The Potential Use of Bar Force Sensor Measurements for Control in Low Consistency Refining

by

Reza Harirforoush

Master of Applied Science, Simon Fraser University, Canada, 2012
Master of Science, Islamic Azad University, Iran, 2003
Bachelor of Science, Islamic Azad University, Iran, 2001

A Dissertation Submitted in Partial Fulfillment
of the Requirements for the Degree of

DOCTOR OF PHILOSOPHY

in the Department of Mechanical Engineering

Supervisory Committee

The Potential Use of Bar Force Sensor Measurements for Control
in Low Consistency Refining

by

Reza Harirforoush

Master of Applied Science, Simon Fraser University, Canada, 2012
Master of Science, Islamic Azad University, Iran, 2003
Bachelor of Science, Islamic Azad University, Iran, 2001

Supervisory Committee

Dr. Peter Wild, Department of Mechanical Engineering
Supervisor

Dr. Ned Djilali, Department of Mechanical Engineering
Departmental Member

Dr. Jens Bornemann, Department of Electrical and Computer Engineering
Outside Member

Abstract

Supervisory Committee
Dr. Peter Wild, Department of Mechanical Engineering
Supervisor
Dr. Ned Djilali, Department of Mechanical Engineering
Departmental Member
Dr. Jens Bornemann, Department of Electrical and Computer Engineering
Outside Member

A crucial parameter in the production of mechanical pulp through refining is energy consumption. Although low consistency (LC) refining has been shown to be more energy efficient than conventional high consistency refining, the degradation of mechanical properties of the end-product paper due to fiber cutting has limited the widespread adoption of LC refining. In conventional control strategies, the onset of fiber cutting is determined by post-refining measurement of pulp properties which does not enable rapid in-process adjustment of refiner operation in response to the onset of fiber cutting.

In this dissertation, we exploit a piezoelectric force sensor to detect the onset of fiber cutting in real time. Detection of the onset of fiber cutting is potentially beneficial in low consistency refining as part of a control system to reduce fiber cutting and increase energy efficiency. The sensor has a probe which replaces a short length of a refiner bar, enabling measurement of normal and shear forces applied to pulp fibers by the refiner bars. The custom-designed sensors are installed in an AIKAWA pilot-scale 16-in. single-disc refiner at the Pulp and Paper Centre at the University of British Columbia. Trials were run using different pulp furnishes and refiner plate patterns at differing rotational speeds and a wide range of plate gaps. Pulp samples were collected at regular intervals and the pulp and paper properties were measured.

We observe distinct transitions in the parameters that characterize the distributions of peak normal and shear forces which consistently correspond to the onset of fiber cutting.

In addition, the analysis of the power spectrum of the sensor data shows that the magnitude of the dominant frequency can be used as an indicator of fiber cutting.

The power of the time domain signal of the normal force is shown to be the most reliable and consistent indication of the onset of fiber cutting. This parameter consistently identifies the onset of fiber cutting, as determined by fiber length data, for all tested pulp furnishes and plate patterns.

In addition, we investigate the effect of pulp furnish and plate pattern on bar forces in LC refining. For tested pulp furnishes and at all plate gaps, the plate with higher bar edge length (which has smaller bar width and groove width) results in lower mean peak normal and shear forces but higher mean coefficient of friction. Moreover, at the onset of fiber cutting, the mean peak normal force of softwood pulp is higher than that for hardwood pulp. Our results also show that the mean coefficient of friction at the onset of fiber cutting is a function of plate gap, pulp furnish, and plate pattern.

Table of Contents

List of Tables

List of Figures

Nomenclature

L_w	Length-weighted fiber length	β	Shape parameter of Weibull distribution
n_i	The number of the fibers in ith class	η	Scale parameter of Weibull distribution
L_i	Mean length of the fiber in ith class	γ	Location parameter of Weibull distribution
f_n	Normal force on a fiber	X(ω)	Continuous Fourier transform of *x(t)*
d_0	Uncompressed outer diameter of fibers	P	Average power of a time domain signal
l	Fiber length	T	Signal length
C_s	Pulp consistency	μ_c	Corner coefficient of friction
K	Fraction of groove width from which fiber captured	μ_f	Surface coefficient of friction
G	Groove width	P_{norm}	Normalized power of normal force
SEL	Specific Edge Load	f_{BP}	Maximum bar-passing frequency
a	Constant in fiber (mat compression parameter)	D	Rotor diameter
g	Gap size	W	Bar width
μ_E	Coefficient of friction	$\emptyset$	Bar angle
s	Sliding distance of bar force	ω	Rotational speed
b	fractional bar coverage of fiber cover width, along length	t	Test duration
z	Fractional distance along unit bar length covered with fiber	HC	High consistency
f_s	Shear force on a fiber	LC	Low consistency
F_N	Average normal force per unit bar length		
F_S	Average shear force per unit bar length		
N	Number of bars on the rotor crossing over the sensor for one revolution		

Acknowledgments

In this acknowledgement I would like to gratefully thank all people who helped me to complete this dissertation.

First and foremost, I would like to express my deep and sincere gratitude to my supervisor and mentor, Dr. Peter Wild, Professor and the chair of the mechanical engineering department, for his continuous support, patience, motivation, enthusiasm and friendly help in various ways. It was a great privilege and honor to work and study under his supervision.

Besides my supervisor, I would like to specially thank Dr. James Olson, Professor and interim dean of the Faculty of Applied Science of the University of British Columbia, for his insightful comments, encouragement, and provide me an opportunity to work with Energy Reduction in Mechanical Pulping research program.

I would also like to thank my committee members, Professors Ned Djilali and Jens Bornemann for letting my defense be an enjoyable moment, and for their brilliant comments and suggestions.

This work is supported by a Collaborative Research and Development grant provided by Natural Sciences and Engineering Research Council of Canada (NSERC) and through the support of our following partners: AB Enzymes, Alberta Newsprint Company, Andritz, BC Hydro, Canfor, Catalyst Paper, FPInnovations, Holmen Paper, Meadow Lake Pulp (Paper Excellence), Millar Western, NORPAC, West Fraser, Westcan Engineering, and Winstone Pulp International.

I would like to thank the staff of Pulp and Paper Centre at the University of British Columbia specifically Mrs. Meaghan Miller, Mrs. Emilia Jahangir, Ms. Reanna Seifert, and Mr. George Soong for their assistance during the preparation and execution of refining trials, and for conducting the sample characterisations and handsheet testing.

I would also to thank my colleagues and friends in the Lab, Geoff Burton, Luis Melo, Elizabeth Trudel, David Bernard, Cameron Wade, Sven Scholtysik, McKenzie Fowler, Kevin Palmer-Wilson, Ben Lyseng, James Donald, Matthias Aigner, and Riccardo Bostock for all of the great times that we have shared. Specially, I would like to thank Institute for

Integrated Energy Systems staffs, Mrs. Susan Walton and Mrs. Pauline Shepherd, for their tremendous supports.

I would like to thank my wonderful parents, Abdolmajid and Batoul, for their love, prayers, caring and sacrifices for educating and preparing me for my future. It was under their watchful eyes that I gained so much drive and an ability to tackle challenges head on. I also want to thank my brother, Mohammad, who has been my best mentor in my life, and my kind sister, Maryam, for their wonderful support and encouragement during my education.

Also, I thank my father-in-low and my mother-in-low, Alireza and Mahvash, and my brothers and sisters-in-law for their wonderful encouragement and support.

Finally, most importantly, I would like to express the profound gratitude from my deep heart to my beloved wife, Mahsa Chitsaz, and our lovely baby on her womb. I could never have accomplished this dissertation without her wonderful support, encouragement, quiet patience, and continued love. Mahsa has been extremely supportive of me throughout entire life and has made countless sacrifices to help me get to this point. I love you dearly!

Dedication

To my wonderful father and mother for always supporting, helping, guiding, unconditionally loving, and standing by me. Without your guidance and love I would not be the man I am.

To my beloved wife Mahsa Chitsaz for all of her love and supports. I am forever thankful for having you in my life.

Chapter 1: Introduction

Canada is strategically positioned in the global pulp and paper market. The nation holds 9% of the world's forest resources [1] and has plentiful water and electrical infrastructure to drive the pulping process. However, the industry is extremely energy intensive. In Canada, in 2015, pulp and paper mills consumed 542 PJ (Petajoule) or one-quarter (26%) of total energy consumed by manufacturing [2]. In British Columbia (BC), in 2010, the 78 refiners used in mechanical pulping consumed 5400 GWh or 11% of BC's total electrical energy production [3]. This energy intensity, coupled with the increasing cost of energy, presents a significant challenge to the competitive position of the Canadian pulp and paper sector.

Refining, an energy intensive process, is used in the pulp and paper industry to separate fibers from wood matrix mechanically and to develop fiber properties to be suitable for papermaking by improving the bonding ability of fibers as well as the strength and smoothness of paper made of the treated fibers.

One method of reducing energy consumption in mechanical pulping is to decrease the number of refining treatments at high consistency[1] (HC) and increase the number of treatments at low consistency (LC). LC refining of mechanical pulp has been shown to be more energy efficient than conventional HC refining [5–7]. It is hypothesized that the higher efficiency of the LC refining process is due to the relative uniformity of treatment [3]. LC refining is also excellent for the removal of shives[2], external fibrillation[3] of fibers, removing latency (fiber twists) in the fiber, and improving fiber networking and bonding capabilities [4,8]. However, at high refining intensities, fiber cutting in the LC process can lead to degradation of the mechanical properties (i.e. tear index) of the end-product paper. This issue has limited the widespread adoption of LC refining.

Conventional refiner control strategies are based on refiner process variables such as rotational speed, plate gap (i.e. the distance between the stationary disc or *stator* and the

[1] *Consistency*: percentage, by weight, of wood fiber in the fiber and water mixture. Typically, pulp with fiber content of 5% or less is considered a low consistency pulp, while pulp with a fiber content of 20% or greater is high consistency pulp. Medium consistency pulp is referred to the pulp with a fiber content of 6-15% [4].

[2] *Shives*: groups of fibers that have not been broken apart into individual fibers.

[3] *External fibrillation*: a change to the external structure of the fiber due to refining, and is defined as the shearing on fiber surface that increases the area of surface fibrils and the bonding area in paper sheet.

rotating disc or *rotor*), pulp consistency, and specific refining energy[4]. In these strategies, fiber cutting is detected only by post-refining measurement of pulp properties. Typically, this approach does not enable rapid in-process adjustment of refiner operation in response to the onset of fiber cutting.

A piezoelectric sensor, referred to here as Refiner Force Sensor (RFS), previously developed for use in LC and HC refining, has been adapted to collect data defining the mechanical interactions between the refiner bars and pulp fibers. The RFS has a sensing probe that replaces a short length (i.e. 5 mm) of a refiner bar, Figure 1-1a, enabling measurement of forces normal and tangential to a refiner bar, as shown in Figure 1-1b. The RFS has been used in studies in both low consistency [9,10] and high consistency refining [11,12]. This sensor has been used to measure forces during individual bar-crossing events (i.e. when a bar of rotating disc passes over the sensor), but has not been used as the basis for advanced refiner control strategies to detect the onset of fiber cutting.

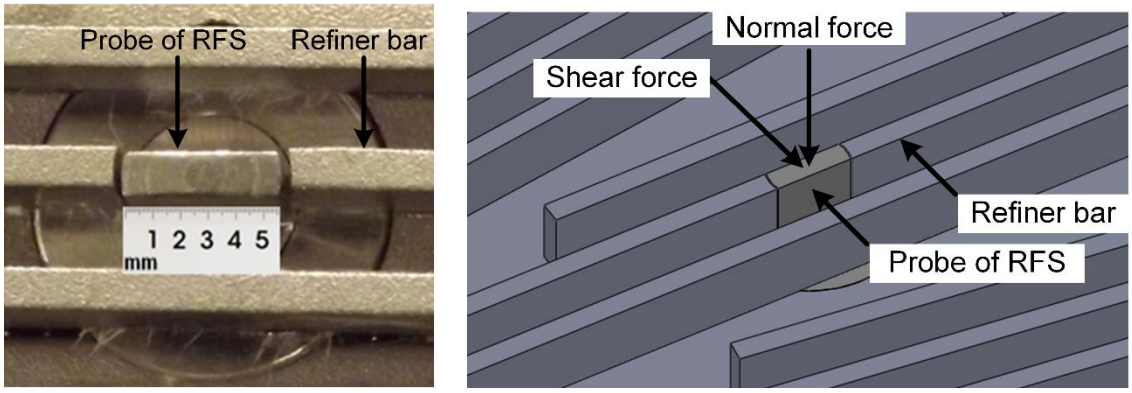

(a) (b)

Figure 1-1. (a) A close-up of the RFS installed in a stator plate, (b) direction of normal and shear forces measured by the RFS

This dissertation investigates the relation between refiner control variables, measured bar forces, and resulting pulp properties by exploiting the latest generation of the RFS. The custom-designed sensors are installed in an AIKAWA pilot-scale 16-in. single-disc refiner at the Pulp and Paper Centre (PPC) at the University of British Columbia (UBC). Trials were run using different pulp furnishes and refiner plate patterns at differing rotational speeds and a wide range of plate gaps. Pulp samples were collected at regular intervals and

[4] *Specific refining energy:* energy transferred to the pulp per unit mass of fiber.

the pulp and paper properties were measured. The sensor data collected in these trials are analyzed and metrics that have potential for in-process detection of the onset of fiber cutting are determined.

This chapter presents a review of mechanical refining, descriptions of the pulp and paper properties reported in our results, and the literature on strategies to detect fiber cutting in LC refining. Previous studies of bar force measurement in HC and LC refining are also reviewed.

1.1. Low Consistency Mechanical Refining

1.1.1. Mechanical Refiners

Mechanical refining, as commercialised in the 1960's [13], is used in the pulp and paper industry to separate fibers from the wood matrix and to develop the properties of the fibers for papermaking. There are several types of mechanical refiners including single-disc, twin, and conical refiners. The most common type of refiner, the single-disc refiner, is composed of opposed stationary (stator) and rotating (rotor) discs that are separated by a small gap, as shown in Figure 1-2a. Replaceable refiner plates that carry patterns of bars and grooves are secured to the facing surfaces of the discs. These plates are characterized by bar width, groove width, groove depth, and bar angle, as depicted in Figure 1-2b.

The axial position of the rotor can move, so that the gap between the stator and rotor can be adjusted. Pulp is fed into this gap at the refiner axis, and flows radially outward between the stator and rotor plates. The fibers flow in the grooves of the plate and are trapped between the leading edges of the opposing bars by reaction forces from the applied compression in the small gap between the rotor and stator. Through repeated cyclic compression and shear forces applied to pulp fibers by the refiner bars, the outer layers of fiber cell wall peel off and become fibrillated, whereas the inner cell wall becomes delaminated. These cause an increase of the surface area and the conformability of fibers which leads to an enhancement in bond area and the strength of paper [14].

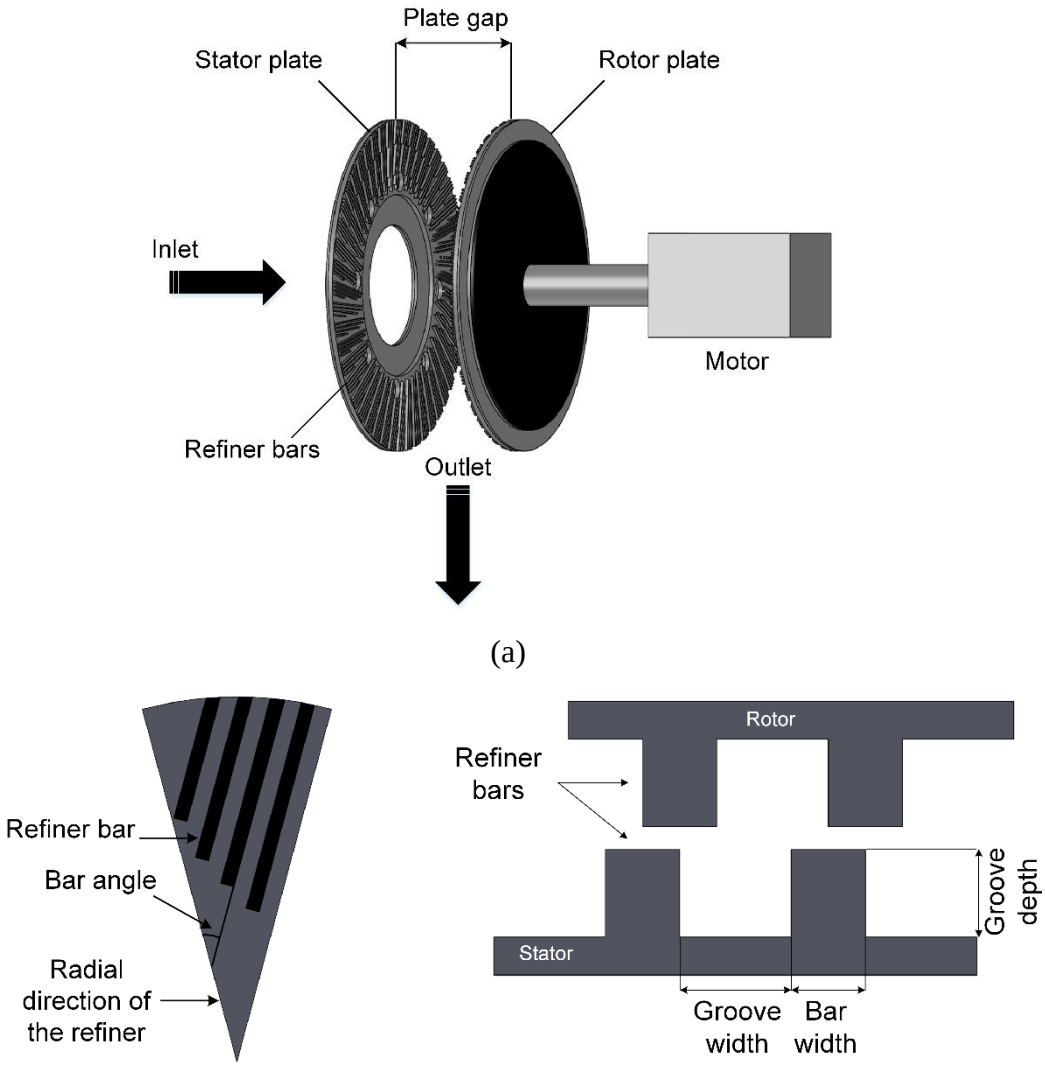

Figure 1-2. (a) Schematic diagram of a single-disc mechanical refiner, (b) a schematic of stator refiner bars with bar angle (left side), bar width, groove width, and groove depth (right side).

1.1.2. Pulp and Paper Properties

In this section, the definitions of the pulp and paper properties reported in our results are presented. These properties include length-weighted fiber length, freeness, tear index, and tensile index.

A. Length-weighted fiber length (mm):

Fiber length is one of the most important fiber properties. Forgacs [15] showed that the physical properties of mechanical pulp can be predicted from two key properties, external

specific surface (commonly measured by freeness test) and fiber length. Fiber length is measured through fractionation with screens or by optical scanners. The most common of these optical instruments are the *Kajaani FS-200* and the *Optest FQA*. In this dissertation, we report the length-weighted fiber length (L_w), the most meaningful measure of fiber length [16], as measured by Fiber Quality Analyzer (HiRes FQA, Optest Equipment Inc.; Hawkesbury, ON, Canada). Equation 1 defines the length-weighted fiber length as follows:

$$L_w = \frac{\sum n_i L_i^2}{\sum n_i L_i} \quad (1)$$

where n_i and L_i are the number of the fibers in the *ith* class and mean length of the *ith* class, respectively.

B. Freeness (ml):

Freeness, the drainage resistance of pulp slurry, is the most widely used control parameter for refining. Freeness is a good predictor of sheet density and it is routinely used to predict strength, opacity[5] and other physical properties of the paper. It is measured by different standards such as Canadian Standard Freeness (CSF), *Schopper Rieglor*, and *William Precisions Slowness* [14]. In this dissertation, we use CSF which is defined as the measure of the rate at which a dilute suspension of pulp (three gram of pulp in one liter of water) is drained through a standard screen (TAPPI standard T227 [17]).

C. Tear index (mNm^2/g):

Tear strength is determined with a pendulum type device that measures the energy absorbed in tearing a paper sample. Tear index is the quotient of paper tear strength (mN) divided by paperweight (g/m^2).

D. Tensile index (Nm/g):

Tensile strength is the maximum tensile force to break a strip of paper sheet when pulled in tension. It is measured by dividing the tensile strength per unit width [N/m] of a paper sheet by its basis weight [g/m^2].

In this work, tear and tensile index are measured based on TAPPI standard T220 [18].

[5] *Opacity:* the property of paper that describes the amount of light which is transmitted through it. The opacity of paper is influenced by thickness, amount of filler and degree of bleaching [14].

1.2. Literature Review

1.2.1. Fiber Cutting in Low Consistency Refining

Low consistency refining is commonly used in three different refining stages including main line stage (second or third stage), reject second stage, and post refining stage [19]. LC refining has been shown to be more energy efficient than conventional HC refining [5–7,20,21]. Although LC is more energy efficient, achieving optimal operating conditions in LC refining is challenging.

In LC refining, the operating plate gap is smaller than in HC refining [22]. Refining at low consistencies with a minimal plate gap increases fiber-bar contact and, consequently, also increases the chance of fiber cutting at high refining energies (i.e. at small plate gaps). Therefore, the plate gap must be controlled to deliver sufficient energy to the fibers to achieve the desired fiber development while avoiding fiber cutting [3,23]. Fiber cutting causes degradation of the mechanical properties of the end-product paper and has limited the widespread adoption of LC refining.

In LC refining, to reduce energy consumption, refiner control strategies often aim to keep net power consumption constant as well as the pulp mass flow rate passing through the refiner. In most of the LC refining operations, power is controlled by plate gap. Thus, understanding the relation between power and plate gap is crucial toward the optimization of LC refining operation.

Several researchers have studied the relation between net refiner power and plate gap, both theoretically and experimentally [24,25]. In many of these studies, refining power is measured at different plate gaps while keeping all other variables constant. As the plate gap is closed, fibers are subjected to increasing compressive and shear forces that leads to an increase in net refiner power.

A linear relationship between refiner power and the inverse of the plate gap in LC refining was suggested by Leider and Nissan [26] who proposed an analytical model to characterize refining as a combination of the number of impacts per single fiber and the intensity of each impact.

The relationship between refiner power and plate gap was experimentally studied by Mohlin [24] in a conical LC refiner. She showed that the refiner power is inversely proportional to the plate gap. The relationship was indicated as an important parameter

relating refiner operation variables to pulp quality changes. An approximate linear relationship between power and plate gap over the range of 0.1-0.2 mm in a two zoned TwinFlo72 LC refining was recently reported by Berg et al. [27].

Using dimensional analysis on the data collected in pilot-scale LC refining trials, Luukkonen et al. [25] developed a predictive model that relates refiner operating conditions to pulp properties. They found that power is related to plate gap, fiber length and plate design. The power varies almost linearly with the inverse of plate gap.

It has been also observed that the relation between power and plate gap is affected by changes in pulp furnish. Berna et al. [28] point out that changing pulp affects the power versus plate gap relationship; the operational plate gap for reject fractions pulp that contain longer, coarser and stiffer fibers are wider than unscreened pulps.

Despite the contribution of these studies, the fiber cutting causing degradation of the mechanical properties of the end-product paper cannot be distinctly determined in the relationship between power and plate gap. As the plate gap is closed, a *critical gap*, which was first introduced by Roux [29], is reached at which significant fiber cutting occurs. Moreover, a rapid increase in refining power occurs after passing the critical gap. The critical gap has been shown to vary with changing rotational speed, plate pattern, consistency, and initial fiber length [14,30,31]. The critical gap decreases with decreasing rotational speed [14]. Lundin [30] showed that increasing consistency increases the critical gap in conical LC refining. The longer the fiber to be refined, the bigger the critical gap is [31]. In addition, using the plate designs with narrower bars and grooves, which provide lower intensity treatments, reduces fiber cutting.

In conventional control strategies, critical gap is detected based on post-refining measurement of pulp properties. For a given feed stock, pulp and paper properties, such as fiber length and tear index, are affected by refiner process variables, in particular, by plate gap, power and rotational speed. The effects of these variables on critical gap have been widely studied.

Based on mill-scale LC refining studies, Luukkonen et al. [3] show that specific energy and plate gap are the two key parameters controlling pulp quality changes during refining. Luukkonen et al. [32] also propose a methodology to correlate operating conditions to pulp quality by relating the refiner operating conditions (i.e. power, flow rate, gap) to fiber

quality (i.e. fiber length and freeness), and then relating fiber quality to pulp handsheet quality (i.e. tensile, tear, and bulk[6]). His work also shows that the changes in pulp quality remain constant until a critical gap was reached. Beyond the critical gap, fiber cutting commences and paper strength properties are reduced. Moreover, beyond this point, the relationship between refining power and plate gap deviates from linearity [33].

Similar results were observed by Nugroho [31] for various mixes of softwood[7] (SW) and hardwood[8] (HW) pulps in LC refining. Refining power increases as the plate gap decreases and, at a critical gap between 0.3 to 0.5 mm, the power sharply increases. Moreover, the fiber length and freeness decrease as the plate gap is reduced below the critical gap. This transition occurs for all of the trial conditions. Nugroho also showed that the critical gap depends on initial fiber length.

Elahimehr et al. [34] studied the effect of plate gap, rotational speed, and plate pattern on LC refining performance in an AIKAWA 16-in pilot-scale LC refiner. They found non-dimensional power-plate gap relationship is a function of refiner plate geometry and pulp furnish. They also found that the mean fiber length was unchanged until the plate gap reached the critical gap, near 0.25 mm, and significantly decreased for the plate gaps smaller than the critical gap.

Moreover, a number of researchers have characterized refining action based upon either the force or energy applied to pulp fibers during bar-crossing events. Specific edge load (SEL[9]) theory, introduced by Brecht [35], is widely used in industry to characterize refining performance. His analysis was based on a laboratory-scale conical refiner and he concluded that the effective power is applied by the edges of the bars. However, Roux and Joris [36] showed that the SEL cannot be used to predict fiber cutting since the effect of plate geometry parameters (i.e. bar width, groove width, and bar angle) are not considered in this theory.

---

[6] *Bulk*: the inverse of sheet density. Density of paper is determined by measuring the weight and thickness of a sheet paper.

[7] *Softwoods*: conifer trees that do not lose their needles during the winter such as spruce, fir, hemlock, Douglas fir. Softwood pulps are long fiber pulps.

[8] *Hardwoods*: deciduous trees, that is, broad leaf trees that lose their leaves in the winter such as maple, aspen, birch. Hardwood pulps are short fiber pulps.

[9] *SEL*: defined as the energy expended per unit refiner bar length over one bar-crossing event.

Modified edge load (MEL) theory, developed by Meltzer [37], is an extension of SEL theory that includes plate geometry parameters, which are absent from SEL theory. However, MEL theory does not account for some important parameters such as consistency, rotational speed, groove depth, and fiber properties [38]. This theory does not enable to predict changes in fiber length [39].

The C-factor theory, which represents the capacity of the refiner to impose impacts upon fibers, was proposed by Kerekes [40] for characterization of pulp refiners by the number and intensity of impact imposed on pulp fibers during bar-crossing events. The C-factor is determined by refiner variables, fiber properties, and pulp consistency. This theory assumes that a large number of impacts of low intensity result in fibrillation while a small number of impacts at high intensity leads to cutting. The C-factor theory has not been tested to detect the onset of fiber cutting.

Elahimehr at el. [39] defined intensity as the net energy per unit length of bar interaction length to predict fiber length reduction and fiber cutting, in an LC refiner. A critical intensity of refining of 0.03 J/m corresponds to the critical gap for all plate patterns and rotational speeds used in this study.

Batchelor [41] introduced a fiber-shortening index based on fiber width, SEL, cross-sectional area of the fiber wall and fibril angle[10]. The index was shown to correlate with the fractional fiber length reduction measured from refining trials on softwood and hardwood pulps. This index has not been reported as the basis for detection of onset of fiber cutting.

Theoretical net tangential and net normal force per number of bar-crossing have also been proposed to assess the refining intensity and to predict changes in fiber length [42]. The correlation between the average weighted fiber length and these two parameters indicates that, among different concepts for assessing the refining intensity, the net normal force per number of bar-crossing is adequate to quantify and predict the cutting effect on fibers. However, this parameter is unable to predict the onset of fiber shortening.

Comminution models have been used in mining and crushing industries to predict particle size distribution change during processing. These models also have been used to

[10] *Fibril angle*: refers to the angle between the direction of the helical windings of cellulose microfibrils in the secondary cell wall of fibers and tracheid and the long axis of cell.

describe fiber length distribution changes during refining [43,44]. Roux and Mayade [45] developed a comminution model for the kinetics of fiber shortening in LC refining. The model predicts the potential of fiber cutting in given conditions as a function of the energy per unit mass consumed by the solid phase and the average impact intensity. Olson et al. [43] found that the probability of fiber cutting in refining is proportional to the applied energy and fiber length, and was independent of consistency.

In all of the reviewed studies, the onset of fiber cutting is not determined in real time and the measurement methods do not enable rapid in-process adjustment of refiner operation in response to the onset of fiber cutting. Recently, the Valmet Pulp Analyzer has been developed for online measurement of micro-scale details of fiber properties using a high definition fiber imaging module.

Refiner control variables affect the pulp properties, and ultimately the paper properties. These control variables also influence the forces that a fiber experiences during refining. A thorough understanding of the relation between refiner control variables, mechanical interactions between refiner bars and pulp fiber, and resulting pulp and paper properties is essential toward the objective of having control over the quality of paper produced. The next section reviews bar force measurement studies in HC and LC refining.

1.2.2. Bar Force Measurements in Mechanical Refining

During bar-passing events, agglomerates of wood fibers, known as *flocs*, are captured repeatedly between the passing bars, and cyclical compression (normal force) and shearing (shear force) of the fibers provide the refining action. These forces are considered as the main mechanism of mechanical refining and are the key parameters governing the properties of product pulp and, ultimately, of the end-product paper [46]. The bar forces, forces applied to pulp fibers by the refiner bars, are distributed among fibers and create stress on fibers which cause the strains that lead to bond-breaking and consequently the refining result. The normal force has been shown to contribute to internal fibrillation of the fiber wall through transverse compression and bending of fibers, while the shear force has been shown to cause external fibrillation of the fibers [47,48]. The progression of a typical bar-passing event is illustrated in Figure 1-3. The encircled figure shows the direction of the normal force, F_N, and the shear force, F_S.

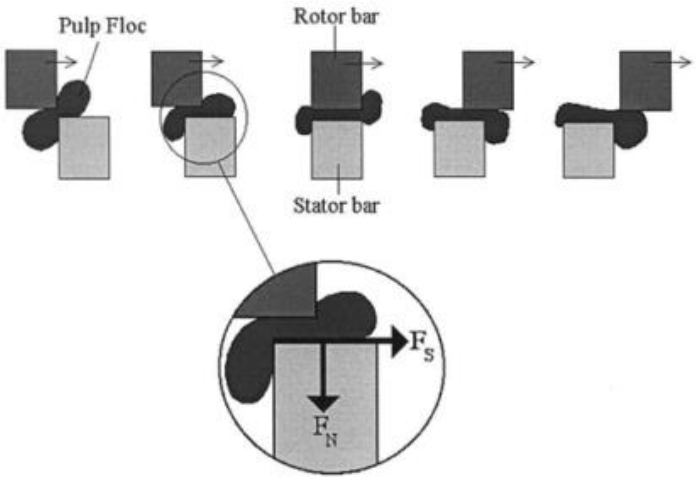

Figure 1-3. Schematic illustration of a typical bar-passing event [49].

A number of researchers have investigated bar forces in LC and HC mechanical refining. The first attempt to experimentally quantify bar forces was by Khlebnikov [50] using strain gauge sensors to measure forces normal to the face of the bar (normal force) and tangential to the bar (shear force) in a conical LC refiner at 2-3% consistency. His results show that the shear force profile increases sharply at the start of the bar-passing event, where flocs were trapped between opposing refiner bars, then decreases to a much lower level and remains relatively constant until the trailing edges of the bars pass each other.

Goncharov et al. [51] developed two strain gauge sensors, the first sensor was based on an L-shaped beam, the top of which protruded into the refining zone as a segment of a refining bar. Beam loading was measured with strain gauges mounted to the base of the beam. However, the accuracy of the sensor was limited to ±2 N, and the sensor only measured bar-passing frequencies less than 2-2.5 kHz due to its first natural frequency limitation. The second sensor was improved in terms of accuracy but the bar-passing frequencies were limited up to 1.3 kHz.

Following this work, Goncharov [52] measured the normal and shear forces in an LC refiner with 300 mm diameter disc using three two-component strain gauge sensors located in three places along the radius of the disc. The pulp consistency was 2.5-3% and the pulp fed through the refiner at a range of plate gaps (0.15-0.3 mm). Measurements of axial thrust, torque and the distribution of hydraulic pressure in the refiner were reported. The

bar width varied between 2 and 10 mm during trials. As shown in Figure 1-4, a peak normal pressure occurs at the initial stage of the bar-passing over the 2-3 mm of the bar width. In Figure 1-4, the horizontal axis represents the overlap between refiner bars while the vertical axis represents the pressure measured by the sensor. Sketch A and B show force and pressure at large and small plate gaps, respectively. The pressure decreased rapidly after 2-3 mm of the bar width and levelled out at only 10-15% of the maximum pressure. Goncharov also found that shortening of fibers increased with increasing pressure. A coefficient of friction of 0.11 (at 720 rpm) was reported.

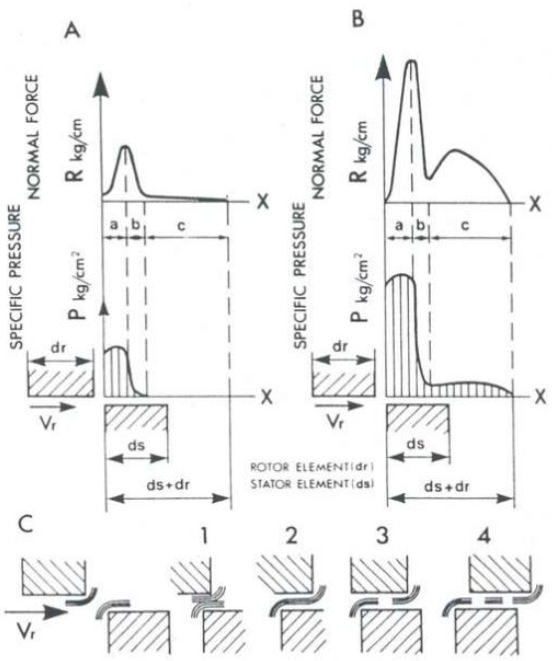

Figure 1-4. The force and pressure distribution as measured by Goncharov [22,52].

Atack and Stationwala measured both temperature and pressure in the refining zone in a 1066 mm (42-in) open discharge HC refiner [53] using custom-made piezoresistive and thermocouple sensors. They observed an irregular peak pressure of up to 6.2 bar (620 kPa) gauge pressure. They suggested that the magnitude of the peak pressure is influenced by the size of flocs.

Nordman et al. [54] used piezoresistive pressure transducers to measure pressure in a small conical LC refiner and in a mill-scale disc refiner. Plate gap, inlet and outlet pressure, pressure in the grooves between the refiner bars and on the top surface of the bar, and temperature were measured. Results show pressures are two orders of magnitude lower

than those of Goncharov but with similar peaks at the leading edge of the bars. They also found that the friction generated during fiber-fiber and fiber-bar contact, as well as transverse compression of fiber bundles are the most critical mechanism in refining. Most of the transducers were damaged by shives [22].

Martinez et al. [55] and Batchelor et al. [56] derived expressions to predict the normal and shear forces acting on a fiber floc in LC refining. The expression was validated experimentally on a single-bar refiner[11] using model nylon flocs at various gaps ranging between 0.7 to 1.3 mm. They found that the forces increase to a peak over the first 2-3 mm of the bar, and then decrease to an essentially constant level over the remaining width of the bar. The study was limited due to the polymer furnish which are considerably larger and coarser than wood pulp fibers. However, the theoretical model was in close agreement with the experiments. Martinez et al. [55] also found that the effect of plate gap on the peak force is strongly dependent on the size of the floc, the mass of fibers trapped between the gap and the compressive modulus of elasticity of the floc.

Gradin et al. [57] used strain gauge sensors, shown as G in Figure 1-5, to measure shear force applied to individual bars inside a 20-in single-disc HC refiner. The shear force was used to find power distribution. Two designs of the sensors were developed. In the first type, shown as type S in Figure 1-5, the refiner bar was cut into segments and the strain gauge installed in each segment while in the second one, shown as type C in Figure 1-5, the strain gauges were installed in a certain distance away from each other in a continuous bar. Strain gauges on the outside of the slit bar sustained only a very short time due to the harsh environment.

One major drawback of the strain gauge sensors is that they are exposed to the harsh environment of refining process and are subject to abrasion from the pulp. Moreover, installing strain gauges inside the grooves is challenging.

[11] *Single-bar refiner*: consists of two opposing plates (stator and rotor) with a single bar protruding from each plate.

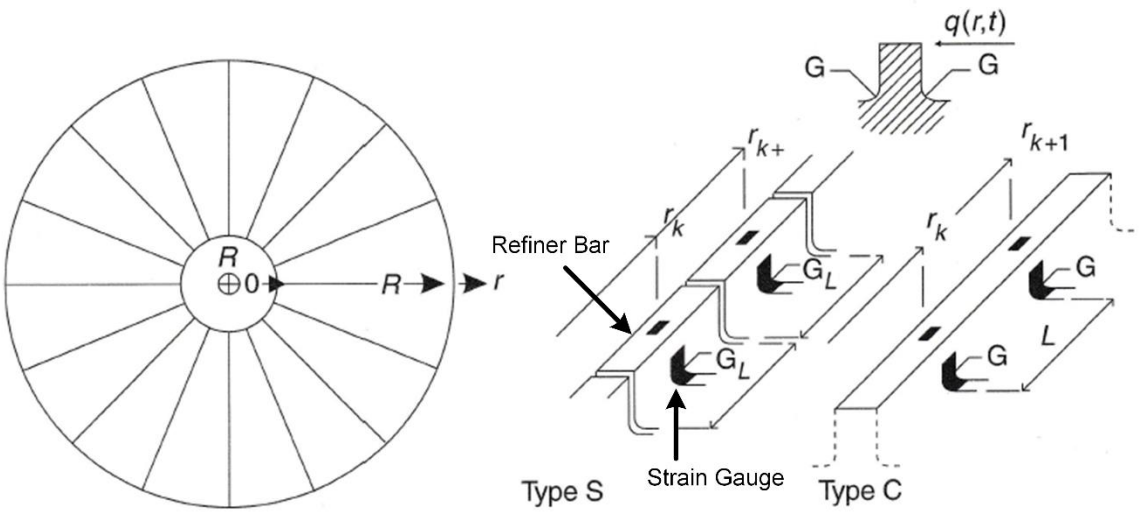

Figure 1-5. Strain gauge sensors developed by Gradin et al. [57]. Tangential force intensity and radial distance are shown by q(r,t) and r_k, respectively.

A similar concept was used and patented by Johansson et al. [58] who installed strain gauges at different points along the refiner bars to measure the shear forces. As discussed earlier, a major problem of these sensors is that they are subject to abrasion.

In a recent work, Gradin et al. [59] attached 16 strain gauge sensors in eight positions on the inside of a hollow radial bar, as shown in Figure 1-6, to determine the tangential force distributions. Trials were run in an atmospheric 20-in single-disc HC refiner at the rotational speed of 600 rpm. However, the tangential force distribution was not determined since the strain-measurement device could only record four channels simultaneously, and it was not possible to get synchronous signals for all sensors. Moreover, the width of the instrumented bar embedded in the refiner is wider than the bar width of the plate that may affect the results. The sensors were only tested in atmospheric condition and more investigations are needed to verify the durability of sensors under high temperature pressurized condition.

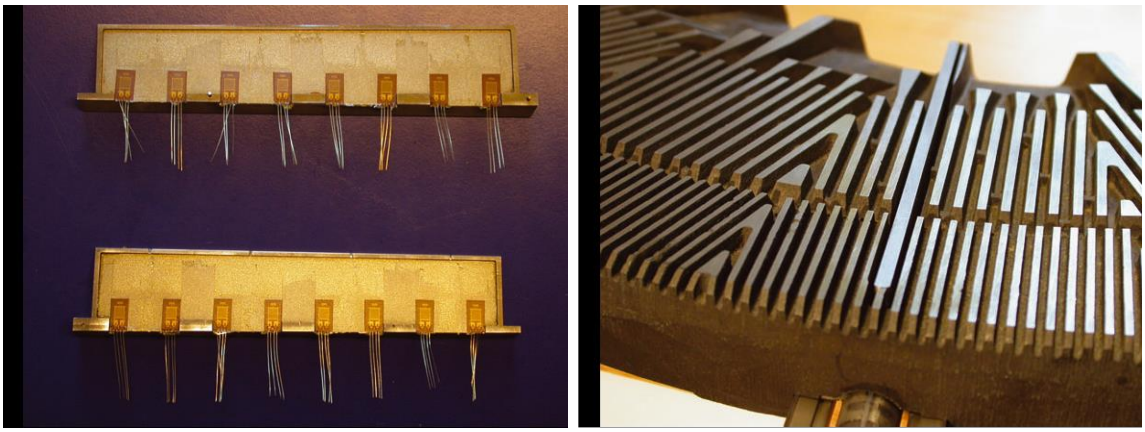

(a) (b)

Figure 1-6. (a) The strain gauge sensors before assembly, (b) refiner disc with the strain gauges [59].

An analytical model was developed by Senger [38] to predict the normal stress resulting from floc compression between the bars of a refiner. The results were compared with experiments that measured normal and shear forces applied to individual flocs of fibers in a single-bar refiner rotating at less than 3 rpm. The gap between the bars could be adjusted by moving the rotor. A single floc is held by a small block mounted adjacent to the bars of the rotor. A linear variable differential transformer (LVDT) mounted on the stator measures the small vertical deflection of the stator during floc compression caused by a bar-passing. A torque sensor measures the torque produced by the event. The experiment setup, shown in Figure 1-7, can measure the normal and shear forces applied to a floc captured between the two passing bars. A typical force profile for a single floc is shown in Figure 1-8. At 5.5 mm, the stator and rotor bar start to overlap while at 8.5 mm, the stator and rotor bar are aligned. At 11.5 mm, stator and rotor bar overlap ends.

Senger et al. [60] also showed that the ratio of the average of shear force to the average normal force, equivalent tangential coefficient of friction, increases with increasing consistency. They also found that the sharpness of the bar edge has a significant effect on shear force. A sharp bar edge acts as a stress concentration point and results in increasing shear force.

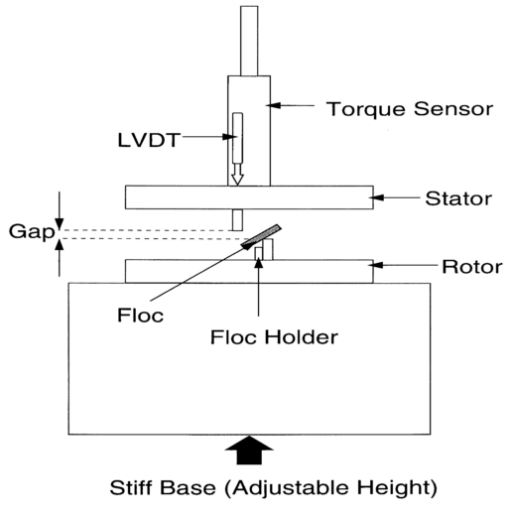

Figure 1-7. Schematic of a single-bar refiner [38].

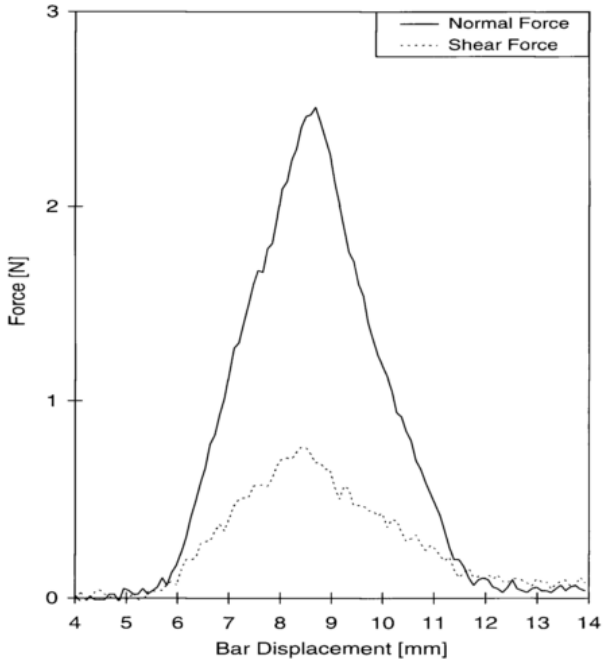

Figure 1-8. A typical force profile of a floc compressed in the single bar refiner [38].

Backlund [61] measured tangential forces in mill-scale 65-in single-disc and conical disc HC refiners using a commercial piezoelectric force and strain gauge sensor, respectively. He concluded that the tangential forces increased along the radius and the highest tangential force was measured at the periphery of the refining zone. However, the sensor could only record an average shear force over many bar-crossings events. Moreover, the large suspended mass of the sensor elements may have caused lateral vibrations close

to or below the bar-passing frequency in a large refiner which would have reduced sensor signal quality.

A family of piezoelectric-based sensors has been developed to measure forces applied to pulp fibers by the refiner bars during individual bar-passing events in both HC and LC refiners [9,11]. The first prototype refiner force sensor (RFS) was tested in a 300 mm HC lab-scale chip refiner at FPInnovations–Paprican division in Vancouver, BC, Canada [49,62,63].

A modified version of this sensor was developed in 2004 for use in both lab and pilot-scale HC refiners, at Paprican's Pointe Claire, QC, Canada [64]. The distribution of peak magnitude of forces followed a decreasing exponential distribution, which suggested substantial heterogeneity of the impacts within the refining zone. Bar forces have been shown to be influenced by radial location in the refining zone. Average normal and shear forces at the beginning of the refining zone were 5-10 times greater in magnitude than those at the end of the intermediate bar section, while peak values at the inner radius were 10-20 times larger than peak values at the outer radius. Senger et al. [64] observed that forces were smallest at the periphery. They also found that the equivalent tangential coefficient of friction ranged between 0.7 and 1.1.

The dynamic range and the durability of the RFS was improved and then used in trials in a 36-in pressurized single-disc HC refiner at the Andritz research facility in Springfield, Ohio [65].

Prairie [66] modifies the RFS to measure normal and tangential shear forces at one location in a Sunds Defibrator Conflo® JC-00 LC conical refiner at FPInnovations, Vancouver laboratory. Trials were undertaken using softwood CTMP (Chemi-Thermo Mechanical Pulp) at a consistency of 3.15% at 900 rpm refiner speed. This study shows that both peak normal and shear force distributions were essentially normal in shape with a slight skew toward smaller force values[9]. It was found that the median normal and shear forces increase with increasing SEL. Moreover, the peak coefficient of friction ranges from 0.13 to 0.16 and decreases slightly with increasing SEL. A two-parameter Weibull function was fit to the normal and shear force data to characterize the force distributions. Prairie et al. [9] found that the shape of force distributions is relatively independent of changes to

SEL. He suggested that the knowledge of the distribution of forces could provide greater insight to predict the probability of forces responsible for fiber cutting at different SEL.

In a separate study [10] , a relationship between refiner tram and force magnitudes was discovered and it was concluded that out of tram plays an important role in the distribution of forces that occur in low consistency refining. Out-of-tram on the order of 40% of the gap can results in variations in peak forces on the order of 300%.

Another RFS was designed by Olender [67] and was installed in two single-disc HC refiners: a pilot-scale primary stage at the Andritz Inc. research facility in Springfield, OH, US, and a mill-scale rejects stage at a Catalyst Paper Corp. mill in Port Alberni, BC, Canada. Olender et al. [11] found that mean normal and shear forces are highest at the periphery of the refining zone in the reject refiner while they were highest at the sensor closest to the refiner axis in the primary stage. In the primary stage, the force distributions were decreasing exponentially while rejects refining showed skewed normal distributions that may indicate the fundamental difference in the treatment of fibers in these refines. Moreover, the equivalent tangential coefficient of friction, defined as the average shear force divided by average normal force, was 0.83 in Springfield trials while it was 0.49 in Port Alberni. The coarse and intact wood fibers in the primary stage, Springfield trials, cause the difference in equivalent tangential coefficient of friction between Springfield and Port Alberni trials.

Olender et al. [12] also investigated the effect of consistency on forces on bars in HC mill-scale refines and found that in the primary refiner, the equivalent tangential coefficient of friction increases by increasing the consistency while no significant changes were observed in the reject refiner.

In a number of studies, bar forces have been analyzed theoretically. Kerekes and Senger [68] derived practical equations to estimate both normal and shear forces on a fiber in LC refining. Forces on a fiber differ from bar forces and depend on how forces are distributed among fibers. Kerekes and Senger [68] found that the average normal (f_n) and shear forces (f_s) on a fiber are estimated by Equation (2) and (3), respectively [69]:

$$f_n = \frac{\sqrt{\pi}\, d_0\, l^{\frac{3}{2}}\, C_s \sqrt{KG}}{4\, a\, g} \left(\frac{\text{SEL}}{\mu_E\, s\, b\, z} \right)^{0.7} \qquad (2)$$

$$f_s = \mu_E \, f_n \tag{3}$$

where d_0 is the uncompressed outer diameter of fibers, l is the fiber length, C_s is the pulp suspension consistency, G is the groove width, g is the gap size, μ_E is the coefficient of friction, s is the sliding distance of bar force, b and z are the fractional bar coverage of fiber cover width, along length, K is the fiber capture factor, and a is a constant in fiber, mat compression equation.

Kerekes [46] also compared the predicted forces on bars, estimated by Equations 4 and 5, with measured forces in a HC primary refiner, reject refiner, and an LC refiner and showed that results for the reject and LC refiner are in good agreement.

$$F_S = \frac{\mathrm{SEL}}{s} \tag{4}$$

$$F_N = \frac{F_N}{\mu_E} \tag{5}$$

where F_S and F_N are the average shear force and normal per unit bar length (N/m), respectively.

Batchelor et al. [56] showed that the bar shear force is the sum of a corner force, at the bar edge, and a surface friction force, on the axial-facing bar surface. These forces are shown in Figure 1-9. The corner force, or ploughing force, strongly depends on bar sharpness (i.e. the radius of curvature of the bar edge). Sharper bars create higher ploughing frictions and higher restrain forces which leads to a cutting action.

They also found that the relationship between the corner force and surface friction force to the normal force is calculated by Equation (6):

$$F_N = \mu_c \, F_s^{\frac{5}{3}} + \mu_f \, F_s \tag{6}$$

where μ_c and μ_f are the corner coefficient of friction and surface coefficient of friction, respectively. μ_c is affected by consistency, fiber length, fiber diameter, fiber modulus of elasticity, and fiber Poisson ration [70].

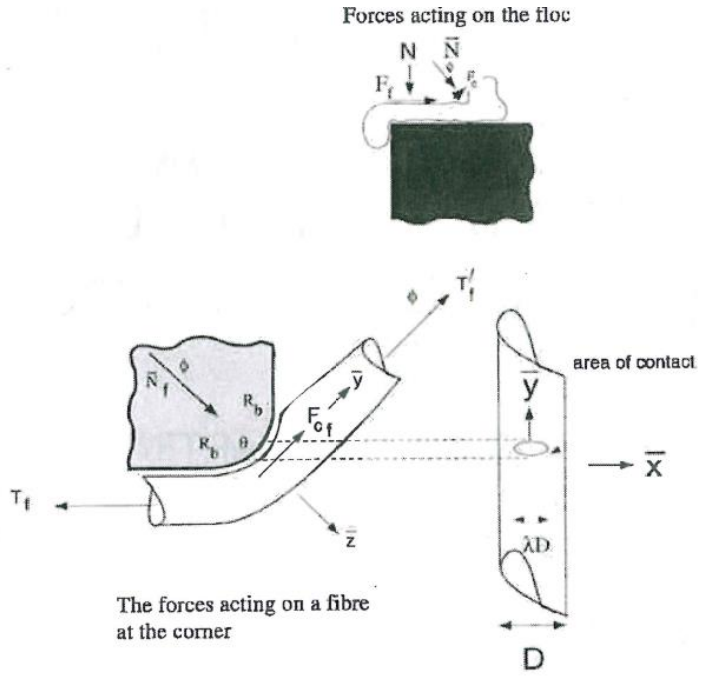

Figure 1-9. The forces acting on a floc in contact with the bar edge, and the force applied by a bar edge to a single fiber in the floc [56].

Kerekes [46] suggests that the force is the key link between bars and fibers in refining that cause important changes in fiber properties. Forces on fibers create stresses which cause three modes of strains including compression, shearing, and tension [68] that lead to bond-breaking and refining action. Compression and surface shearing are likely to cause internal fibrillation[12] and external fibrillation, respectively. Tension is assumed as the cause of straitening and fiber shortening. Page [71] indicated that fibers are shortened in refining by tension failure, not by scissor-like cutting or compression.

None of the bar force studies discussed above investigated the relation between refiner control variables, bar forces, and the resulting pulp and paper properties in order to detect the onset of fiber cutting in real time. Moreover, although the RFS has been used to measure shear and normal forces during individual bar-passing events, it has not been applied as the basis of refiner control strategy to detect the onset of fiber cutting.

[12] *Internal fibrillation*: defined as the degradation of the fiber wall.

1.3. Objectives of Dissertation

The objective of this work is to exploit the latest generation of the RFS for in-process detection of the onset of fiber cutting in LC refining. The first objective is, therefore, to detect the onset of fiber cutting in real time based on RFS data. The second objective of this dissertation is to investigate the effect of pulp furnishes and plate pattern on measured bar forces and, more specifically, on the detection of fiber cutting.

1.4. Research Contributions

Custom-designed piezoelectric force sensors measure normal and shear forces applied to pulp fibers by the refiner bars. The sensors are installed in an AIKAWA pilot-scale 16-inch single-disc LC refiner at PPC-UBC. Trials were run using different pulp furnishes and refiner plate patterns (with differing bar and groove width), at different rotational speeds and a wide range of plate gaps. The contributions of this work are as follows:

i. Identify the relationships between bar forces, plate gap, and fiber length: We find a non-linear relationship between measured bar forces and length-weighted fiber length that mirrors the established relationship between length-weighted fiber length and the inverse of plate gap [Chapter 2].

ii. Detection of the onset of fiber cutting in real time: Based on time and frequency domain analysis of the sensor data, we identify four fiber cutting metrics which detect the onset of fiber cutting in real time in LC refining [Chapter 3]. The most reliable and sensitive indication of the onset of fiber cutting is the *power* of the time domain signal of the normal force [Chapter 4]. For pulp mills, detection of the onset of fiber cutting conditions is potentially beneficial in low consistency refining as part of a control system to reduce fiber cutting and increase energy efficiency.

iii. Identify the effect of pulp furnish on bar forces: Mean peak normal force, mean peak shear force, and mean coefficient of friction, at the onset of fiber cutting, depend on pulp furnishes. Moreover, at the onset of fiber cutting, the mean peak normal force of softwood pulp is higher than for the hardwood pulp [Chapter 4]. This study provides new insights into the fundamental knowledge in understanding the treatment of hardwood and softwood fibers in mechanical refining.

iv. Identify the effect of plate pattern on bar forces: For tested pulp furnishes and at all plate gaps, the plate with smaller bar width and groove width results in lower mean peak normal and shear forces but higher mean coefficient of friction. In addition, mean peak normal force, mean peak shear force, and mean coefficient of friction at the onset of fiber cutting depend on plate pattern [Chapter 5]. Meanwhile, we hypothesize that the normal forces are the dominant forces in LC refining. The results of this study are advantageous for researchers and pulp mills to understand the effect of plate geometry parameters in the interaction of bar forces and pulp fibers in LC refining.

Contributions of this dissertation are presented in four journal articles, two conference papers, and a conference oral presentation.

1.5. Dissertation Organization

The dissertation is organized in five chapters, Chapters 2 to 6. Chapters 2 to 5 are synopsis of four journal papers. An expanded version is available in Appendixes. In each Chapter, the experiment and methodology are explained in Sections 1 and 2, respectively, while the discussion of significant findings are presented in Section 3.

Chapter 2 investigates the relationship between measured bar forces, net power, plate gap, and length-weighted fiber length in a single-disc low consistency refiner. This Chapter was published in:

- **Harirforoush, R.**, Wild, P., Olson, J. (2016): The relation between net power, gap, and forces on bars in low consistency refining. Nordic Pulp and Paper Research Journal, 31(1), 71-78. http://dx.doi.org/10.3183/NPPRJ-2016-31-01-p071-078

Chapter 3 presents the indications of the onset of fiber cutting in real time using custom-designed piezoelectric force sensors. This Chapter was published in:

- **Harirforoush, R.**, Olson, J., Wild, P. (2017): In-process detection of fiber cutting in low consistency refining based on measurement of forces on refiner bars. TAPPI Journal, 16(4), 189-199.

In Chapter 4, the effect of pulp furnish on measured bar forces is investigated. Moreover, the most reliable and sensitive indication of the onset of fiber cutting is determined. This Chapter is recently published in:

- **Harirforoush, R.**, Olson, J., Wild, P. (2018): Indications of the onset of fiber cutting in low consistency refining using a refiner force sensor: the effect of pulp furnish. Nordic Pulp and Paper Research Journal, 33(1).

Chapter 5 assesses the effect of plate patterns on measured bar forces. In addition, the validation of the indications of the onset of fiber cutting found in Chapters 3 to 4 are also investigated. This Chapter is under review in:

- **Harirforoush, R.**, Olson, J., Wild, P. (2017): Bar force measueremnets in low consistency refinin: the effect of plate pattern. Under Review, Nordic Pulp and Paper Research Journal.

Chapter 6 presents the conclusions of the combined articles, and outlines potential future work.

Chapter 2: The Relationships between Refiner Control Variables, Bar Forces, and Resulting Pulp Properties

The objective of this chapter is to investigate the relationship between bar forces, net power, plate gap, and length-weighted fiber length in a single-disc low consistency refiner. This chapter was published in the journal of Nordic Pulp and Paper Research Journal, Appendix A.

Harirforoush, R., Wild, P., Olson, J. (2016): The relation between net power, gap, and forces on bars in low consistency refining. Nordic Pulp and Paper Research Journal, 31(1), 71-78. http://dx.doi.org/10.3183/NPPRJ-2016-31-01-p071-078

2.1. Experiments

Experimental pilot-scale trials are conducted at the PPC-UBC in which two RFS-type sensors are used to define bar forces over a wide range of refiner control parameters to characterize the magnitudes and distribution of normal and shear forces. This chapter presents the experimental facilities at the PPC, trial preparations, data acquisition system, and operating conditions. The design and frequency response of the sensors are discussed in Appendix B while the fabrication and calibration of the sensors are explained in Appendix C.

The Pulp and Paper Centre at UBC is equipped with an advanced LC refining pilot facility. The facility includes two tanks with the capacity of 4 m^3 each, a centrifugal pump, an AIKAWA 16-inch single-disc refiner with a 112 kW motor, and a variable frequency drive to power the refiner and to provide variable speed refining up to 1750 rpm. The refiner is instrumented with magnetic flow meters, pressure, and temperature sensors in the inlet and outlet of refiner. The refiner is equipped with a linear variable differential transformer to measure plate gap. The zero-point of plate gap is determined by bringing the plates together and calibrating before each trial. A schematic illustration of the UBC pilot LC refiner is shown in Figure 2-1.

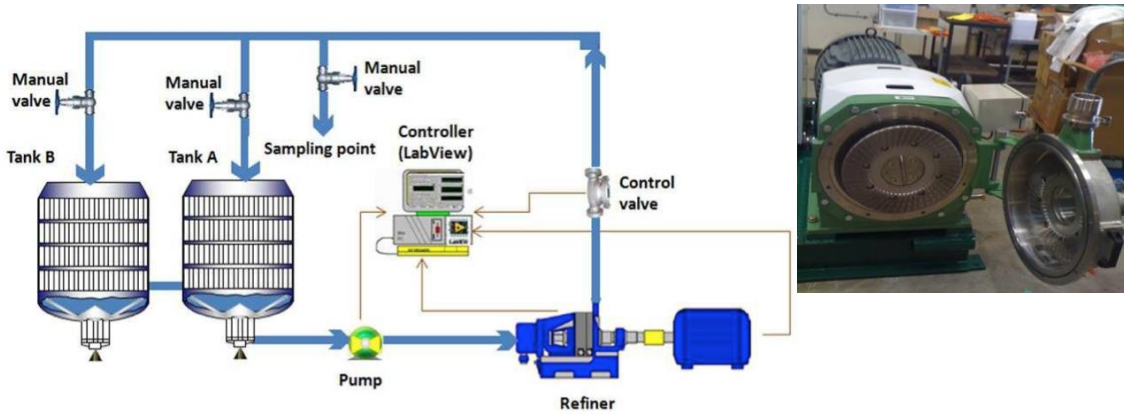

Figure 2-1. Illustration of the UBC pilot LC refiner [72].

The plate used in these trials is the AIKAWA FINEBAR®, which has bar edge length[13] (BEL) of 2.74 km/rev and bar angle of 15^0 from radial. The bar width, groove width, and groove depth of the plate are 1.6 mm, 3.2 mm, and 4.8 mm, respectively.

RFS-type sensors were custom designed and fabricated based on the design used in previous refiner trials [73]. The sensors include the probe that replaces a short length of the refiner bar (i.e. 5 mm), as shown in Appendix A, Figure 1. For these trials, two RFS-type sensors were used. RFS#1 measures shear force perpendicular to the major axis of the refiner bar while, for the first time, RFS#2 measures shear force parallel to the major axis of the refiner bar (Appendix A, Figure 2). The sensors also measure force normal to the plate surface (i.e. parallel to the axis of the refiner). A detailed description of the installation of the sensors and calibrations is presented in Appendix A.

In December 2014, commissioning trials were run and, based on the results, a number of improvements were applied and the first trials were planned. The set up and experiments of the first trials took place over the last week in February 2015 at Pulp and Paper Centre, UBC. The operating conditions are tabulated in Table 1, Appendix D.

The details of the data acquisition system, shown in Figure 2-2, are presented in Appendix A. A sampling rate of 150 kHz is used which is more than twenty times the maximum bar-passing frequency occurring during the trials.

[13] *Bar edge length (BEL)*: the total length of bar edges swept by bar-crossing during a single rotation of disc.

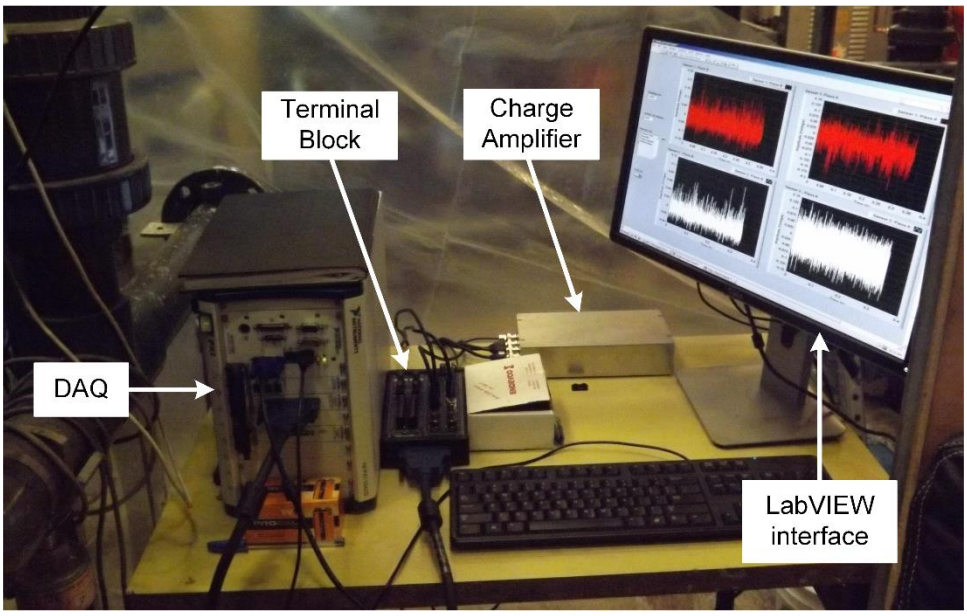

Figure 2-2. Data acquisition for refiner trials at Pulp and Paper Centre, UBC, Canada.

During the experiments, the flow rate was held constant at 250 liter/min while three different rotational speeds and a wide range of plate gaps were tested, as tabulated in Table 1, Appendix D. Mechanical SPF (spruce, pine and fir) softwood pulp with freeness starting at 378 ml CSF at 3.5% consistency was used in all trials. The procedure of recording signals and collecting pulp samples are explained in Appendix A.

Pulp samples were collected and the Fiber Quality Analyzer located at UBC Pulp and Paper Centre was used to assess the length-weighted fiber length. The length-weighted fiber length data, plate gap, and net power for three different rotational speeds are tabulated in Table 2, Appendix D.

Data analysis and the key findings of the trials are described in Sections 2.2 and 2.3, respectively.

2.2. Data Analysis

Based on data collected in the pilot-scale study, data analysis is carried out to investigate the relationship between plate gap, bar forces, and measured pulp properties. An algorithm was created in MATLAB to identify bar-passing events in the force data. A bar-passing event is defined to occur when the passage of a rotor bar over the sensor results in a maximum or peak value in the force data that exceeds a predefined threshold value. This threshold criterion is applied to eliminate data peaks associated with non bar-passing

events, including signal noise. This threshold value affects the number of bar-passing events detected by the algorithm.

Equation 7 calculates the maximum possible number of bar-passing events as follows:

$$\text{Number of bar-passing events} = N\ \omega\ t \tag{7}$$

where N is the number of the bars of the rotor crossing over the sensor for one revolution (N equals 144 for the plate with BEL=2.74 km/rev), ω is the rotational speed in radians per second, and t is the test duration.

The occurrence ratio is defined as the number of bar-passing events detected by the algorithm divided by the maximum possible number of bar-passing events. In this study, we assume that sufficient pulp is always present between the sensor and crossing refiner bars such that all of the bar-passing events are detected by the algorithm, then the occurrence ratio is 100%. An occurrence ratio of 95% was obtained in previous LC refiner bar-passing event's algorithm [66]. The algorithm of bar-passing event is described in Appendix A and is verified by manually scanning samples of the time domain data.

For each bar-passing event, the magnitudes of the peak normal and shear forces are determined as the difference between the force at the base of the preceding local valley and the following peak [9]. Distributions of these peak forces are determined for each operating condition, as in previous LC and HC refining trials [9,11]. These distributions allow comparison between refining conditions on the basis data taken throughout operation at each condition.

Each distribution is characterized using statistical values such as mean and median values. In this chapter, the sensor data are analyzed by investigating the mean values of peak normal and shear force distributions. The correlation between mean peak forces and measured pulp property, length-weighted fiber length, is analyzed.

2.3. Results and Discussion

The peaks appear in the shear and normal force data, highlighted by dashed rectangles in Figure 2-3, representing bar-passing events. The shape of each event depends on a number of factors including the amount and the properties of pulp located between the rotor and stator at the location of the sensor. The normal force peak values are much higher than their shear counterparts. For this plate, the bars of the rotor that cross over the force sensor

are grouped in three-bar clusters. Therefore, bar-passing events appear as clusters of three peaks.

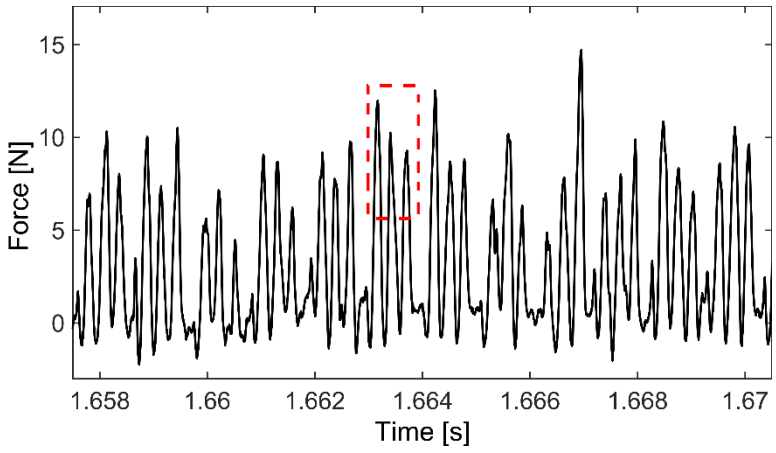

(a)

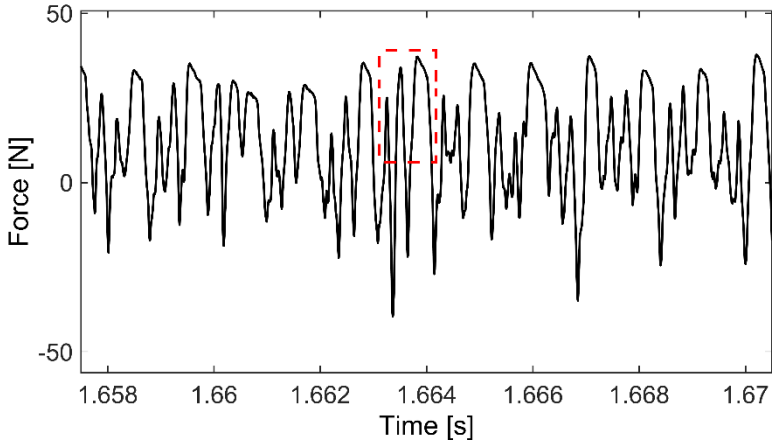

(b)

Figure 2-3. (a) Typical unfiltered shear force and (b) normal force at 1200 rpm and 0.25 mm plate gap.

Power spectra of the force sensor data are characterized by maxima at frequencies that correspond to the passage of individual bars and clusters of bars. The power spectrum of the normal force data at 1200 rpm, plate gap of 0.25 mm, shows four local maxima at frequencies of 3.82, 2.87, 1.90 and 0.95 kHz, Figure 2-4. These four local maxima, corresponded to the passage of individual bars and clusters of bars, are explained in detail in Appendix A.

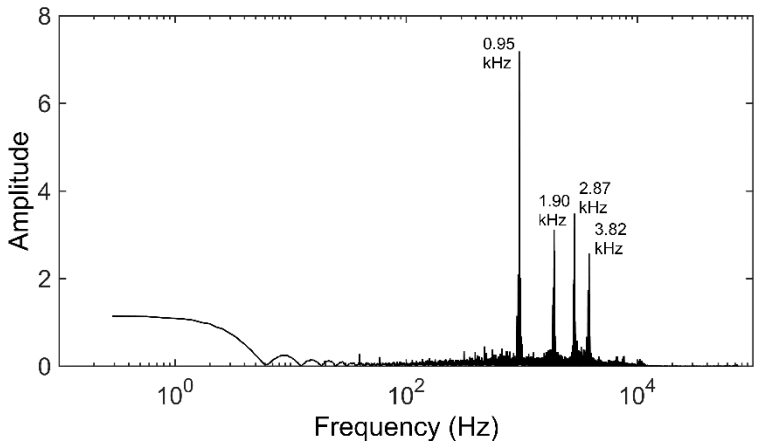

Figure 2-4. Spectrum of normal force at 1200 rpm and 0.25 mm plate gap.

The normalized distribution of peak normal force values indicates that when the plate gap is decreased, the median peak force increases, the peak normal forces tend to be clustered around a single value, and the spread of distribution is decreased. Normal distributions with a slight skew towards smaller force values for both peak normal and shear forces were found in a conical LC refiner for the SEL values of 0.33-0.5 J/m at 900 rpm refiner speed [9].

Moreover, as the plate gap decreases, the net refiner power increases. However, the effect of increasing the net power is more significant for the gap sizes of less than 0.5 mm. A linear relationship between the power and the inverse of the plate gap was reported by Mohlin et al. [24], Luukkonen et al. [3], Elahimehr et al. [34], and Nugroho [31]. The relation deviates from linearity for plate gaps smaller than the critical gap. The critical gap at which the transition from linearity to nonlinearity occurs is not apparent until the L_w is plotted versus the inverse of the plate gap.

However, as the plate gap is closed, length-weighted fiber length is unchanged until the plate gap reaches a critical gap, as highlighted in Figure 2-5 for the rotational speed of 1200 rpm. Below this point, the L_w decreases and the fiber cutting begins. Similar trends occur at 1000 pm and 800 rpm, Appendix A, Figure 9. However, the trend is not apparent at 1000 rpm due to the pulp shortage at the storage tank. Comparing the critical gaps for three rotational speeds shows that the critical gap decreases as the rotational speed decreases. The same trend has been reported in previous studies [3,31,34].

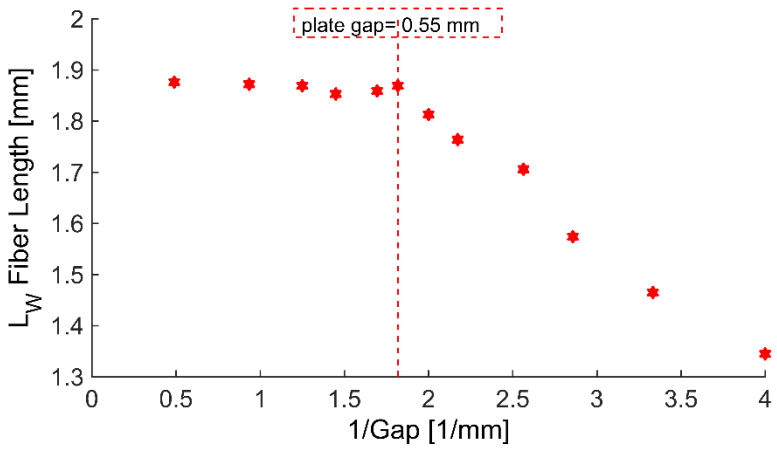

Figure 2-5. The L_w versus the inverse of plate gap for rotational speed of 1200 rpm.

The relationship between forces and fiber length is investigated by plotting length-weighted fiber length versus the mean peak normal and shear forces, as shown in Figure 2-6. As the plate gap is reduced, the L_w remains relatively constant and mean peak normal and shear forces increase up to the threshold values, highlighted by dashed lines, which corresponds to the critical gap. The threshold values of mean peak normal and shear forces are approximately 8 N and 2.4 N, respectively.

Note that only the results of RFS#2 are presented in this study since an anomaly in normal sensitivity was detected in post-trial calibration of RFS#1. This anomaly was found to be due to damage to sensor wires which occurred during installation into the refiner.

This study indicates that there is a non-linear relationship between measured bar forces and length-weighted fiber length that mirrors the established relationship between length-weighted fiber length and inverse plate gap. Moreover, the results of this study suggest that the RFS has a promising potential for in-process detection of the onset of fiber cutting. The investigation of the onset of fiber cutting using RFS data is studied in Chapter 3.

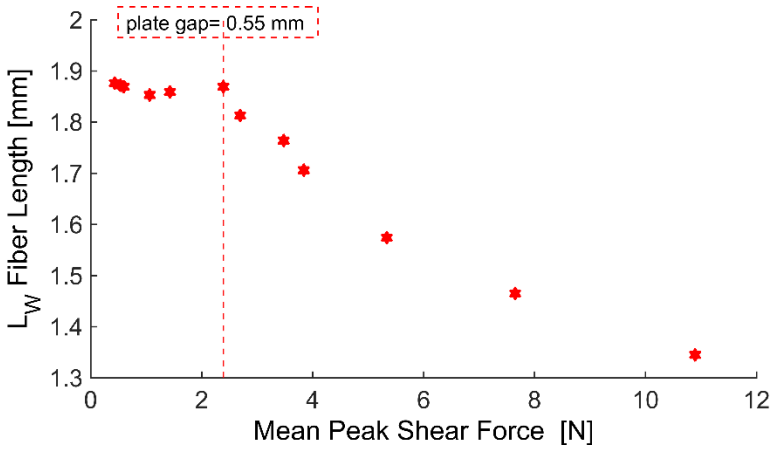

(a)

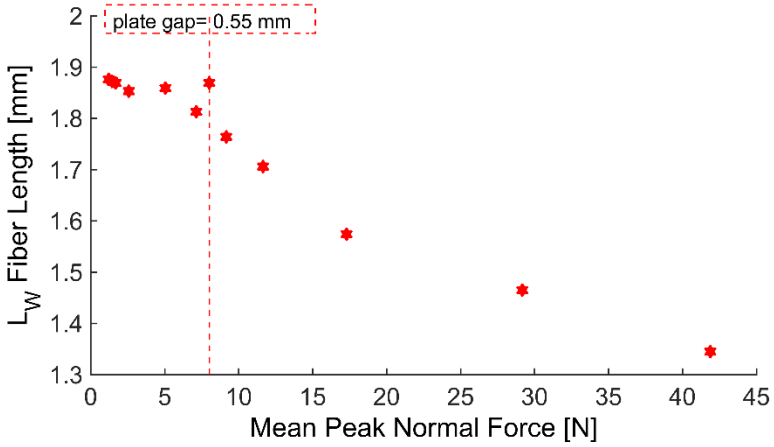

(b)

Figure 2-6. (a) The L_w versus mean peak shear and (b) normal force for rotational speed of 1200 rpm.

Chapter 3: In-process Detection of Fiber Cutting in Low Consistency Refining

The objective of the work presented in this chapter is to investigate in-process detection of the onset of fiber cutting by using custom-designed piezoelectric force sensors that measure real time shear and normal forces applied to pulp fibers by the refiner bars. This chapter was published in the TAPPI Journal, Appendix H.

Harirforoush, R., Olson, J., Wild, P. (2017): In-process detection of fiber cutting in low consistency refining based on measurement of forces on refiner bars. TAPPI Journal, 16(4), 189-199.

3.1. Experiments

Experimental trials are carried out at the PPC-UBC in which two RFS-type sensors are used to measure force normal to the plate surface (i.e., parallel to the axis of the refiner bar) and the shear force perpendicular to the major axis of the refiner bar (similar to RFS#1 in Chapter 2). This chapter presents trial preparations, data acquisition system, and operating conditions. The design, frequency response of the sensors, and fabrication and the calibration of the sensors are explained in Appendix B, and Appendix C.

For these trials, the AIKAWA FINEBAR® plate with BEL of 2.74 km/rev, the same plate employed in Chapter 2, is used. Bar angle, bar width, groove width, and groove depth of the plate are previously discussed in Section 2.1.

The sensors include a probe that replaces a short length of the refiner bar (i.e. 5 mm), as shown in Appendix H, Figure 1. The installation of the sensors in the stator plate and the calibration of the sensors are presented in Appendix H.

The data acquisition system, described in Appendix H, is similar to that described in Chapter 2. Mechanical SPF softwood pulp, produced at Quesnel River Pulp Mill, with 378 ml CSF at 2.5% and 3.5% consistency at rotational speeds of 800 rpm, 1000 rpm, and 1200 rpm was used in all trials. During the experiments, the flow rate was held constant at 250 liter/min. The operating conditions for the trials are tabulated in Table 3, Appendix D. The procedure of recording signals and collecting pulp samples are detailed explained in Appendix H.

At each operating condition, 2-liter pulp samples were collected, and the Fiber Quality Analyzer located at PPC-UBC measured the length-weighted fiber length, fine

percentage[14], curl index[15], and kink index[16]. The length-weighted fiber length, fine percentage, curl index, kink index, plate gap, and net power data for three different rotational speeds at 2.5% and 3.5% consistency are tabulated in Table 4, Appendix D.

Data analysis and the key findings of the trials are presented in Sections 3.2 and 3.3.

3.2. Data Analysis

Bar force sensor data collected in these trials are analyzed to assess indications of the onset of fiber cutting. Bar-passing events in the force data are detected based on an algorithm described in Appendix A. In this algorithm, the threshold values are set to identify all bar-passing events, i.e. an *occurrence ratio* of 100%.

The method for determination of mean peak normal and mean peak shear force is explained in Appendix H. The peak coefficient of friction is calculated by dividing the peak shear force by the peak normal force. The peak forces and peak coefficient of friction data are assessed in the form of distributions to which the two-parameter Weibull distribution function is fit. The Weibull distribution function is widely used because of its ability to characterize a wide variety of distributions, and it has been used in previous HC and LC refining studies [9,11]. The Weibull distribution function is shown in Equation 8 [77]:

$$f(x) = \frac{\beta}{\eta}\left(\frac{X-\gamma}{\eta}\right) exp^{-\left(\frac{x-\gamma}{\eta}\right)^{\beta}} \tag{8}$$

where β, η, and γ are shape, scale, and location parameters, respectively. The effect of changing the Weibull parameters on the Weibull distribution is explained in [66]. The two-parameter Weibull distribution function is obtained by setting $\gamma = 0$ in Equation 8. The location parameter, γ, is considered zero since both the peak normal and shear force distributions begin at zero.

For these trials, the Weibull scale and shape parameters of the peak normal force, peak shear force, and peak coefficient of friction distributions are calculated for each operating condition. Mean values of peak normal force, peak shear force, and peak coefficient of friction distributions are also determined.

---

[14] *Fine percentage*: the percentage of fines. This consists of particles measuring less than 0.2 mm in length.

[15] *Curl index*: defined as the $(1/f - 1)$, where f, the length factor, is the ratio of projected fiber length to real fiber length [74]. Curly fibers will lead to low tensile index, but it may also lead to high tear index [75].

[16] *Kink index*: a measure of fiber curvature. Pulp with a high kink index behaves as a shorter length pulp [76].

As the plate gap decreases, net power and the energy transferred to pulp fibers increases that appear as the change in the peak magnitude of forces as shown in Figure 3-1a and 3-2b. According to Parseval's theorem, explained by Equation 9, the sum (or integral) of the square of a signal is equal to the sum of the square of its transform in the frequency domain. This theory implies that the total energy of a signal (i.e. $x(t)$) over time must be equal to the total energy of this signal over all frequencies:

$$\int_{-\infty}^{+\infty}(x(t))^2\,dt = \frac{1}{2\pi}\int_{-\infty}^{+\infty}(\mathrm{X}(\omega))^2\,d\omega \qquad (9)$$

where $\mathrm{X}(\omega)$ represents the continuous Fourier transform of $x(t)$ and ω is the frequency in radians per second.

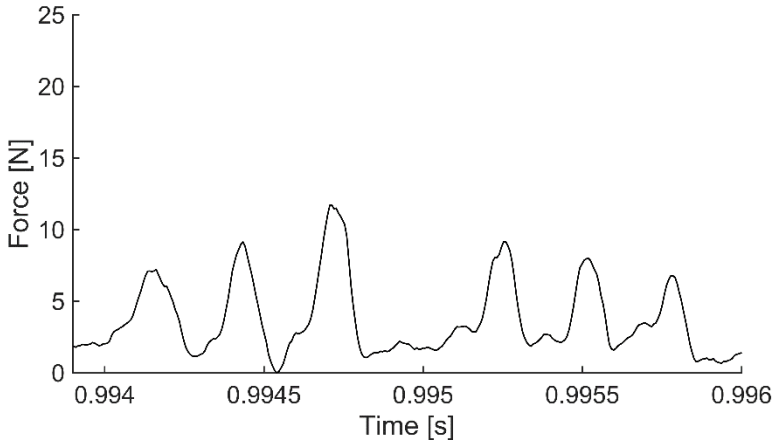

(a)

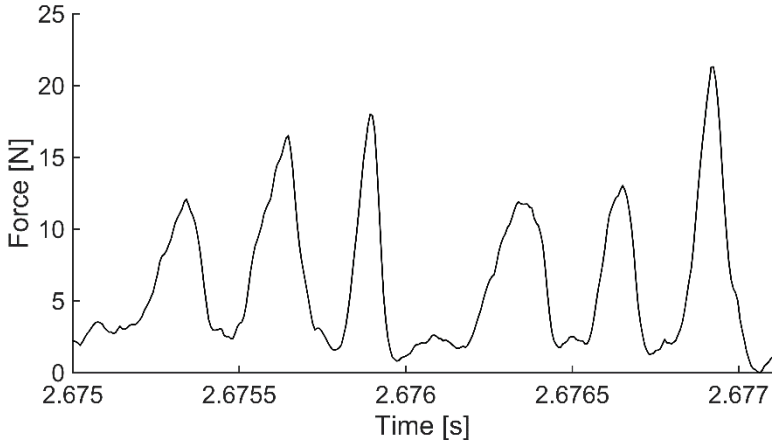

(b)

Figure 3-1. Typical unfiltered normal force data of mechanical SPF softwood pulp, 378 ml CSF, at 1200 rpm (a) 0.55 mm plate gap, and (b) 0.45 mm plate gap.

Based on this theory, the change in peak magnitude of forces will results in change in the amplitude of the spectrum at the bar-passing frequencies. As stated earlier, in Section 2.3, the frequency spectrum of bar force data shows four local maxima at frequencies of 3.82, 2.87, 1.90 and 0.95 kHz, Appendix A, Figure 6. The highest amplitude maximum corresponds to the passage, over the stator bar in which the sensor is located, of equivalent edges of three-bar clusters on the rotor, for all of the operating conditions. The amplitude of this frequency, referred to here as the *dominant frequency*, increases as the plate gap decreases, as showed in Appendix H, Figure 11. To find the transition in the spectrum analysis of the force data, the magnitude of the dominant frequency is determined at each operating condition and is plotted versus the plate gap.

3.3. Results and Discussion

The net power increases as the plate gap decreases, as previously described in Chapter 2. At a constant rotational speed (i.e. 1200 rpm), the net power for two different consistencies, 3.5% and 2.5%, are approximately equal.

The relation between length-weighted fiber length and the inverse of the plate gap, Appendix H, Figure 3, shows that the L_w remains relatively constant as the plate gap reduces until the plate gap reaches the critical values, critical gaps. This trend is consistent with the result shown in Figure 2-5. Similar to the results found in Chapter 2, the critical gaps influenced by the rotational speed. Increasing the rotational speed increases the critical gaps. At the same rotational speed, decreasing the consistency slightly increases the critical gap which is not consistent with Lundin [30] who found that decreasing the consistency decreases the critical gap.

The unfiltered normal force profile, shown in Appendix H, Figure 4, shows the cluster of three peaks that is in accordance with crossing the rotor bars over the sensor grouped in three-bar clusters, and is in agreement with the Figure 2-3. However, the magnitude of the peaks of bar-passing events are different which may be related to an uneven distribution of pulp captured between rotor and the probe of the sensor.

As the plate gap is reduced, the mean value of the peak force distribution increases, the distributions are extended to the right, its height decreases, and the shape of the distribution changes from positively skewed to an approximately normal distribution.

Moreover, transitions are seen in the relation between L_w and mean peak normal and shear forces, Figure 3-2 which is consistent with the trend seen in Figure 2-6. As the plate gap decreases, the length-weighted fiber length remains relatively unchanged and mean peak forces increase up to the threshold values that correspond to the critical gaps. The L_w value decreases in an approximately linear manner beyond the critical gap threshold. The threshold values are relatively independent of rotational speed at 3.5% consistency and the values are 7 N and 3.8 N for mean peak normal and shear force, respectively. We found that decreasing the consistency from 3.5% to 2.5% slightly increases the threshold value for mean peak normal force.

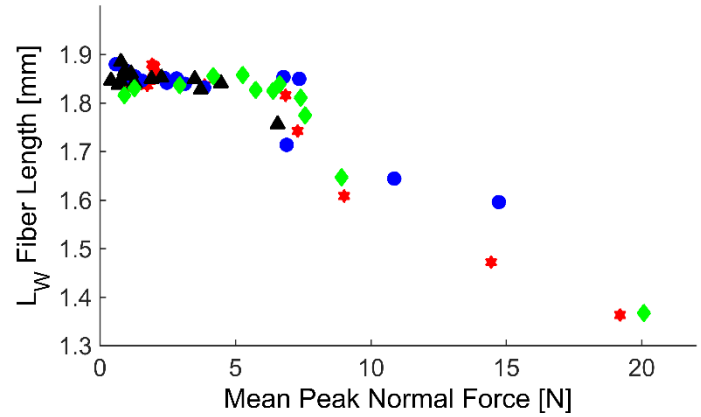

(a)

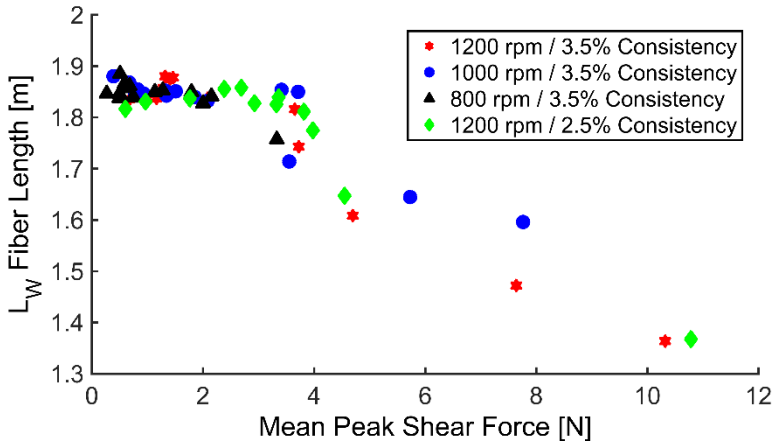

(b)

Figure 3-2. L_w versus mean peak (a) normal and (b) shear force for three rotational speeds (i.e., 1200 rpm, 1000 rpm, and 800 rpm) at 3.5% consistency. Data is also shown for 1200 rpm at 2.5% consistency.

A distinct transition occurs in the relation between L_w and the values of the Weibull scale parameter of the peak force distribution, as shown in Figure 3-3, for data taken at 1200 rpm, that consistently corresponds to the onset of fiber cutting. The position of this transition, highlighted by the dashed line, corresponds to the transition in the plot of L_w versus the inverse of plate gap.

The transition seen in Figure 3-3 also appears in the relation between the Weibull scale parameter of peak normal force distribution and plate gap, and this transition corresponds to the onset of fiber cutting. The plot is not shown here in the interest of brevity but is depicted in Appendix H, Figure 7.

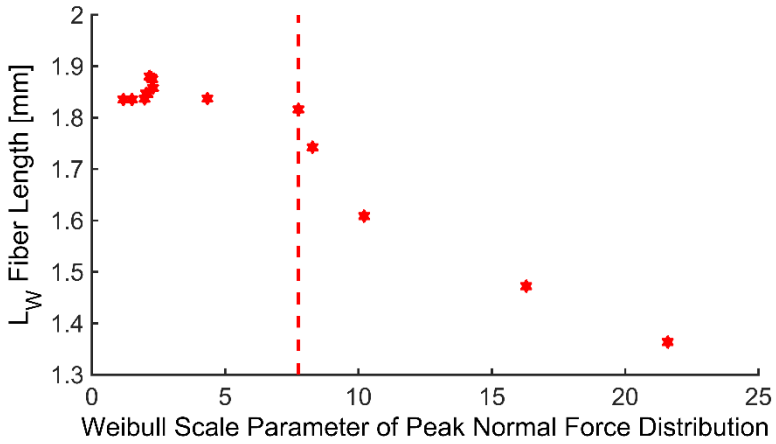

Figure 3-3. L_w versus the Weibull scale parameter of peak normal force distribution for rotational speed of 1200 rpm at 3.5% consistency.

A transition occurs in the relation between the magnitude of the dominant frequency and the plate gap at 1200 rpm at 3.5% consistency, as shown in Figure 3-4. The magnitude remains relatively constant while the plate gap is decreased up to a threshold value that corresponds to the onset of fiber cutting. The transition may be due to a fundamental change in the mode of energy transfer to the pulp at the onset of fiber cutting.

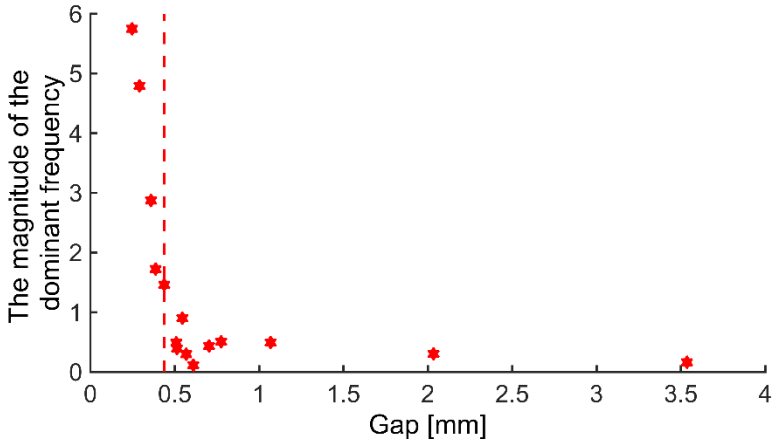

Figure 3-4. The magnitude of the dominant frequency versus the plate gap for the rotational speed of 1200 rpm.

Similar trends seen in Figures 3-3 and 3-4 also occur in the data for the rotational speeds of 1000 rpm and 800 rpm at 3.5% consistency and 1200 rpm at 2.5% consistency, as shown in Appendix H, Figures 8 and 12. These trends are less definitive in the data taken at 800 rpm. At this speed, the pulp flow rate was observed to be unstable which may reflect unstable conditions in the refiner and may also be the cause of anomalous data.

The mean coefficient of friction decreases as the plate gap is reduced, Appendix H, Figure 9b. This finding is in agreement with Siadat [63] and Senger et al. [78] who showed that in HC refining at the consistency of 20%, the coefficient of friction decreases with decreasing plate gap at a given rotational speed.

In a separate analysis, we investigated the correlation between measured pulp properties (i.e. length-weighted fiber length, fine percentage, curl index, and kink index) and bar forces [79]. We found that distinct transitions in the indications of the onset of fiber cutting are only seen in the relation of L_w and mean peak force, and Weibull scale parameter. No correlation has been found in the relation between fine percentage, curl index, kink index and bar forces.

In conclusion, the time domain analysis of data from these trials show that the mean peak normal and shear forces, the Weibull scale parameter of peak force distributions are promising candidates for in-process detection of fiber cutting. The magnitude of the dominant frequency identified in the frequency domain analysis also provides an indication of the onset of fiber cutting. Detection of the onset of fiber cutting conditions is potentially beneficial in low consistency refining as part of a control system to reduce fiber cutting,

optimize fiber quality improvements by operating at gaps just wider than the critical gap, avoid decreasing the strength properties of paper, and increase energy efficiency.

The data presented in this chapter are based solely on data taken with mechanical SPF softwood pulp. Further investigation is needed to determine whether or not these fiber cutting metrics can be extended to different pulp furnishes and operating conditions. This investigation is the subject of Chapter 4.

Chapter 4: The Effect of Pulp Furnish on Bar Forces and on Indications of the Onset of Fiber Cutting

The objective of this chapter is to understand the effect of pulp furnish on measured bar forces. Moreover, the effect of pulp furnish on the detection of fiber cutting is investigated. This chapter is recently published in Nordic Pulp and Paper Research Journal, Appendix I.

Harirforoush, R., Olson, J., Wild, P. (2018): Indications of the onset of fiber cutting in low consistency refining using a refiner force sensor: the effect of pulp furnish. Nordic Pulp and Paper Research Journal, 33 (1).

4.1. Experiments

Experimental trials are performed at the Pulp and Paper Centre, UBC, using two RFS-type sensors to measure forces normal to the plate surface (i.e., parallel to the axis of the refiner bar) and the shear force perpendicular to the major axis of the refiner bar (similar to RFS#1 in Chapter 2). This chapter presents trial preparations, data acquisition system, and operating conditions. The design, frequency response of the sensors, fabrication and the calibration of the sensors are explained in Appendix B, and Appendix C, respectively.

The plate, BEL=2.74 km/rev, used in Chapter 2, and 3 is also employed for these trials. Bar angle, bar width, groove width, and groove depth of the plate are described in Section 2.1. The sensors include the probe that replaces a short length of the refiner bar (i.e. 5 mm), as shown in Appendix I, Figure 1. The installation of the sensors in the stator plate is detailed presented in Appendix I. The set up and experiments of the third trials were planned in August 2016 at PPC-UBC.

The data acquisition system, described in Appendix I, is similar to Chapter 2 and 3. Trials are conducted with four different pulp furnishes: hemlock/balsam softwood thermomechanical (TMP) pulp (240 ml CSF), SPF softwood TMP pulp (630 ml CSF), northern bleached softwood kraft (NBSK) pulp (700 ml CSF), and aspen hardwood TMP pulp (500 ml CSF) at 3.0 to 3.5% consistency at rotational speeds of 1200 and 1400 rpm. During the experiments, the flow rate was held constant at 250 liter/min. The operating conditions for the trials are tabulated in Table 5, Appendix D. The procedure of recording signals and collecting pulp samples are detailed described in Appendix I.

All pulp samples were collected and measured for length-weighted fiber length (L_w) using a Fiber Quality Analyzer, and freeness (using TAPPI standard T227). Handsheets were made and paper properties of bulk, tear index and tensile index (using TAPPI standard T220) were measured at PPC-UBC. The length-weighted fiber length, freeness, tear index, tensile index, plate gap, and net power data for different operating conditions are tabulated in Table 6, Appendix D.

Data analysis and the key findings of the trials are presented in Sections 4.2 and 4.3.

4.2. Data Analysis

Bar force sensor data are analyzed to investigate the effect of pulp furnish on measured bar forces and on the detection of the onset of fiber cutting. The algorithm for the detection of bar-passing events in the force data is described in Appendix A. As stated earlier, peak forces are defined as the difference between the force at the base of the local valley that precedes the peak and the force at the peak.

The critical gaps, highlighted as dashed lines in Appendix I, Figure 3, is identified based on fiber length data and Equations 10 and 11:

$$\frac{(L_w)_{i+1}-(L_w)_i}{(L_w)_i} < -2\% \qquad i = 1, \dots, n-1 \tag{10}$$

$$\begin{Bmatrix} (L_w)_{i+2} - (L_w)_{i+1} < 0 \\ (L_w)_{i+3} - (L_w)_{i+2} < 0 \\ (L_w)_{i+4} - (L_w)_{i+3} < 0 \end{Bmatrix} \tag{11}$$

In these Equations, L_w, is the length-weighted fiber length, *i*, is the index of data point, and *n* is the total number of data points at each trial. The data point index, *i*, ascends as the gap is closed. When the conditions presented in Equations 10 and 11 are both satisfied, then fiber cutting is determined to have begun.

Note that this algorithm of the detection of the critical gap has not been used in Chapters 2 and 3. However, our analysis shows that the critical gaps previously found in the results of Chapters 2 and 3 are consistent with the critical gaps determined based on Equation 10 and 11.

The average "*power*" (*P*) of a time domain signal $x(t)$ is defined as the sum of absolute squares of time-domain samples divided by the signal length, and defined by Equation 12 [80]:

$$P = \lim_{T\to\infty} \frac{1}{2T} \int_{-T}^{T} (x(t))^2 dt \quad (12)$$

where *T* is the signal length. Note that this term is not equal to the mechanical power that is dissipated on the sensor probe. Rather this is a signal processing term which is equivalent to the square of RMS (root-mean-square) magnitude of a signal.

As the plate gap is closed, the value of the power of normal force signals changes, as depicted in Figure 4-1. In this study, the power of the normal force signals and the shear force signals are calculated at each operating condition and plotted versus the plate gap. The transition in the relation between the power of the normal force signal and the plate gap, referred to here as *transition gap* is identified when the conditions shown in Equations 13 and 14 are satisfied:

$$\Delta_j = (P_{norm})_{j+1} - (P_{norm})_j > 0.01 \qquad j = 1, \dots, n-1 \quad (13)$$

$$\begin{Bmatrix} \Delta_{j+1} > 0.01 \\ \Delta_{j+2} > 0.01 \end{Bmatrix} \quad (14)$$

where $(P_{norm})_j$ is the normalized power of normal force and is defined by Equation 15:

$$(P_{norm})_j = \frac{P_j - \min(P_1 \dots P_i)}{\max(P_1 \dots P_i) - \min(P_1 \dots P_i)} \qquad i = 1, \dots, n-1 \quad (15)$$

In these Equations, P_j is the power of normal force signal, *i* and *j* are the indexes of data point and *n* is the total number of data points at each trial. This transition point is indicated by blue dotted lines in Appendix I, Figure 4 for different pulp furnish.

For these trials, the mean peak normal and shear force, the mean of coefficient of friction, and the Weibull scale parameter of peak force distributions are calculated at each operating condition.

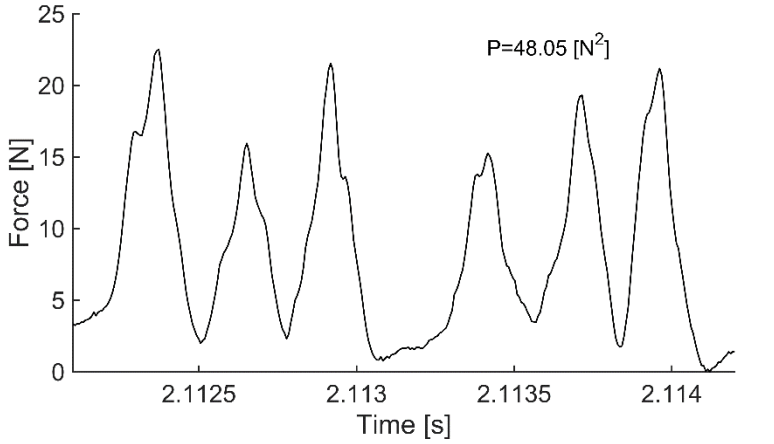

(a)

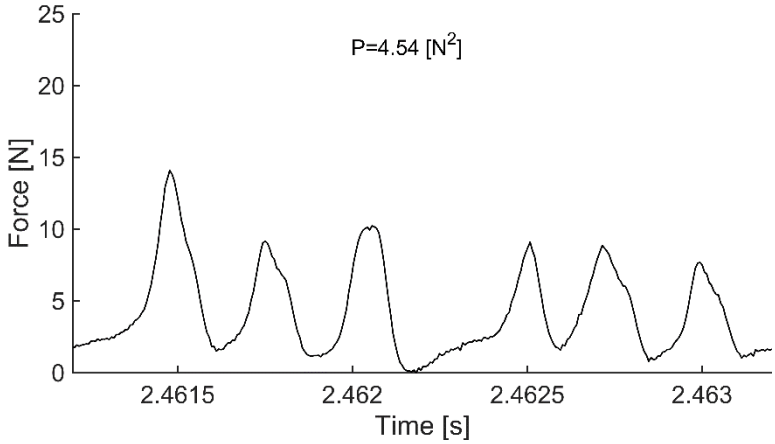

(b)

Figure 4-1. Typical unfiltered normal force profile data and the value of power of normal force *(P)* for hemlock/balsam softwood TMP at 1200 rpm at (a) 0.3 mm plate gap and (b) 0.55 mm plate gap.

4.3. Results and Discussion

Similar to the trends seen in Chapters 2 and 3, the net power increases as the plate gap is reduced. At the same plate gap, more energy is transferred to softwood pulp than to hardwood pulp.

The relation between the length-weighted fiber length and the inverse of the plate gap, is in agreement with the results of [81,82] and is similar to the trend shown in Figure 2-5. The critical gaps, except for NBSK pulp, are determined based on an algorithm described in Equations 10 and 11. During the NBSK pulp trials, the flow rate was unstable, and this is thought to be the cause of the anomalous data. The critical gaps depend on both pulp

furnishes and rotational speed and they happen at different SEL values. In addition, the SEL at the onset of fiber cutting for softwood pulp is higher than the hardwood pulp. For example, the SEL at the onset of fiber cutting is 0.42 J/m for SPF softwood TMP while it is 0.12 J/m for aspen hardwood TMP.

A distinct transition gap, based on the algorithm expressed in Equations 13-14, occurs in the relation between the power of normal force and the plate gap. The power of normal force is relatively constant down to a gap, highlighted by the blue dotted line, at which there is a transition below which the power increases sharply, as shown in Figure 4-2 for hemlock/balsam SW TMP. There is an agreement between the transition gap and the critical gap, highlighted by the dashed line and detected based on fiber length data (Equations 10-11). This power of normal force consistently identifies the critical gaps for all pulp furnishes except the NBSK pulp, Appendix I, Figure 4. The instability of flow rate during NBSK pulp trials may be the cause of the anomalous data for this pulp.

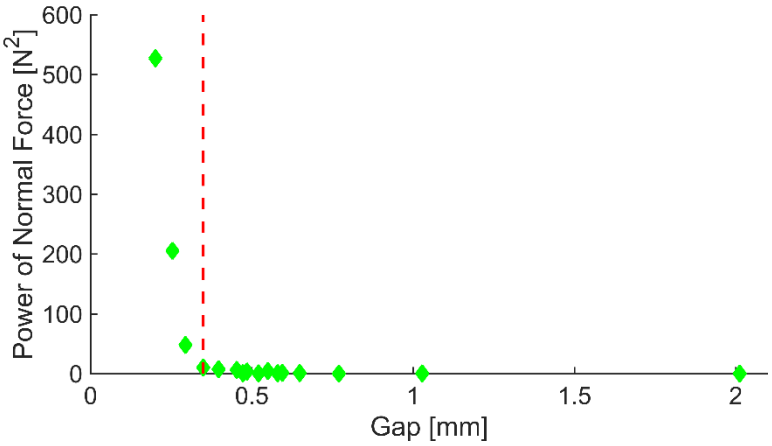

Figure 4-2. Power of normal force versus plate gap for hemlock/balsam SW TMP at 1200 rpm.

A substantial reduction of freeness occurs for the plates gaps smaller than the critical gap, which is consistent with the results of [33, 40]. The relation between handsheet properties, tear index and tensile index, and the inverse of the plate gap, shown in Appendix I, Figure 5, indicates that tear index is relatively constant as the plate gap is decreased until the critical gap. After the critical gap, fibers start to cut and tear index drops significantly. However, the trend is different for hardwood pulp. The increasing of tensile index with decreasing tear index is in agreement with the results of [3].

The results also show that the mean peak normal and shear force at the onset of fiber cutting depend on pulp furnish. At the onset of fiber cutting, the mean peak normal force of softwood pulp (9 N) is much higher than for the hardwood pulp (3 N), Appendix I, Figure 6. However, the mean peak shear force for hardwood and softwood pulps at the onset of fiber cutting are approximately equivalent, 1.4 N, Appendix I, Figure 7.

Kerekes and Senger [68] estimated that, for low consistency refining, the normal force on a fiber is proportional to fiber length taken to the power of 3/2 and uncompressed fiber diameter, as explained in Equation 2. Hardwood and softwood fibres have different typical geometries (e.g. SW fibers are longer than HW fibers). This results in different normal force on a fiber, different level of compressive strain in fibers, and different normal force at the onset of fiber cutting.

However, as stated in Chapter 1, Equation 4, the shear force is comprised of a corner or ploughing force at the bar edge and a friction force on the axial-facing bar surface. Due to the dissimilar geometries of hardwood and softwood fibers, we expect that the magnitudes of the corner force and the friction force for hardwood pulp will be different from those of the softwood pulp. However, this data shows that, in these trials, the sum of these forces is approximately equal for hardwood and softwood pulps at the onset of fiber cutting.

The result also shows that the mean coefficient of friction decreases as the plate gap is closed, Figure 4-3a. However, the trend is different for hardwood pulp, Figure 4-3b. The mean coefficient of friction increases up to the plate gap of 0.65 mm, and decreases beyond this point. At the same plate gap, the mean coefficient of friction is relatively constant at two different rotational speeds. In this study, we also found that the mean coefficient of friction at the onset of fiber cutting depends on pulp furnish. At 1200 rpm, the mean coefficient of friction is 0.22, 0.54, 0.41, and 0.49 for hemlock/balsam SW TMP, SPF SW TMP, NBSK, and aspen HW TMP, respectively.

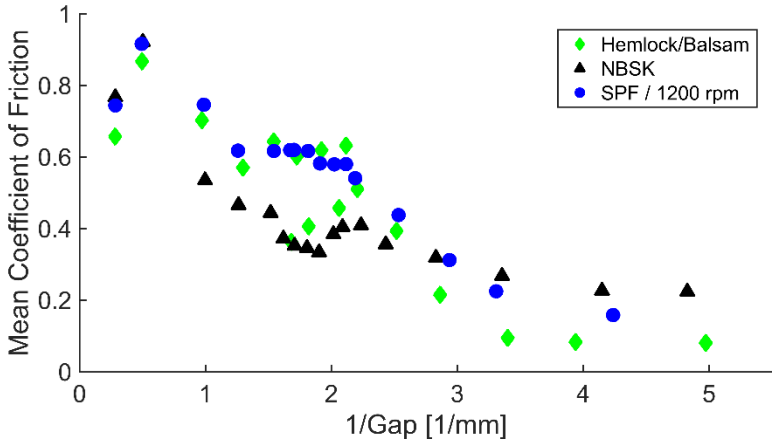

(a)

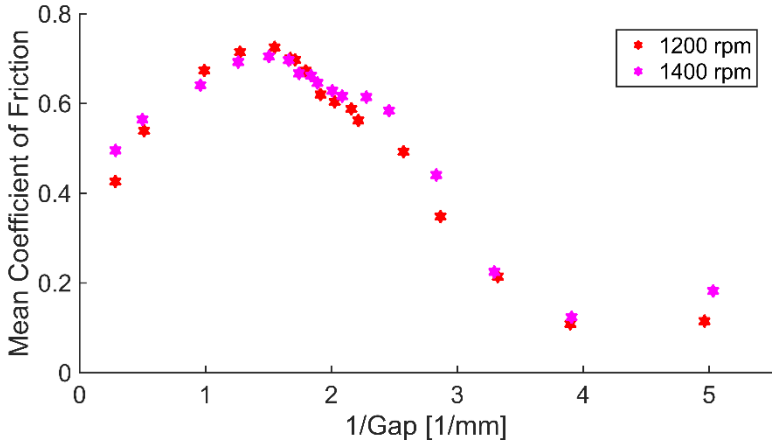

(b)

Figure 4-3. Mean coefficient of friction versus the inverse of plate gap for (a) hemlock/balsam SW TMP, SPF SWTMP, NBSK, and (b) aspen HW TMP.

In summary, in this study, distinct transitions occur in the plot of the power of time domain signal of measured normal force versus plate gap which consistently identifies the critical gap, as determined by fibre length data. This indication is a sensitive and reliable metric for in-process detection of fiber cutting for all tested pulp furnishes. This method is independent of the algorithm used for detection of bar-passing events. In addition, it is shown that the onset of fiber cutting, mean peak normal and shear forces and the mean coefficient of friction all depend on pulp furnishes.

The indications of the onset of fiber cutting, presented in Chapters 3-4, are based on trials with the plate having BEL=2.74 k/rev. Further investigation is required to determine whether or not the fiber cutting metrics identified here can be used for different plate patterns, operating conditions and pulp furnishes. This work is presented in Chapter 5.

Chapter 5: The Effect of Plate Pattern on Bar Forces and on Indications of the Onset of Fiber Cutting

To reduce fiber cutting, one approach is to use a plate pattern with narrower bars and grooves which provides lower intensity treatments [3]. However, the effect of plate pattern on the relationship between refiner operating conditions, measured bar forces, and resulting pulp properties is not well understood. The objective of the work presented in this chapter is to assess the effect of plate pattern on measured bar forces and on the detection of fiber cutting. The manuscript on which this chapter is based is under review by Nordic Pulp and Paper Research Journal, Appendix J.

Harirforoush, R., Olson, J., Wild, P. (2017): Bar force measurement in low consistency refining: the effect of plate pattern. Under Review, Nordic Pulp and Paper Research Journal.

5.1. Experiments

Experimental trials are carried out at the PPC-UBC using two RFS-type sensors to measure force normal to the plate surface (i.e., parallel to the axis of the refiner bar) and the shear force normal to the bar edge and in the plane of the refiner plate (similar to RFS#1 in Chapter 2). This chapter presents trial preparations, data acquisition system, and operating conditions. The design, frequency response of the sensors, fabrication and the calibration of the sensors are described in Appendix B, and Appendix C.

The plate used in this chapter is manufactured by AIKAWA FINEBAR®, and has a bar edge length of 5.59 km/rev and bar angle of 15º from radial. The bar width, groove width, and groove depth of the plate are 1 mm, 2.4 mm, and 4.8 mm, respectively.

To compare the bar force results of the plate patterns with BEL=2.74 km/rev and BEL=5.59 km/rev, the RFS sensors are installed at the same radial position of the sensors previously accommodated in the plate with BEL=2.74 km/rev to avoid the effect of radial position on bar forces. The sensors are positioned in the second bar of a four-bar cluster. At this position, 192 bars on the rotor, grouped into 48 four-bar clusters, cross over the sensor in one revolution of the rotor.

The sensors include a probe that replaces a short length of the refiner bar (i.e. 5 mm), as shown in Appendix J, Figure 1. The installation of the sensors in the stator plate is presented in Appendix J.

The data acquisition system, as described in Appendix J, is similar to the system used for the work described in Chapters 2 to 4. However, the ratio of the first natural frequency of the sensor to the maximum bar-passing frequency is approximately 4, compared to a ratio of 8.2 for the plate with BEL=2.74 km/rev. The data for these trials show that this ratio provides an adequate margin above the bar-passing frequency.

Three different pulp furnishes, SPF softwood TMP pulp (666 ml CSF and 456 ml CSF), NBSK pulp (686 ml CSF), and aspen hardwood TMP pulp (566 ml CSF) at 3.3 to 3.6% consistency at rotational speeds of 1200 and 1400 were used in these trials. During the experiments, the flow rate was held constant at 250 liter/min. The operating conditions for the trials are tabulated in Table 7, Appendix D. The procedure of recording signals and collecting pulp samples are detailed explained in Appendix J.

All pulp samples were collected and measured for length-weighted fiber length (L_w) using a Fiber Quality Analyzer, and freeness (using TAPPI standard T227) at PPC-UBC. Handsheets were made and paper properties of bulk, tear index and tensile index (using TAPPI standard T220) were measured at PPC-UBC. The length-weighted fiber length, freeness, tear index, tensile index, plate gap, and net power data for different operating conditions are tabulated in Table 8, Appendix D.

Data analysis and the key findings of the trials are presented in Sections 5.2 and 5.3.

5.2. Data Analysis

Bar force sensor data are analyzed to investigate the effect of plate pattern on measured bar forces and on the detection of the onset of fiber cutting. The algorithm of the detection of bar-passing events in the force data is described in Appendix A. As stated earlier, peak forces are defined as the difference between the force at the base of the local valley that precedes the peak and the force at the peak.

The critical gaps are identified based on fiber length data and the algorithm explained in Chapter 4, Section 4.2, Equations 10-11. The transition in the relation between the power of the normal force signal and the plate gap, *transition gap*, is determined based on the algorithm described in Chapter 4, Section 4.2, Equations 13-15.

For these trials, the mean peak normal and shear force, the mean coefficient of friction, the Weibull scale parameter of peak force distributions, and the power of the normal force signal are calculated at each operating condition. Moreover, the normal and shear stresses are calculated by dividing the peak normal and shear forces by the area of the "top" of the sensor probe, i.e., the product of bar width and probe length, respectively. The bar forces and stresses are compared with the results for the trials with the plate having BEL=2.74 km/rev.

5.3. Results and Discussion

Typical unfiltered normal and shear force data, taken at 1200 rpm and a plate gap of 0.15 mm, for aspen HW TMP is shown in Figure 5-1. Bar-passing events appear as clusters of four peaks because the bars of the rotor that cross over the force sensor are grouped in four-bar clusters.

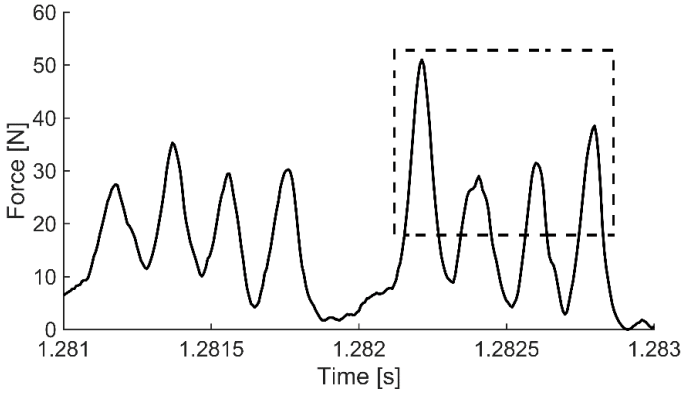

(a)

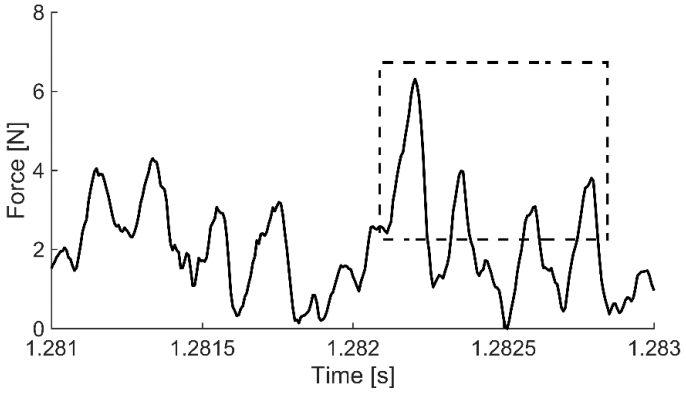

(b)

Figure 5-1. Typical unfiltered (a) normal force and (b) shear force at 1200 rpm and 0.15 mm plate gap for aspen HW TMP.

The relation between specific refining energy (SRE), defined as the ratio of the net power to the mass of the flow rate of fibers, and the inverse of plate gap is shown in Figure 5-2. At the same plate gap and pulp furnish, the energy transferred to pulp fibers is relatively equivalent for two plate patterns. Moreover, for all plate gaps, more energy is transferred to SW pulp than to HW pulp, which is consistent with the results for the plate with BEL=2.74 km/rev described in Chapter 4.

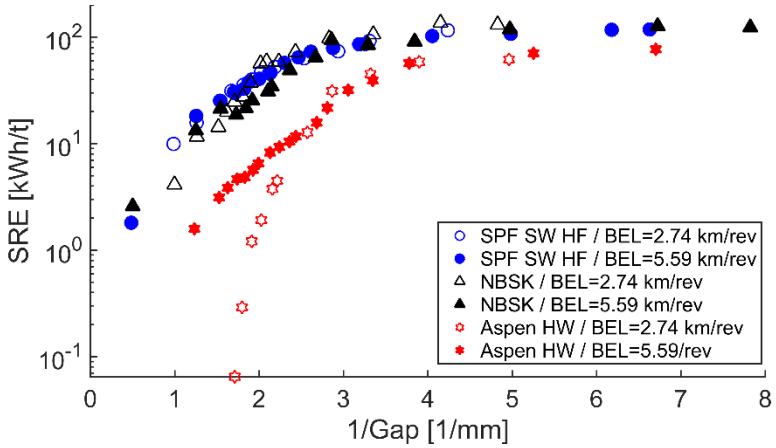

Figure 5-2. Specific refining energy versus the inverse of plate gap for SPF SW HF TMP (circle),NBSK (triangle), and aspen HW TMP (hexagon) at 1200 rpm for the plates of BEL =5.59 km/rev and BEL=2.74 km/rev.

The relation between length-weighted fiber length and the inverse of plate gap is shown in Appendix J, Figure 5. The results are similar to the trend seen in Figure 2-5. L_w remains relatively constant as the plate gap is reduced until the plate gap reaches the critical gap which is determined based on fiber length data using the algorithm described in Equations 10-11. Beyond this point, L_w decreases in an approximately linear manner. The trend is in agreement with the results of [81,82]. Comparing the critical gap values of the plates of BEL=5.59 km/rev and BEL=2.74 km/rev shows that for the same pulp furnish, the critical gap decreases with the plate pattern having higher BEL. However, this is more considerable for NBSK pulp. In addition, for the plate with BEL=5.59 km/rev, the critical gaps happen at different SEL values which is consistent with the results of the plate with BEL=2.74 km/rev. At the critical gaps, the SEL value of SW pulp is much higher than that of the HW pulp.

As shown in the relation between freeness versus the inverse of plate gap in Appendix J, Figure 6, freeness changes with decreasing plate gap which is in accordance with the results of [3,39] that showed the changes of freeness with SRE. For SW pulp, at the same gap, the freeness is relatively constant for the plate patterns of BEL=5.59 km/rev and BEL=2.74 km/rev. However, for HW pulp, at the same gap, the freeness slightly increases with the plate having higher BEL. The trend seen in the relationship between the tear index and tensile index versus the inverse of plate gap for the plate with BEL=5.59 km/rev is similar to the plate with BEL=2.74 km /rev.

For tested pulp furnishes and at all plate gaps, the plate with higher BEL, which has smaller bar width and groove width, results in lower mean peak normal force, Figure 5-3. However, this is less definitive for NBSK pulp. A similar result was found for mean peak shear force data when it is plotted versus the inverse of plate gap, Appendix J, Figure 8.

SRE is the product of the number of impacts per unit mass of the pulp and the intensity of each impact [83]. The number of impacts per unit mass of pulp is higher for the plate pattern with higher BEL. In one revolution, the number of rotor bars cross over the sensor for the plate with BEL=5.59 km/rev and the plate with BEL=2.74 km/rev are 192 and 144, respectively. As shown in Figure 5-2, at the same plate gap and pulp furnish, the SRE for the two plates are approximately equivalent. So, we expect that the intensity of the plate with BEL=2.74 km/rev is higher than that of the plate with BEL=5.59 km/rev. Decreasing intensity by increasing BEL is consistent with our results that show higher BEL plate results in lower mean peak forces.

This study also shows that the mean peak normal and shear force at the onset of fiber cutting depend on pulp furnish and plate pattern and that these parameters are lower for the higher BEL plate, as shown in Table 2, Appendix J. At the onset of fiber cutting, the mean peak normal force of the SW pulp is higher than for the HW pulp which is in agreement with the results of the plate with BEL=2.74 km/rev. However, the difference between mean peak normal force at the onset of fiber cutting for two plate patterns is more significant for SW pulp than HW pulp.

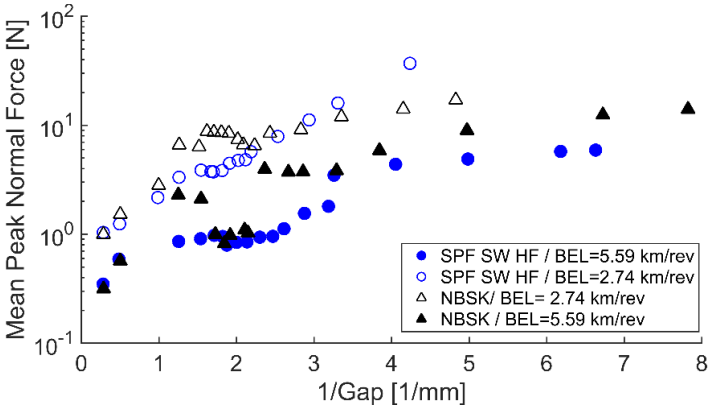

(a)

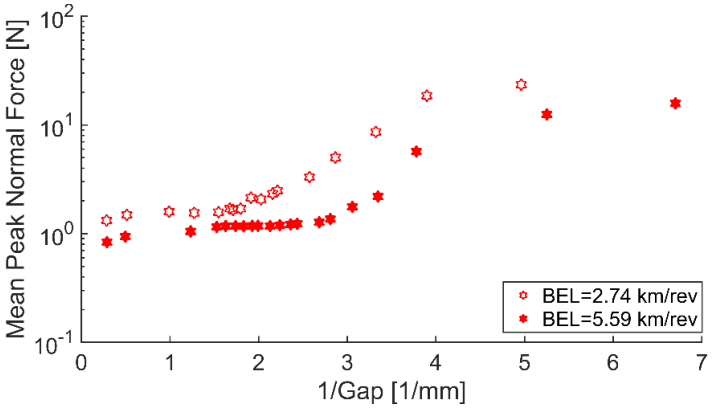

(b)

Figure 5-3. Mean peak normal force versus the inverse of plate gap for (a) SPF SW HF TMP, NBSK, and (b) aspen HW TMP at 1200 rpm for the plates of BEL =5.59 km/rev and BEL=2.74 km/rev.

For the plate with BEL=5.59 km/rev, the mean peak shear force at the onset of fiber cutting is different for HW and SW. This is not in agreement with the results of the plate with BEL=2.74 km/rev. We hypothesize that the relative magnitudes of two components of shear force including a corner or ploughing force, at the bar edge, and a friction force, on the axial-facing bar surface, differ for these two plates. For the plate with BEL=2.74 km/rev, these two forces vary such that their sum is approximately equivalent for HW and SW pulps, at the onset of fiber cutting. However, for the plate with BEL=5.59 km/rev, the magnitude of the friction force/corner force for HW pulp will be different from the friction force/corner force for SW pulp that cause different mean peak shear forces at the onset of fiber cutting.

As shown in Appendix J, Figure 9, at the same plate gap and pulp furnish, normal stress decreases with a higher BEL plate. However, for SW pulp, shear stress is relatively similar for both plates, while, for HW pulp, shear stress slightly increases with the plate pattern with higher BEL.

The mean coefficient of friction is plotted in Figure 5-4 as a function of the inverse of plate gap for SPF SW HF TMP, aspen HW TMP, and NBSK pulp at 1200 rpm for two plate patterns, BEL=2.74 km/rev and BEL=5.59 km/rev. At all plate gaps and for all pulp furnishes, the mean coefficient of friction is higher for the plate pattern having higher BEL. Moreover, the mean coefficient of friction decreases as the plate gap is reduced. However, for HW pulp, the mean coefficient of friction increases up to a peak value, and decreases beyond this point.

The results tabulated in Table 2, Appendix J, indicate that the mean coefficient of friction at the onset of fiber cutting is a function of plate gap, pulp furnish, and plate pattern. The plate with smaller bar width and groove width resulted in higher mean coefficient of friction at the onset of fiber cutting.

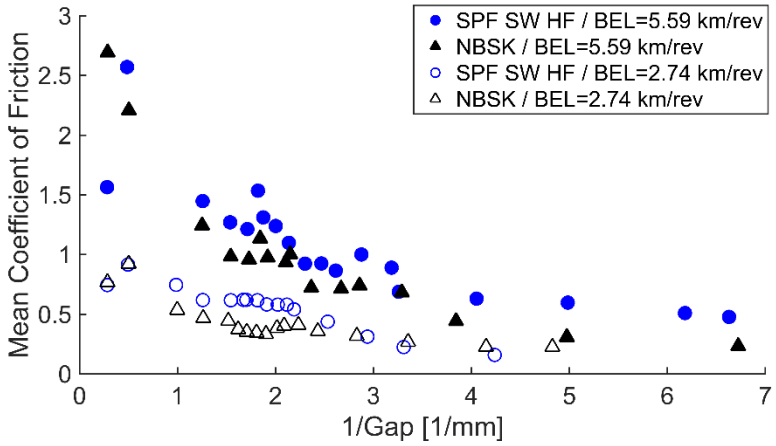

(a)

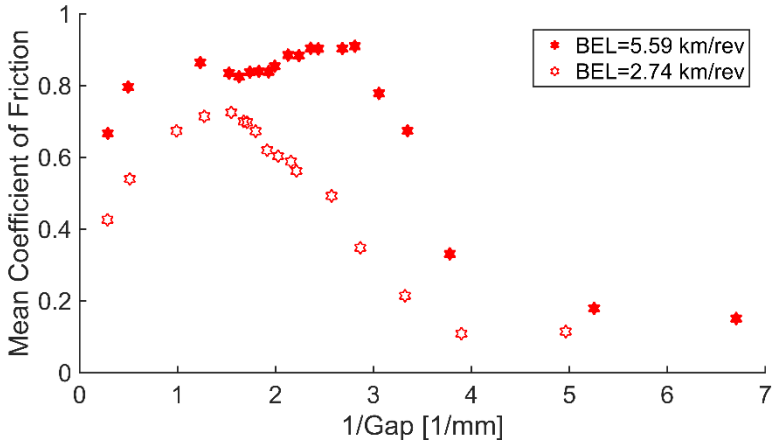

(b)

Figure 5-4. Mean coefficient of friction versus the inverse of plate gap for (a) SPF SW HF TMP (circle), NBSK (triangle), and (b) aspen HW TMP at 1200 rpm for the plates of BEL =5.59 km/rev and BEL=2.74 km/rev.

As an aside, the results also indicate that the fiber cutting metrics previously found in Chapters 3 and 4 can be used with different plate patterns. As an example, Figure 5-5 shows the relation between the power of normal force and the plate gap for two plate patterns for aspen hardwood TMP at 1400 rpm. Here, the transition gap, indicated by a dotted blue line, is based on the power of the normal force while the dashed red line highlights the critical gap, based on the fiber length data. There is an agreement between the transition gap and the critical gap.

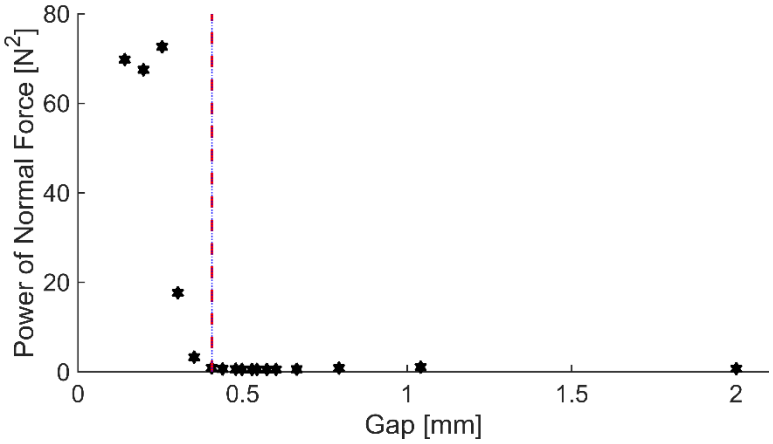

(a)

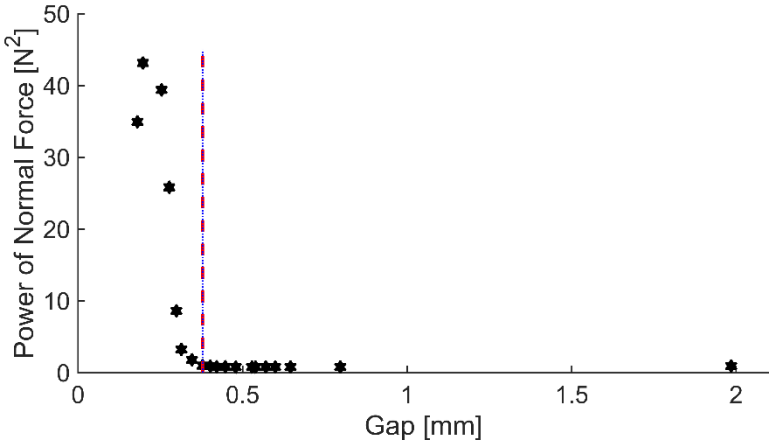

(b)

Figure 5-5. Power of normal force versus plate gap for aspen hardwood TMP at 1400 rpm (a) the plate gap of BEL=2.74 km/rev, and (b) the plate gap of BEL=5.59 km/rev.

In summary, for tested pulp furnishes and at all plate gaps, the plate with smaller bar width and groove width results in lower mean peak normal and shear forces but higher mean coefficient of friction. In addition, mean peak normal force, mean peak shear force, and mean coefficient of friction at the onset of fiber cutting depend on the plate pattern.

Moreover, as the plate gap is closed, mean peak normal and shear forces increase but mean coefficient of friction decreases. However, an increase in mean peak normal force is more significant than the increase in mean peak shear force which implies that the normal forces are the dominant forces in LC refining that are responsible for development of fibre and paper properties, particularly those properties affected by fiber cutting. This is in accordance with [84].

Chapter 6: Conclusions and Future Work

6.1. Conclusions

The primary objective of this work was to detect the onset of fiber cutting, in real time, based on time and frequency domain analysis of the RFS signals. We observed distinct transitions in the parameters that characterize the distribution of peak normal and shear forces, namely mean peak force and the Weibull scale parameter, as measured by the RFS during LC refining. These transitions consistently correspond to the onset of fiber cutting. In addition, the analysis of the power spectrum of the sensor data indicates that the magnitude of the dominant frequency can be used as an indicator of fiber cutting.

We found that the most reliable and consistent indication of the onset of fiber cutting was the power of the time domain signal of the normal force. This parameter, which is a signal processing term that is equivalent to the square of RMS magnitude of the signal, consistently determines the onset of fiber cutting, as identified by fiber length data.

The generality of these fiber cutting metrics have been investigated for a range of pulp furnishes and two different plate patterns. The results show that the RFS-type based indications of the onset of fiber cutting apply to all of the tested pulp furnishes and plate patterns. For pulp mills, detection of the onset of fiber cutting conditions is beneficial in low consistency refining as it can be used as the major part of a control system to reduce fiber cutting and increase energy efficiency.

In addition, we investigated the effect of pulp furnish and plate pattern on bar forces in LC refining. For the plate with BEL=2.74 km/rev, at the onset of fiber cutting, the mean peak normal force of the softwood pulp is much higher than for the hardwood pulp. However, the mean peak shear force for hardwood and softwood pulps at the onset of fiber cutting are approximately equivalent. We expect that the magnitude of the corner force for hardwood pulp will be different from the corner force of softwood pulp. Similarly, we expect that the magnitude of the friction force for hardwood pulp will be different from the friction force for softwood pulp. Our results suggest, however, that these two forces vary such that their sum is approximately equivalent for hardwood and softwood pulps, at the onset of fiber cutting.

For the plate with BEL=5.59 km/rev, at the onset of fiber cutting, the mean peak normal force of the softwood pulp is higher than for the hardwood pulp. The mean peak shear force

at the onset of fibre cutting is different for hardwood and softwood pulp. We expect that for the plate with BEL=5.59 km/rev, the magnitude of either the friction force or the corner force for hardwood pulp will be different from the softwood pulp that cause different mean peak shear forces at the onset of fiber cutting.

For tested pulp furnishes and at all plate gaps, the plate with higher BEL (which has smaller bar width and groove width) resulted in lower mean peak normal and shear forces. Mean peak normal and shear forces at the onset of fiber cutting depend on pulp furnish and plate pattern and are lower with the plate pattern having higher BEL.

The mean coefficient of friction decreases as the plate gap is closed. Our results also show that the mean coefficient of friction at the onset of fiber cutting is a function of plate gap, pulp furnish, and plate pattern. The plate with smaller bar width and groove width resulted in higher mean coefficient of friction.

This research provides new insights into the fundamental knowledge in characterizing refining action in low consistency refining. This work contributes to the understanding of the effect of pulp furnish and plate design on the interaction of bar forces and pulp fibers in LC refining.

Our work provides direct evidence, based on measurements of bar forces, that the normal forces are the dominant forces in LC refining that are responsible for the development of fibre and paper properties, particularly those properties affected by fiber cutting. As the plate gap is closed, mean peak normal and shear forces increase but the mean coefficient of friction decreases. However, an increase in mean peak normal force is more significant than the increase in mean peak shear force which implies the importance of normal forces in LC refining.

6.2. Future Work

We recommend pilot and mill-scale trails in the future that focus on the following research areas:

- Assess the applicability of the indications of the onset of fiber cutting found in data from the pilot-scale refiner trials at mill-scale;
- Assess use of the RFS to detect refining zone imbalance in twin-flow refiners to prevent production of non-homogenous pulp;

- Use multiple sensors to investigate the radial distribution of bar forces in LC refining;
- Use RFS to investigate the effect of consistency on bar forces and critical gaps at mill-scale.

References

[1] Global forest resources assessment (2015). Published by Food and Agriculture Organization of the United Nations. Retrieved from http://www.fao.org/3/a-i4793e.pdf.

[2] Energy consumption by the manufacturing sector (2016). Published by Statistics Canada. Retrieved from http://www.statcan.gc.ca/daily-quotidien/161031/dq161031d-eng.pdf.

[3] Luukkonen, A., Olson, J.A., Martinez, D.M. (2010): Low consistency refining of mechanical pulp, effect of gap, speed and power. J. Pulp Pap. Sci., 36, 28–34.

[4] Kappel, J. (1999): Mechanical pulps: From wood to bleached pulp. Tappi press, Atlanta, GA.

[5] Muenster, H., Ferritsius, O., Lecourt, M. & Petit-Conil, M. (2005): Energy savings in TMP by high temperature LC/MC refining. Proc. Intl. Mech. Pulp. Conf., Oslo, Norway, 213-223.

[6] Zha, Q., Lanouette, R., Law, K.N., Bousquet, J-P., Bussieres, S. (2008): Refining of long fibre fractions after fractionation. Preprint 94th Ann. Mtg., PAPTAC, Montreal, QC, Canada, B481–B487.

[7] Musselmann, R., Letarte, D., Simard, R. (1997): Third stage low consistency refining of TMP for energy savings and quality enhancement. 4th International Refining Conference, Italy, 141-147.

[8] Smook, G.A. (1998): Handbook for Pulp & Paper Technologists. Tappi Press, Angus Wilde Publications.

[9] Prairie, B., Wild, P., Byrnes, P., Olender, D., Ouellet, D. and Francis, D.W. (2008): Forces during bar-passing events in low consistency refining: distributions and relations to specific edge load. J. Pulp Paper Sci., 34(1), 1-8.

[10] Prairie, B., Wild, P., Byrnes, P., Olender, D., Francis, D. W., Ouellet, D. (2007): Forces during bar-passing events in low consistency refining: Effects of refiner tram. Pulp Pap. Canada, 108(9), 34–37.

[11] Olender, D., Wild, P., Byrnes, P., Ouellet, D. and Sabourin, M. (2007): Forces on bars in high-consistency mill-scale refiners: trends in primary and rejects stage refiners. J. Pulp Paper Sci., 33(3), 163-171.

[12] Olender, D., Wild, P., Byrnes, P., Ouellet, D., Sabourin, M. (2008): Forces on bars in high-consistency mill-scale refiners: Effect of Consistency. Nord. Pulp Pap. Res. J., 23(2) 218–223.

[13] Hamad, W.Y. (2002): Cellulosic Materials: Fibers, Networks and Composites. Springer Science & Business Media, New York.

[14] Elahimehr, A. (2014): Low consistency refining of mechanical pulp: the relationship between plate pattern, operational variables and pulp properties. Ph.D. Thesis, The University of British Columbia.

[15] Forgacs, O.L. (1963): The characterization of mechanical pulps. Pulp Pap. Mag. Can., 64 (C), T89-T118.

[16] Ilvessalo-P, M.-S. (1956): On the determination of fiber length. Pap. Ja Puu-Pap. Timber. 38(9), 443–449.

[17] College of Natural Resources. Retrieved from https://research.cnr.ncsu.edu/wpsanalytical/documents/T227.PDF.

[18] College of Natural Resources. Retrieved from https://research.cnr.ncsu.edu/wpsanalytical/documents/T220.PDF

[19] Andersson, S., Sandberg, C., Engstrand, P. (2012): The effect of rotor position on pulp properties in a two- zoned low consistency refiner. Nord. Pulp Pap. Res. J., 27(3), 525–530.

[20] Hammar L-A., Htun M., Svensson, B. (1997): A two-stage refining process to save energy for mechanical pulps. International mechanical pulping conference, Stockholm, Sweden, 257–262.

[21] Eriksen O., Hammar, L.-Å. (2007): Refining mechanisms and development of TMP properties in a low-consistency refiner. Int. Mech. Pulp. Conf., Tappi, Minneapolis, Minnesota, USA, 62-75.

[22] Eriksen, O., Hammar, L.-Å. (2005): Literature survey measurement techniques suitable for the refining zone of disc and conical LC refiners, STFI-PACKFORSK.

[23] Martinez, D. M., and Kerekes, R. J. (1994): Forces on fibers in low consistency refining. Tappi J. 77(12), 119-123.

[24] Mohlin, U-B. (2006): Refining intensity and gap clearance. 9th PIRA International Refining Conference, No.14, Vienna, Austria.

[25] Luukkonen, A., Olson, J., Martinez, D.M. (2012): Low consistency refining of mechanical pulp: Relationships between refiner operating conditions and pulp properties. Nord. Pulp Pap. Re. J., 27(5), 882-885.

[26] Leider, P.J. and Nissan, A.H. (1977): Understanding disc refiners: The mechanical treatment of fibres. TAPPI Journal, 60(10), 85-89.

[27] Berg, J.-K., Sandberg, C., Engberg, B.A., and Engstrand, P. (2015): Low consistency refining of mechanical pulp in the light of forces on fibres. Nord. Pulp Pap. Res. J. 30(2), 225-229.

[28] Berna R., J.E., Martinez, D.M., Olson, J.A. (2017): A comminution model parametrization for low consistency refining. Power Technology, 1(1).

[29] Roux, J.C. (2001): Review paper on pulp treatment process, The Science of Papermaking, Trans. 12th Fund. Res. Symposium, Oxford, 19-80.

[30] Lundin, T. (2008): Tailoring pulp fiber properties in low consistency refining. Ph.D. Thesis, Laboratory of Fibre and Cellulose Technology, Abo Academy University, Finland.

[31] Nugroho, D.D.P. (2012): Low consistency refining of mixtures of softwood and hardwood bleached kraft pulp: Effects of refining power. M.Sc. thesis, Asian Institute of Technology, Thailand.

[32] Luukkonen, A., Olson, J.A., Martinez, D.M. (2010): Low Consistency Refining of Mechanical Pulp: A Methodology to Relate Operating Conditions to Paper Properties, J. Pulp Pap. Sci. 36, 107–111.

[33] Luukkonen, A. (2011): Development of methodology to optimize low consistency refining of mechanical pulp. Ph.D. thesis, University of British Columbia.

[34] Elahimehr, A., Olson, J.A., Martinez, D.M. (2013): Understanding LC refining: The effect of plate pattern and refiner operation, Nord Pulp Paper Res J, 28(3), 386-391.

[35] Brecht, W. (1967): A Method for the Comparative Evaluation of Bar Equipped Beating Devices, TAPPI Journal of Technical Association of the Pulp and Paper Industry, 50(8), 40-44

[36] Roux, J.C., Joris, J. (2005): Angular parameters beyond specific edge load, TAPPSA Journal, Technical Association Pulp and Paper Industry South Africa.

[37] Meltzer, F., Rautenbach, R. (1994): Neue moeglichkeiten zur vorherbestimmung des technologischen mahlergebnisses. Das Papier, 48(9), 578-583, 1994.

[38] Senger, J.J., (1998): The forces on pulp fibres during refining, M.A.Sc. Thesis, Dept. of Mechanical Engineering, University of British Columbia, Vancouver, BC.

[39] Elahimehr, A., Olson, J.A., Martinez, D.M. (2015): Low consistency refining of mechanical pulp: how plate pattern and refiner operating conditions change the final pulp properties. Nord. Pulp Pap. Res. J., 30 (4), 609–616.

[40] Kerekes, R.J. (1990): Characterization of pulp refiners by a C - factor. Nord. Pulp Pap. Res. J., 5(1), 3-8.

[41] Batchelor, W. J. (2001). Effects of flocculation and floc trapping on fibre treatment in low-consistency refining. J. Pulp. Pap. Sci. 27(7), 249-253.

[42] Roux, J.-C., Bloch, J.-F., Bordin, R., Nortier P. (2009): The Net Normal Force per Crossing Point: A Unified Concept for the Low Consistency Refining of Pulp Suspensions, 14th Fundamental Research Symposium. Oxford, 72(2), 172-179.

[43] Olson, J.A., Drozdiak, J., Martinez, M., Garner, R., Robertson, A., Kerekes, R.J. (2003): Characterizing fibre shortening in a low-consistency refining using a comminution model, Powder Technology 129, 122– 129.

[44] Meyer, R., Almin, K.E., Steenberg, B. (1966): Length reduction of fibres subject to breakage. British Journal of Applied Physics. 17, 409–416.

[45] Roux, J.C., Mayade, T.L. (1999): Modeling of the particle breakage kinetics in the wet mills for the paper industry, Powder Technology, 105 (1), 237–242.

[46] Kerekes, R. J. (2011): Force-Based characterization of refining intensity. Nordic Pulp and Paper Res. J., 26(1), 14-20.

[47] Hartman, R.R. (1984): Mechanical treatment of pulp fibres for property development. Ph.D. Thesis, Lawrence Univ., Appleton, WI, USA.

[48] Biasca, J.E. (1989): Oriented fiber refining: application of individual modes of mechanical action to single pulp fibers. Ph.D. dissertation, The institute of Paper Chemistry, Appleton, WI, 1989.

[49] Siadat, A., Bankes, A., Wild P.M., Senger, J. and Ouellet, D. (2003): Development of a piezoelectric force sensor for a chip refiner, Proc IMechE Part E: Journal of Process Mechanical Engineering, 217(2), 133.

[50] Khlebnikov, A. A., Pashinskii, V. F., Goncharov, V. N., and Smirnova, E. A. (1969): Analysis of forces involved in the operation of conical refiner. Bumażna Prom. (10)22, 129-136.

[51] Goncharov, V.N., Smirnova, E.A. and Shemyakin, E.V. (1970): Method for the determination of stresses between refiner blades, Bumazh. Prom. (27):134-138, English Trans.

[52] Goncharov, V.N. (1971): Force factors in a disk refiner and their effect on the beating process, Bumazh. Prom. 5:12-14, English Trans.

[53] Atack, D. and Stationwala, M.I. (1975): On the measurement of temperature and pressure in the refining zone of an open discharge refiner. Transactions of the technical section, CPPA, 1 (3), 71-76.

[54] Nordman, L., Levlin, J.E., Makkonen, T., and Jokisalo, H. (1981): Conditions in an LC-refiner as observed by physical measurements. Paperi ja Puu. 63(4):169-180.

[55] Martinez, D.M., Batchelor, W.J., Kerekes, R.J., and Ouellet, D. (1997): Forces on fibres in refining: normal force. Journal of Pulp and Paper Science, 23(1), 11-18.

[56] Batchelor, W.J., Martinez, D.M., Kerekes, R.J., and Ouellet, D. (1997): Forces on fibres in refining: shear force. Journal of Pulp and Paper Science, 23(1), 40-45.

[57] Gradin, P.A., Johansson, O., Berg, J.-E., Nyström, S. (1999): Measurement of the power distribution in a single-disc refiner. J. Pulp Pap. Sci., 25(11), 384–387.

[58] Johansson et al., U.S. Patent 5,747,707, May 1998.

[59] Gradin, P.A., Berg, J.-E., Nyström, S.K. (2014): Measuring tangential forces in a pulp refiner: a novel approach. Exp. Tech., 40, 789-793.

[60] Senger, J.J. and Ouellet, D. (2002): Factors affecting the shear forces in high-consistency refining. J. Pulp Paper Sci., 28(11), 364-369.

[61] Backlund, H.-O. (2002): Measurement of shear force, temperature profiles and fibre development in mill-scale tmp refiners. Ph.D. Thesis, Mid Sweden University, Sweden.

[62] Bankes, A. (2000): The design and development of a mechanical wood pulp force sensor. M.A.Sc. Thesis, Dept. of Mechanical Engineering, Queen's University, Kingston, ON.

[63] Siadat, A. (2001): Measurement of Forces on Refiner Bars. M.A.Sc. Thesis, Dept. of Mechanical Engineering, University of British Columbia, Vancouver, BC.

[64] Senger, J., Olmstead, M., Ouellet, D., Wild, P. (2005): Measurement of Normal and Shear forces in the refining zone of a TMP refiner. J. Pulp Pap. Sci., 31 (1),28-32.

[65] Senger, J., Ouellet, D., Wild, P., Byrnes, P., Sabourin, M. and Olender, D. (2006): A technique to measure mean residence time in TMP refiners based on inherent process fluctuations, J. Pulp Paper Sci. 32(2), 83.

[66] Prairie, B.C. (2005): Measurement of forces in a low consistency refiner, M.A.Sc. Thesis, University of Victoria, British Columbia, Canada.

[67] Olender, D.J. (2007): Forces on Bars in High-Consistency Mill-Scale Refiners. Ph.D. Thesis, University of Victoria, Canada.

[68] Kerekes, R.J., Senger, J.J. (2006): Characterizing Refining Action in Low-Consistency Refiners by Forces on Fibres. Journal of Pulp and Paper Science 32(1):1-8.

[69] Kerekes, R.J. (2010): Energy and Forces in Refining. J. Pulp Paper Sci., 36, 10-15.

[70] Kerekes, R.J., Meltzer, F. (2017): The Influence of Bar Width on Bar Forces and Fibre Shortening in Pulp Refining, Dresden, Germany.

[71] Page, D.H. (1989): The beating of chemical pulps – the action and the effects. 9th Fundamental Research Symposium, "Fundamentals of Papermaking", 1-38.

[72] Pulp and Paper Centre. Retrieved from http://www.lcrl.ppc.ubc.ca/facilities.

[73] Olender, D., Wild, P., Byrnes, P. (2008): A piezoelectric force sensor for mill-scale chip refiners. Proceedings of the Institution of Mechanical Engineers, Part E: J Process Mech. Eng., 222(2), 115–122.

[74] Beghello, L., Toivakka, M., Eklund, D. and Lindstriim, T., (1996): A device for measuring fiber floc sizes in highly turbulent fiber suspensions. Nordic Pulp and Paper Research Journal, 11, 249-253.

[75] Johansson, A. (2011): Correlations between fibre properties and paper properties. M.Sc. Thesis. KTH, School of Chemical Science and Engineering, Sweden.

[76] Welch, L.V.S. (1999): Low consistency refining of mechanical pulps. Ph.D. Thesis, University of British Columbia.

[77] Murthy, D.N.P, Xie, M.R.J. (2003): Weibull Models.Wiley Series in Probability and Statistics, 2003.

[78] Senger, J., Siadat, A., Ouellete, D., Wild, P. (2004): Measurement of Shear and Normal Forces in the Refining Zone of a TMP Refiner. Journal of Pulp and Paper Science, 30(9), 247-251.

[79] Harirforoush, R., Olson, J, Wild, P. (2017): The Correlation between pulp properties and bar forces in LC refining using a piezoelectric sensor. 26th Canadian Congress of Applied Mechanics, University of Victoria, Canada.

[80] Papoulis, A. (1962): The Fourier Integral and Its Applications. New York: McGraw-Hill.

[81] Harirforoush, R., Olson, J., Wild, P. (2017): In-process detection of fiber cutting in low consistency refining based on measurement of forces on refiner bars, Tappi J., 16(4), 189-199.

[82] Harirforoush, R., Wild, P., Olson, J. (2016): The relation between net power, gap, and forces on bars in low consistency refining. Nord. Pulp Pap. Res. J., 31(1), 71–78.

[83] Kerekes, R.J. (2015): Perspectives on High and Low Consistency Refining in Mechanical Pulping, BioResources, 10(4), 8795-8811.

[84] Fernando, D., Gorski, D., Sabourin, M., and Daniel, G. (2013). Characterization of fiber development in high- and low-consistency refining of primary mechanical pulp. Holzforschung 67(7), 735–745.

Appendix A

Harirforoush, R., Wild, P., Olson, J. (2016): The relation between net power, gap, and forces on bars in low consistency refining. Nordic Pulp and Paper Research Journal, 31(1), 71-78. http://dx.doi.org/10.3183/NPPRJ-2016-31-01-p071-078

MECHANICAL PULPING
Nordic Pulp & Paper Research Journal Vol 31 no (1) 2016

The relation between net power, gap, and forces on bars in low consistency refining

Reza Harirforoush, Peter Wild, and James Olson

KEYWORDS: Force measurement, low consistency refining, pulp, sensor

SUMMARY: The objective of this study is to experimentally investigate the relationships between local bar forces, plate gap and fiber length in a single-disc low consistency refiner. Piezoelectric sensors are used to measure normal and shear forces applied to pulp fibers by the refiner bars. It is shown that there is a non-linear relationship between measured bar forces and length-weighted fiber length that mirrors the established relationship between length-weighted fiber length and the inverse of plate gap. As the plate gap is reduced, the length-weighted fiber length remains relatively constant while net refiner power and the mean peak normal and shear forces increase. These trends continue up to a threshold values of mean peak normal and shear forces of approximately 8 N and 2.4 N, respectively. Above this threshold, mean peak normal and shear forces continue to increase but the length-weighted fiber length exhibits negative linear relationships with these forces. These results can be used as the initial study for onset detection of fiber cutting and that these sensors have promising potential to be used as the basis for advanced refiner control strategies.

ADDRESSES OF THE AUTHORS: Reza Harirforoush (rharirfo@uvic.ca) and **Peter Wild** (pwild@uvic.ca): University of Victoria, Department of Mechanical Engineering, P.O. Box 3055 STN CSC, V8W 3P6, Victoria, BC, Canada. **James Olson** (james.olson@ubc.ca): University of British Columbia, Department of Mechanical Engineering, Point Grey Campus, 5000-2332 Main Mall, V6T 1Z4,Vancouver, BC, Canada.

Corresponding author: Reza Harirforoush

Mechanical refining is an energy intensive process. For example, in British Columbia (BC), mechanical refiners consume about 10% of BC's total electrical energy production (Luukkonen et al. 2010). With the ever increasing costs of energy, the long term survival of mechanical pulping depends on the ability to decrease energy consumption per ton of pulp.

Low consistency (LC) refining has been introduced to reduce energy consumption in mechanical pulping (Andersson et al. 2012; Hammar et al. 1997; Sabourin et al. 2011). LC refining of mechanical pulp consumes less energy than conventional high consistency (HC) refining (Muenster et al. 2005; Zha et al. 2008). However, a key limitation of LC refining is the degradation of mechanical properties due to fiber cutting at high refining energies (Luukkonen et al. 2010). This issue has limited the widespread adoption of LC refining.

In mechanical refining, friction between the plate and the fiber increases as the plate gap, the distance between the stator and rotor plates, is reduced. The reduction of plate gap causes the fibers to be compressed and sheared and results in an increase in net power. A linear relationship between refining power and the inverse of plate gap was suggested by Leider et al. (1977) who proposed an analytical model to describe refining as a combination of the number of impacts received by a fiber and their intensity. A similar relationship was found by May et al. (1988) for HC refiners.

The relationship between refining power and the plate gap was experimentally studied by Mohlin (2006) in an LC conical refiner at a flow rate of 600 liter/min. She showed that the plate gap is inversely proportional to the refiner power; as the plate gap decreases the refining power increases, and vice versa. The relationship was indicated as an important parameter relating refiner operation variables to pulp quality changes.

Luukkonen et al. (2010) demonstrated a linear correlation between the dimensionless power and dimensionless plate gap for a range of different refiner operating conditions and diameters in pilot and mill scale LC refiners. His work also investigated the relationship between the plate gap and pulp quality and showing that the changes in pulp quality remained constant until a *critical gap* was reached. Beyond the critical gap, fiber cutting commenced and paper strength properties were reduced. Moreover, beyond this point, the relationship between refining power and plate gap deviated from linearity (Luukkonen 2011).

Similar results were found by Nugroho (2012) for various mixes of softwood and hardwood pulps in LC refining. Refining power increased as the plate gap decreased and, at a critical gap between 0.3 to 0.5 mm, the power sharply increased. Moreover, the fiber length decreased when the plate gap reached the critical gap. This transition occurred for all of the trial conditions.

In a recent study, Elahimehr et al. (2013) studied the relationship between power and gap in an LC refiner. The trials were run at three different rotational speeds, with three different refiner plate patterns, and at 3% consistency. The flow rate was constant at 250 liter/min for all trials. He found that the relationship between net power and the inverse of plate gap was linear, up to a critical gap. He also showed that the fiber length was unchanged until the plate gap reached the critical gap. An approximate linear relationship between power and plate gap over the narrow range of 0.1-0.2 mm in a two zoned TwinFlo72 LC refining was recently reported by Berg et al. (2015).

Detection of the onset of critical gap conditions is potentially beneficial in LC refining as it may reduce fiber cutting and increase energy efficiency. In the studies discussed above, the critical gap is determined by investigation of the relation between plate gap and pulp properties, measured after refining. In-process detection of critical gap conditions has not been well studied.

In a number of previous studies, bar forces have been analyzed both theoretically and experimentally. Kerekes and Senger (2006) derived practical equations to estimate both normal and shear forces on a fiber in LC refining. Kerekes (2011) suggested that the force is the key link between bars and fibers in refining that cause important changes in fiber properties. His work also demonstrated the strong influence of gap size and specific edge load on fiber shortening. A sensor has been developed to measure local forces applied to refiner bars. This sensor, referred to here as the refiner force sensor (RFS), has a sensing probe which replaces a short length of a refiner bar enabling measurement of forces normal to and tangential to the refiner bars. The RFS has been applied in a number of studies in both low consistency (Prairie et al. 2007; Prairie et al. 2008) and high consistency refining (Olender et al. 2007; Senger et al. 2004).

The objective of the present study is to experimentally investigate the relationships between local bar forces, measured with the RFS, plate gap and fiber length in a single-disc LC refiner. Two RFS-type sensors measure the forces applied to the fibers by the refiner bars for different rotational speeds and a range of plate gaps. The net refiner power and the mean peak forces increase as the plate gap is reduced while the length-weighted fiber length remains relatively constant up to a threshold value at which fiber cutting begins.

Materials and Methods

Trials were performed in the AIKAWA 16'' single-disc refiner at the Pulp and Paper Center at the University of British Columbia, Canada. The refiner is equipped with power meter, plate actuation and variable speed drives on the pump. The plate used in these trials is the AIKAWA FINEBAR®, which has bar edge length of 2.74 km/rev and bar angle of 15° from radial. The bar width, groove width, and groove depth of the plates were 1.6 mm, 3.2 mm, and 4.8 mm, respectively.

Two RFS-type sensors, were custom designed and fabricated based on the design previously used in refiner trials (Olender et al. 2008). A photograph of one of the RFS used in this work is shown in *Fig 1a*. Each sensor is installed in a custom recess that is machined into the back side of the stator plate. The recess is located so that the tip of the sensor replaces a short length of the refiner bar (i.e. 5 mm), as shown in *Fig 1b*. To know the magnitude and the direction of the shear force, two components of the shear force need to be measured. RFS#1 measures shear force perpendicular to the major axis of the refiner bar (*Fig 2a*) while RFS#2 measures shear force parallel to the major axis of the refiner bar (*Fig 2b*). Both sensors also measure force normal to the plate surface (*i.e.* parallel to the axis of the refiner).

The sensors are located on opposite sides of the stator plate, as shown in *Fig 3*.

Each sensor is positioned in the second bar of a three-bar cluster at a radius of 151 mm. At this radius, 48 bars on the rotor, grouped into 16 three-bar clusters, pass over the sensor in one revolution of the refiner. The radial location of the sensors ensures that the heads of the bolts securing the rotor plate do not pass over the sensor and that the sensor body resides in one of the "pockets" in the

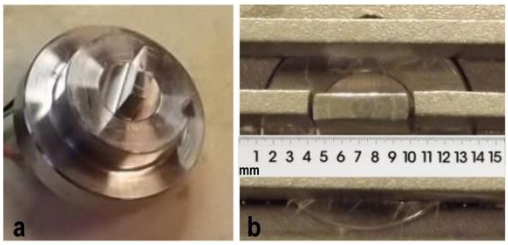

Fig 1 - a) RFS sensor used in Pulp and Paper Center, UBC, Canada trials and b) A close-up of RFS installed in the stator plate

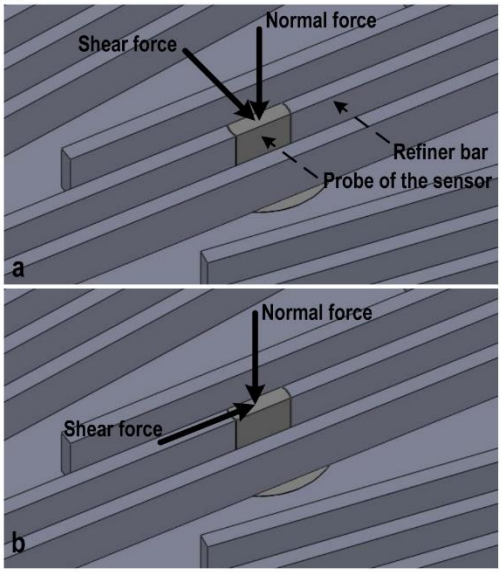

Fig 2 - Direction of forces measured by the a) RFS#1 sensor and b) RFS#2 sensor

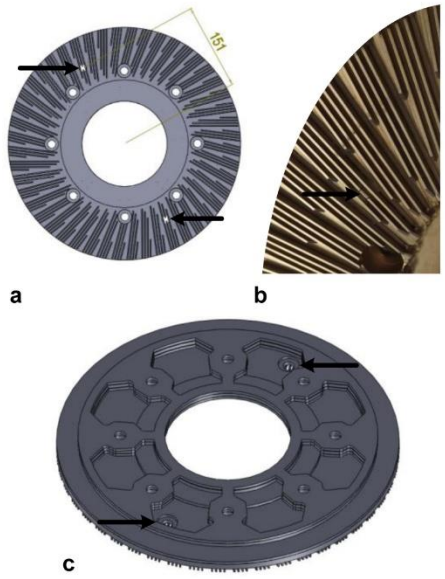

Fig 3 - a) The location of the sensors in the stator plate (front view) b) Close up of the stator plate with sensor c) The location of the sensors in the stator plate (back view)

back side of the stator plate. The sensor wires pass from the back side of the sensors through a custom gland located in door of the refiner, to which the stator plate is secured. Each sensor was calibrated by applying successive impacts (i.e. ~20 impacts) with a modal hammer to the tip of the sensor in the normal and shear directions. Each sensor generates two voltage signals, which are related to normal and shear force signals based on the method described by Prairie (2005). Environmental tests were also performed to ensure that the sensors are not compromised by refiner conditions. In these tests, the sensors were placed inside a water-filled custom pressure vessel located in an oven set to the temperature of the planned refiner trials (i.e. 100ºC). After four hours, the sensors were cooled and then calibrated.

To prevent phase and magnitude distortion of the signal due to sensor resonance, modal tests were performed to ensure that the first natural frequency of the sensor is well above the bar-passing frequency of the refiner. The first natural frequency of the sensors was determined to be 42 kHz based on the frequency response function obtained during calibration. The maximum bar-passing frequency of the refiner, based on bar spacing and rotor speed, was calculated to be 5.1 kHz. The ratio of the first natural frequency of the sensor to the maximum bar-passing frequency is 8.2 which provides a sufficient margin above the bar passing frequency.

A custom charge amplifier converts the high impedance charge output of the sensors to a low impedance voltage signal which is read by a National Instruments (Austin, TX, USA) PXI 1042 Q high-speed board. National Instrument BNC-2110, Shielded Connector Blocks are used to connect the high-speed DAQ board to the charge amplifier. A custom LabVIEW™ interface is used to control data acquisition. A sampling rate of 150 kHz is used which is more than twenty times the maximum bar-passing frequency occurring during the trials.

The set up and experiments in the Pulp and Paper Center took place over one week at the end of February 2015. Mechanical SPF softwood pulp with 378 CSF and 3.5% consistency was used in all trials. The operating conditions for the trials are shown in *Table 1*. The refining operating mode was mono-flo with one inlet perpendicular to the outlet. The refining temperature was about 60°C. The refiner speed was set with a Variable Frequency Drive (VFD). The plate gaps were digitally adjusted through a controller from no-load position (3.5 mm) to the smaller plate gaps. The flow rate was held constant at 250 liter/min. Once reaching stable condition at each target point, piezo signals were recorded using the LabVIEW™ interface for approximately 10 s. At each operating condition, the refiner was held steady for about 10 s to give the pulp time to move from the refining zone to the sample collection port and a two liter pulp sample was collected over 5 s interval. The process was repeated until all of the target points were achieved for one rotational speed (e.g. 1200 rpm). Then the plate gap was increased to the no-load position and the refiner was adjusted to the next rotational speed (e.g. 1000 rpm) using the VFD.

Table 1 - Operating conditions for the pilot-scale low consistency refining trials at Pulp and Paper Centre, UBC, Canada

Parameter	Condition
Refiner speed	800 rpm, 1000 rpm, 1200 rpm
Consistency	3.5 %
Flow rate	250 l/min
Plate gap	1200 rpm, 2.0 mm - 0.25 mm (12 gaps) 800 rpm, 2.0 mm - 0.25 mm (12 gaps) 1000 rpm, 2.0 mm - 0.40 mm (9 gaps)
Refining temperature	60°C
Quantity of pulp	3500 liter
Operating mode	Mono-flo
Pulp type	Mechanical SPF softwood pulp, 378 CSF

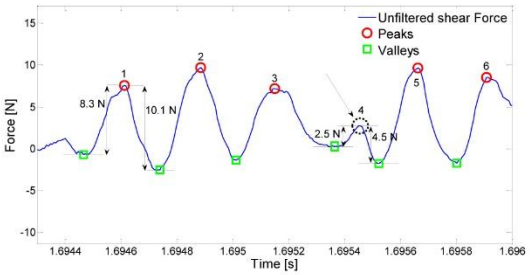

Fig 4 - Typical unfiltered shear force data for RFS#2 (i.e. parallel to the major axis of the refiner bar)

All pulp samples were analyzed using the Fiber Quality Analyzer (HiRes FQA, Optest Equipment Inc.) located at the UBC Pulp and Paper Center calculated the *length-weighted fiber length* for all pulp samples taken in trials. Length-weighted fiber length (L_w) is defined as follows (Graca et al. 1997):

$$L_w = \frac{\sum n_i L_i^2}{\sum n_i L_i} \qquad [1]$$

Where n_i and L_i are the number of the fibers in the *i*th class and mean length of the *i*th class respectively. This is the key pulp property that was used in the analysis.

An algorithm was created in MATLAB to identify *bar-passing events* in the force data. A bar–passing event is defined to occur when the passage of a rotor bar over the sensor results in a maximum or peak value in the force data that exceeds a predefined threshold value. This threshold criteria is applied to eliminate data peaks associated with non-bar-passing events, including signal noise. In the algorithm, potential bar-passing events are first identified as all local maxima in the force data. If the differences between a given local maxima and the preceding and the subsequent minimum both exceed a threshold value, then the peak is defined as bar-passing event. Otherwise, the peak is discarded. Examples of potential bar-passing events are shown in *Fig 4*. The threshold value for the typical unfiltered shear force data shown in *Fig 4* is 3.473 N. The peak No.1 is determined as a bar-passing event since the differences between the peak and its valleys are both greater than the threshold value. The peak No.4, marked with dashed circle, is not accepted as a bar-passing event as the difference between the peak and its preceding minimum is less than the

threshold value. Maxima that are defined by the algorithm as bar-passing events are marked with solid red circles.

The threshold value affects the number of bar-passing events detected by the algorithm. If the threshold is set too high, many legitimate bar-passing events will not be identified while if it is set too low, features in the data may be improperly identified as bar-passing events. The maximum possible number of bar-passing events is calculated as follows:

$$Number\ of\ bar-passing\ events = N \times \omega \times T \quad [2]$$

Where N is the number of the bars of the rotor crossing over the sensor for one revolution (N=48), ω is the rotational speed in revolution per second, and T is the test duration.

The occurrence ratio is defined as the number of bar-passing events detected by the algorithm divided by the maximum possible number of bar-passing events. If the pulp always exists between the refiner bars, and all of the bar-passing events are detected by the algorithm, then the occurrence ratio would be 100%. The occurrence ratio of 95% ±1% was obtained in previous LC refiner bar-passing event's algorithm (Prairie 2005). In this study, all of the bar-passing events are counted (occurrence ratio=100%) by manually changing the threshold value in each set of data. The algorithm is verified by manually scanning a data sample from each set of force data. For each bar-passing event, peak force is defined as the difference between the forces at the base of the local valley and the following peak (Prairie et al. 2007).

Results

Typical unfiltered RFS#2 normal and shear force data, taken at 1200 rpm and a plate gap of 0.25 mm, is shown in *Fig 5*. Each peak represents a bar-passing event. The shape of each event depends on number of factors including the amount and the properties of pulp located between the rotor and stator at the location of the sensor. As noted earlier, the bars of the rotor that cross over the force sensor are grouped in three-bar clusters. Therefore, bar-passing events appear in *Fig 5* as clusters of three peaks, an example of which is highlighted in the dashed rectangle.

Negative values appear in the force data due to charge decay which is a fundamental characteristic of piezo-based sensors. However, the magnitude of a load that is applied over a relatively short time frame can be determined from the change in the state of charge of the sensor, regardless of its initial state (Gautschi 2002). Therefore, for bar-passing events that begin when the force signal is negative, the magnitude of the applied force is measured from the base of the valley preceding the peak, as discussed earlier.

The power spectrum of the RFS#2 data at 1200 rpm and plate gap of 0.25 mm shows four local maxima at frequencies of 3.82, 2.87, 1.90 and 0.95 kHz (*Fig 6*). The maximum at 3.82 kHz, corresponds to passage of the leading edges (or trailing edges) of adjacent bars within each three-bar cluster. The leading edges of adjacent bars are illustrated and marked as 1 and 2 in *Fig 6b.* The maximum at 2.87 kHz, corresponded to passage of the leading edge and then the trailing edge of adjacent bars

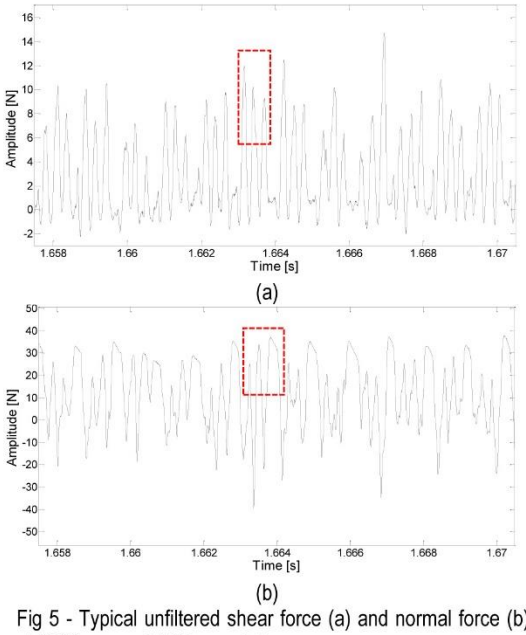

Fig 5 - Typical unfiltered shear force (a) and normal force (b) at 1200 rpm and 0.25 mm plate gap

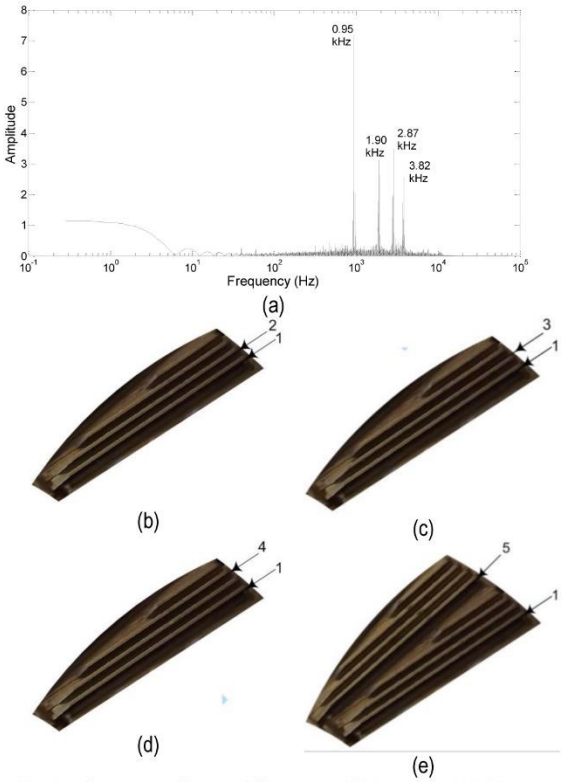

Fig 6 - Spectrum of normal forces at 1200 rpm and 0.25 mm plate gap (a) a segment of the stator plate showing the leading edges of adjacent bars (b) the leading and the trailing edges of adjacent bars (c) the leading edges of the first and the third bars (d) the equivalent edges in adjacent three-bar clusters (e)

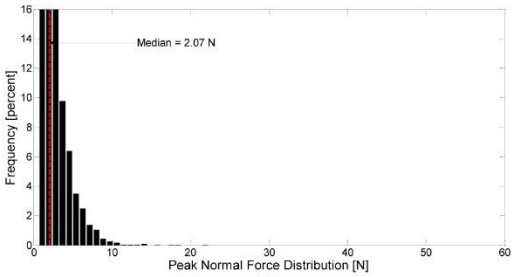

(a)

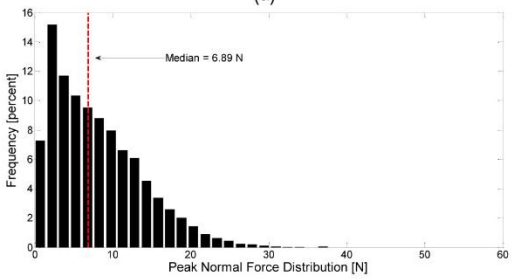

(b)

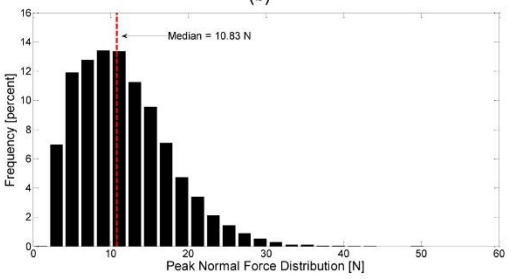

(c)

Fig 7 - Normalized distributions of peak normal force for plate gaps of 0.7 mm (a), 0.55 mm (b), and 0.4 mm (c) for 1200 rpm rotational speed.

within each three-bar cluster. The leading and the trailing edges of adjacent bars are shown and marked as 1 and 3 in *Fig 6c*. The maximum at 1.90 kHz corresponds to the passage of the leading edge (or trailing edge) of the first and third bars within each three-bar cluster. The leading edges of the first and the third bars are depicted and marked as 1 and 4 in *Fig 6d*. Finally, the maximum at 0.95 kHz, corresponds to the passage of equivalent edges in adjacent three-bar clusters. The equivalent edges in adjacent three-bar clusters are illustrated and marked as 1 and 5 in *Fig 6e*.

Typical RFS#2 normalized distributions of peak normal force values for three different plate gaps, 0.4 mm, 0.55 mm, and 0.7 mm, at 1200 rpm are shown in *Fig 7*. Both the median magnitude and the *spread* of the peak normal force distributions increase as the gap decreases. The median of the distributions for the plate gaps of 0.4 mm, 0.55 mm, and 0.7 mm are 10.83 N, 6.89 N, and 2.07 N respectively.

The relationships between the net power and the inverse of the plate gap for three rotational speeds: 1200 rpm, 1000 rpm, and 800 rpm are shown in *Fig* 8. These relationships are similar to the result of Nugroho (2012) and Elahimehr et al. (2013). As the plate gap is reduced,

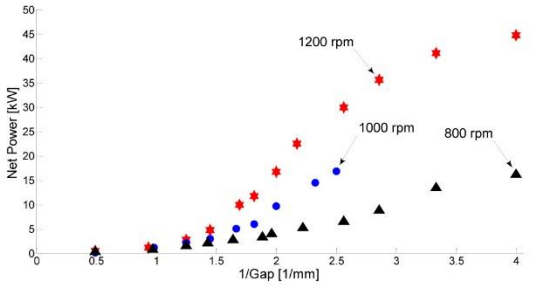

Fig 8 - The net power versus the inverse of the plate gap for three rotational speeds of 1200rpm, 1000 rpm, and 800 rpm

the net power increases. However, the effect of increasing the net power is more significant for gap sizes of less than 0.5 mm. At a constant gap, increasing the rotational speed increases the amount of energy transferred to the fibers. The critical gap at which the transition from linear to non-linear behaviour occurs is not apparent in these plots.

The relation between the L_w and the inverse of plate gap is shown in *Fig 9* for three rotational speeds, 1200 rpm, 1000 rpm, and 800 rpm. At 1200 rpm (*Fig 9a*), L_w remains constant as the gap is closed until the plate gap reaches a critical value of 0.55 mm, indicated by the dashed line. Beyond this point, L_w decreases in an approximately linear manner. A similar trend occurs at 800 rpm (*Fig 9b*). At this speed, the critical gap is 0.39 mm. The trend cannot be followed at 1000 rpm (*Fig 9c*) since nine plate gaps were tested due to the pulp shortage at the storage tank and only one data is available for the plate gaps less than the critical gap of 0.43 mm. Comparing the critical gaps for these three rotational speeds shows that the critical gap decreases at lower rotational speed. This finding is consistent with the results of Elahimehr et al. (2013) and Nugroho (2012). As an aside, it can be seen from *Fig 8*, and *Fig 9* that the fiber cutting at 1200 rpm, and 800 rpm starts once 11.77 KW, and 6.52 KW power is applied, respectively. This result is similar to the results of Elahimehr et al. (2013).

To explore the relationship between forces and fiber length, L_w is plotted against the mean of peak normal forces and the mean of peak shear forces for RFS#2 data taken at 1200 rpm. As shown in *Fig 10a*, L_w remains relatively constant as mean peak shear force increases up to a value of approximately 2.4 N, which corresponds to the critical gap of 0.55 mm. Beyond this point, L_w decreases in an approximately linear manner. A similar trend is seen in the relationship between mean peak normal force and L_w (*Fig 10b)*. However, the linear trend is not definitive beyond a mean peak normal force of approximately 8 N, which corresponds to the critical gap of 0.55 mm.

For 1000 rpm, because of the insufficient data for the plate gaps less than the critical gap of 0.43 mm, as previously mentioned, the relationship between the L_w and mean peak forces cannot be investigated. In addition, the force data for 1000 rpm and 800 rpm was of poor quality at several plate gaps. Therefore, the results of L_w versus mean peak normal and shear forces for 1000 rpm and 800 rpm are not discussed in this work.

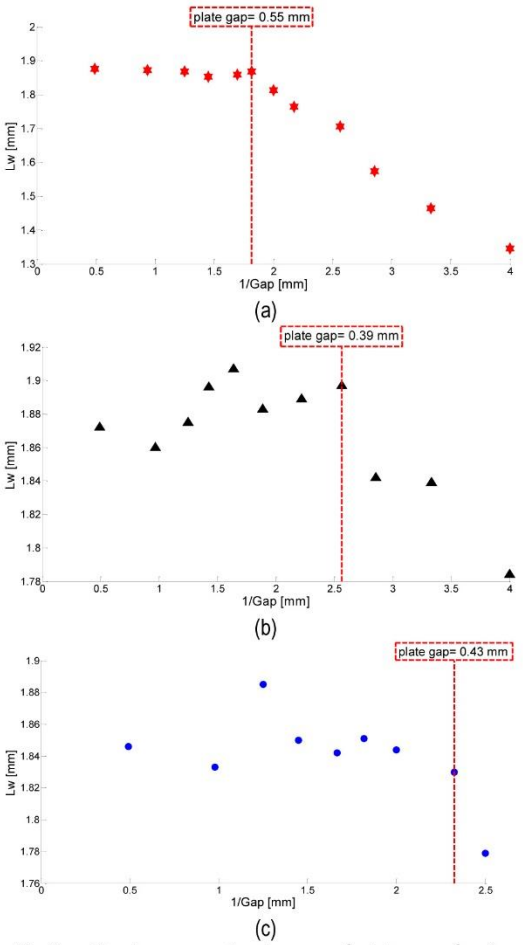

Fig 9 - The L_w versus the inverse of plate gap for three rotational speeds of 1200 rpm (a), 800 rpm (b), and 1000 rpm (c) during Pulp and Paper Center trials

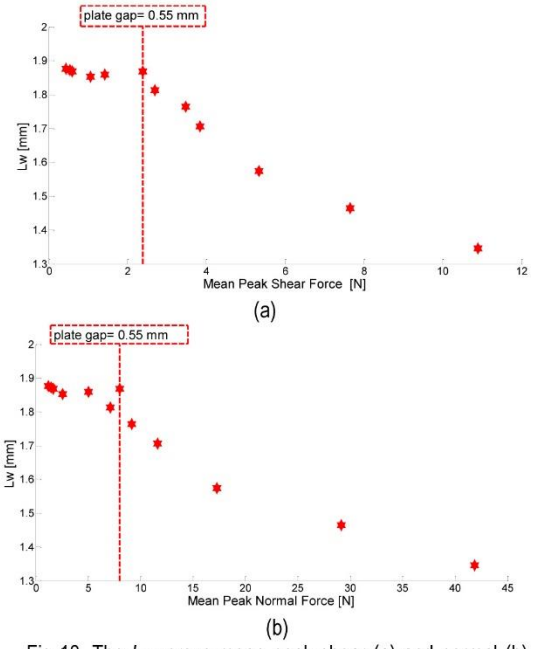

Fig 10. The L_w versus mean peak shear (a) and normal (b) force for rotational speed of 1200 rpm

Post–trial calibration of the RFS#2 showed less than 10% variance with respect to initial pre-trial calibration, verifying the viability of the RFS#2 data. However, an anomaly in normal sensitivity was detected in post-trial calibration of RFS#1. This anomaly was found to be due to damage to sensor wires which occurred during installation into the refiner. As a result, RFS#1 data is not presented in this study.

Discussion

RFS#2 measures normal and shear forces, parallel to the refiner bar, in a single-disc LC refiner. Clusters of three peaks appear in both normal and shear force time domain data (*Fig* 5), corresponding to passage of three-bar clusters on rotor over the force sensor. Power spectra of the force sensor data is characterized by maxima at frequencies that correspond to the passage of individual bars and clusters of bars. These results support the validity of the sensor measurements.

Peaks in the time domain data are subjected to a threshold algorithm to identify those peaks that correspond to bar-passing events. The algorithm eliminates the peaks related to non-bar-passing events such as noises. Moreover, since the algorithm counts all bar-passing events by manually changing the threshold value for each set of data, the occurrence ratio, defined previously, is always 100%.

Since each bar-passing event is unique, a useful way of characterizing the bar-passing events is with distributions of event parameters such as peak normal and shear force. These distributions allow comparison between refining conditions on the basis data taken throughout operation at each condition. As shown in *Fig 7*, the median peak force and the *spread* of peak force distributions increase as the plate gap decreases. The increase in median peak force is consistent with the increase in refiner power which accompanies reduction in plate gap. Increasing the *spread* of peak force distribution may be related to changes in refiner operating condition. When the plate gap is increased, the peak normal forces tend to be clustered around a single value and the spread of distribution is decreased. Studying the distribution of peak forces provides a great insight in understanding the mechanical interactions between fibers and refiner bars. Further investigation is needed to explore the relation between the shape of these force distributions and changes in pulp properties.

As shown in *Fig 8*, net refiner power increases as plate gap decreases. A linear relationship between the power and inverse of the plate gap was reported by Mohlin et al. (2006), Luukkonen et al. (2010), Elahimehr et al. (2013), and Nugroho (2012). The relation deviates from linearity for the plate gaps smaller than critical gap. However, the transition from linearity to nonlinearity cannot be easily determined until the L_w is plotted versus the inverse of plate gap. L_w is unchanged until the plate gap reaches a

critical gap. Below this point, the L_w decreases and the fiber cutting begins (*Fig 9*). In addition, the critical gap decreases as the rotational speed decreases. The same trend has been reported in previous studies (Luukkonen et al. 2010; Nugroho 2012; Elahimehr et al. 2013).

As shown in *Fig 10*, the L_w remains relatively constant and the mean peak shear and normal forces increase up to a threshold, at which mean peak normal and shear forces are equal to approximately 8 N and 2.4 N , respectively. At this point the fiber cutting happens and L_w decreases. This point corresponds to the critical gap, at which point the relation between power and inverse of the gap deviates from linearity.

Current control strategies rely on global process variables such as rotational speed, specific energy, and inlet pulp consistency. In these control strategies, the critical gap is determined by investigation of the relation between plate gap and pulp properties measured after refining. The details of mechanical interactions between refiner bars and pulp are not considered. To reduce fiber cutting and increase energy efficiency, in-process detection of critical gap conditions is crucial in LC refining. The results of this study suggest that there is promising potential for force sensor data to detect the onset of fiber cutting. However, the trends in this study exist over a limited range of operating conditions. Further trials are needed before the authors will be able to conclude that the trends seen in this study hold over a wide range of conditions. For instance, consistency, type of pulp, and flow rate can be suggested as independent variables and the effect of each parameter on bar forces can be investigated separately.

Conclusions

This study presents the relation between refiner operation, fiber length, and RFS data in a pilot-scale LC refiner. Two RFS-type sensors were custom designed and fabricated to measure normal and shear forces, perpendicular to and parallel to the major axis of the refiner bars, in an AIKAWA 16" refiner. These sensors replaced a short length of the refiner bar and measured normal and shear forces applied to the tip of the sensors. The experiments were performed using 378 CSF softwood pulp at 3.5% consistency for three rotational speeds (1200, 1000, and 800 rpm) and a range of plate gaps. The pulp was sampled at regular intervals and the L_w was determined for each sample. The data recorded from the sensors were processed by an algorithm to detect bar-passing events, and to measure bar-passing characteristic features.

It is shown that there is a non-linear relationship between measured bar forces and length-weighted fiber length that mirrors the established relationship between length-weighted fiber length and inverse plate gap. As the plate gap is reduced, the net refiner power and the mean peak normal and shear forces increase but the length-weighted fiber length remains relatively constant. When the mean peak normal and shear forces reach to approximately 8N and 2.4 N , respectively, a transition occurs. Above this threshold, mean peak normal and shear forces continue to increase but the length-weighted fiber length exhibits negative linear relationships with these forces. However, this negative linear trend is not definitive in the relationship between the L_w and mean peak normal force.

These trends are based on limited range of operating conditions in a pilot-scale LC refiner and additional studies in both pilot and mill scales are suggested to draw more general conclusions. These results suggest that the onset of fiber cutting could be detected, in process, using the force sensor data.

Acknowledgements

The authors gratefully acknowledge the assistance of M. Miller, and E. Jahangir during the preparation and execution of the refining trials at the Pulp and Paper Centre at UBC. The work was funded by the Natural Sciences and Engineering Research Council of Canada. A special thanks to our partners AFT-Aikawa Group, Alberta Newsprint Company, Andritz, Arkema, BC Hydro, Canfor, Catalyst Paper, FPInnovations, Holmen, Howe Sound Pulp and Paper Corporation, Millar Western, NORPAC, West Fraser, Westcan Engineering, and Winstone Pulp International.

Literature

Andersson, S., Sandberg, C., Engstrand, P. (2012): Comparison of mechanical pulps from two stage HC single disc and HC double disc-LC refining, Appita J.65 (1), 57–62.

Berg, J. E., Sandberg, C., Engberg, B. A., & Engstrand, P. (2015): Low-consistency refining of mechanical pulp in the light of forces on fibers, Nord Pulp Paper Res J, 30(2), 225-229.

Elahimehr, A., Olson, J.A., Martinez, D.M. (2013): Understanding LC refining: The effect of plate pattern and refiner operation, Nord Pulp Paper Res J, 28(3), 386-391.

Gautschi, G. (2002): Piezoelectric sensorics, Springer.

Graca Carvalho, M., Ferriera, P.J., Martins, A.A., Figueiredo, M.M. (1997): A comparative study of two auto-mated techniques for measuring fiber length, Tappi J 80(2), 137–142.

Hammar, L-Å, Htun, M., Svensson, B. (1997): A two-stage refining process to save energy for mechanical pulps, International mechanical pulping conference, SPCI. Stockholm, Sweden, pp. 257–262.

Kerekes, R.J, Senger, J.J. (2006) : Characterizing refining actionb in low-consistency refiners by forces on fibers, J Pulp Paper Sci., 32(1), 1-8.

Kerekes, R.J. (2011): Force-based characterization of refining intensity, Nord Pulp Paper Res J, 26(1), 14-20.

Leider, P. J. and Nissan, A. H. (1977): Understanding the disk refiner; The mechanical treatment of the fibers, Tappi J, 60(10), 85–89.

Luukkonen, A. (2011): Development of methodology to optimize low consistency refining of mechanical pulp, Ph.D. Thesis, The University of British Columbia, British Columbia, Canada.

Luukkonen, A., Olson, J.A., Martinez D.M. (2010): Low consistency refining of mechanical pulp, effect of gap, speed and power, J Pulp Paper Sci.36, 28–34.

May, W. D., Miles, K. B., McRay, M.R., Lunan, W. A. (1988): An approach to the measurement of the residence time in a chip refiner, J Pulp Paper Sci.,14(3), J47-J53.

Mohlin, U-B. (2006): Refining intensity and gap clearance. 9th International Refining Conference, No14, Vienna, Austria.

Muenster, H., Ferritsius, O., Lecourt, M., Petit-Conil, M. (2005): Energy savings in TMP by high temperature LC/MC refining, Proc. Intl. Mech. Pulping Conf., Olso, Norway, p.213-223.

Nugroho, D.D.P. (2012): Low consistency refining of mixtures of softwood & hardwood bleached kraft pulp: effects of refining power. M.Sc. Thesis, Asian Institute of Technology School of Environmen, resources and development, Thailand.

Olender, D., Wild, P., Byrnes, P., Ouellet, D., Sabourin, M. (2007): Forces on bars in HC mill-scale refiners:Trends in primary and rejects stage refiners. Journal of Pulp and Paper Science,33(3),163-171.

Olender, D., Wild, P., Byrnes, P. (2008):A piezoelectric force sensor for mill-scale chip refiners. Proceedings of the Institution of Mechanical Engineers, Part E: J Process Mech Eng, 222(2), 115–122.

Prairie, B.C. (2005): Measurement of forces in a low consistenct refiner, M.A.Sc. Thesis,University of Victoria,British Columbia, Canada.

Prairie, B.C., Wild, P., Olender, D., Francis, D.W., Ouellet, D. (2007): Forces during bar-passing events in low consistency refining:Effects of refiner tram. Pulp Pap Can, 9, T153–T156.

Prairie, B.C., Wild, P., Byrnes, P., Olender, D., Francis, B., Ouellet, D. (2008): Forces during bar-passing events in low-consistency refining: distributions and relationships to specific edge load, J Pulp Paper Sci 34(1), 1-8.

Sabourin M., Antensteiner P., Luukkonen A. (2011): Aggressive low consistency refining in thermomechanical pulping: energy consumption and fibre development, International mechanical pulping conference, China Light Industry Press, Xi'an, China,pp. 248–252.

Senger, J., Olmstead,M., Ouellet,D., Wild, P. (2004): Measurement of normal and shear forces in the refining zone of a TMP refiner, Journal of Pulp and Paper Sci., 30(9), 247-251.

Zha, Q., Lanouette,R., Law, K.N., Bousquet, J.P., Bussieres, S. (2008): Refining of long fibre fractions after fractionation, Preprint 94th Ann. Mtg., PAPTAC, B481-B487.

Manuscript received November 25, 2015
Accepted February 12, 2016

Appendix B

Design and Frequency Response of the Refiner Force Sensor

The refiner force sensor measures shear and normal forces applied to pulp fibers by the refiner bar. It includes a probe that replaces a short length of the refiner bar. Integration of the sensor into the AIKAWA 16-in single-disc LC refiner at the PPC required designing of the probe length and width to match the bar geometry of the stator plate. The design of the probe of the sensor changes from plates with BEL=2.74 km/rev to the plate with BEL=5.59 km/rev since each plate has a specific bar geometry. The sensors, installed in these two plates, were custom designed based on the design previously used in refiner trials [73]. However, some modifications were applied to the sensors' electrical system that decrease the complexity in fabrication of the sensors and improve the sensor performance.

Two piezoelectric elements, lead metaniobate material, are used in each sensor. The orientations of the piezo elements for measuring the shear forces perpendicular and parallel to the major axis of the refiner bar are shown in Appendix E, Figure E1.

The critical issue in design considerations of a sensor is its dynamic range. The sensor should be properly designed to record frequencies in a range well below its lowest natural frequency to prevent phase and magnitude distortion of the signal due to sensor resonance. The ratio of the lowest natural frequency of the sensor, the first resonance frequency, to the maximum bar-passing frequency, f_{BP}, is important as it determines the acceptable level of signal distortion because of the resonance frequency of the sensor. The maximum bar-passing frequency is calculated in [85] and presented in Appendix E.

The modal analysis of the sensor has been carried out using ANSYS software to investigate the resonance frequencies of the sensor. The probe of the sensor was modeled in SolidWorks and imported to Finite Element Analysis (FEA) software for resonance frequency analyses. The element solid tetrahedral 4 nodes 187 was used in meshing since the element has a quadratic displacement behaviour and is well suited to modelling irregular meshes. The material of the probe is AISI 316 stainless steel. The first natural

frequency of the sensor, installed in the plate with BEL=2.74 km/rev, is shown in Appendix E, Figure E2.

To measure the frequency response function[17] (FRF) of the RFS, the sensor is excited in the normal and shear directions by a miniature impact hammer (PCB Piezotronics Model 086D80) while secured in a test plate. The test plate simulates the refiner plate and was manufactured for mounting the sensor, as shown in Figure B1a. The probe of the impact hammer was positioned at the mid-point along the length and width of the probe surface. Olender et al. [73] showed that the sensor was relatively insensitive to the point of the impact. The typical FRFs of the sensors installed in the plate with BEL=2.74 km/rev and BEL=5.59 km/rev are shown in Figure B1b and B1c, respectively. The first natural frequency of the sensor installed in the plate with BEL=2.74 km/rev and BEL=5.59 km/rev were determined to be 42 kHz and 28 kHz, respectively. The ratio of the first natural frequency of the sensor to the maximum bar-passing frequency, shown as dashed lines in Figure B1b and Figure B1c, is 8.2 for the plate with BEL=2.74 km/rev while it is 4 for the plate with BEL=5.59 km/rev which provides a sufficient margin above the bar passing frequency.

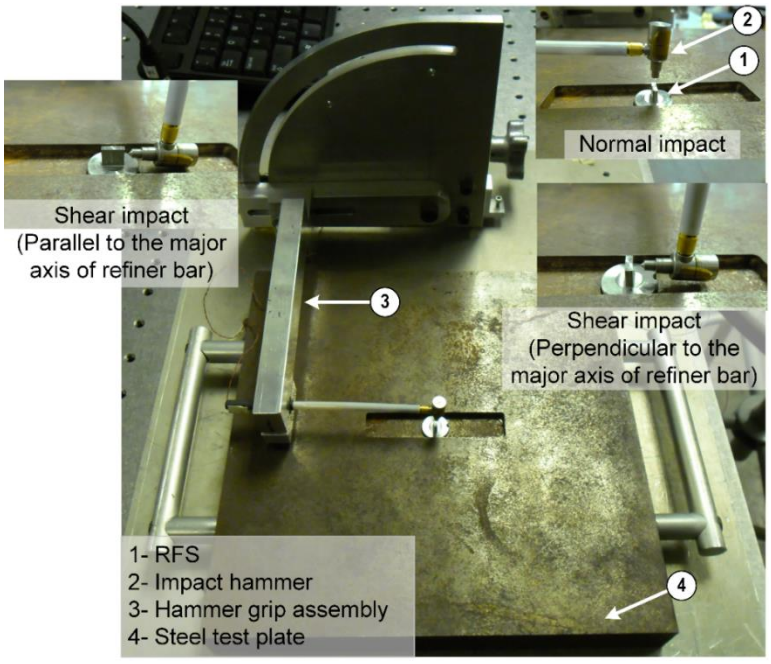

(a)

[17] FRF: the measure of the output spectrum of a system in response to an input force and is used to characterize the dynamics of the system.

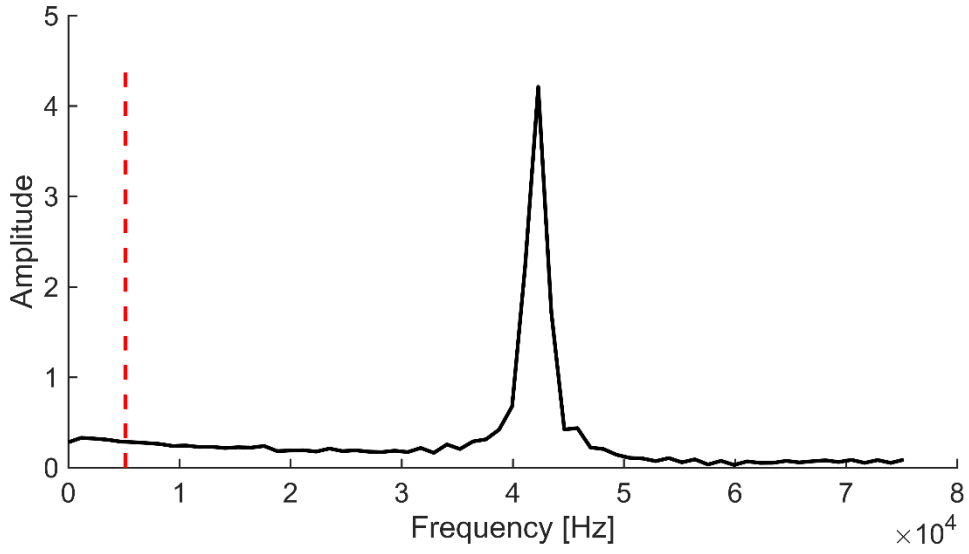

(b)

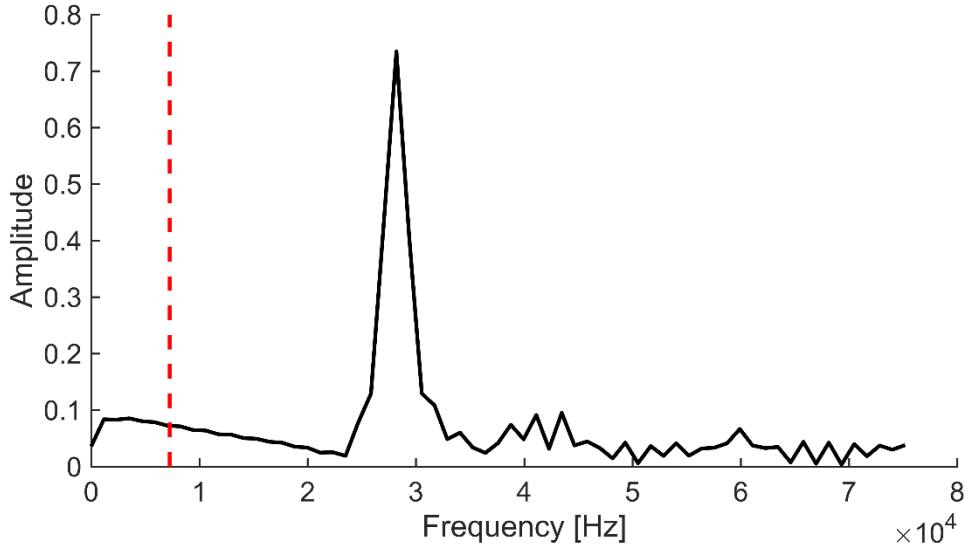

(c)

Figure B1. (a) The sensor secured in the test plate to measure the frequency response function, (b) typical frequency response function of the RFS installed in the plate with BEL=2.74 km/rev, and (c) BEL=5.59 km/rev. Dashed lines show the maximum bar-passing frequencies.

Appendix C

Fabrication and Calibration of the Refiner Force Sensor

A great effort has been made in fabrication of the sensors and machining of the stator plate. The plate to be used in the pilot trials has been manufactured by the AFT-Aikawa Group. More details on the fabrication of the sensors are presented in Appendix F.

The refiner force sensors were calibrated by applying successive impacts (i.e. 20 impacts) with a miniature modal hammer to the probe of the sensor in the normal and shear directions. The force hammer voltage response and the voltage responses of the piezo elements (two piezo elements are used in each sensor) are captured by a custom LabVIEW^{TM} interface, created by R. Harirforoush. Typical responses of force hammer and piezo for normal impact are shown in Figure C1.

An algorithm was created in MATLAB to read the force hammer and piezo voltage responses. The algorithm finds the peak voltages and plots the peak voltage of piezo versus peak forces to determine the liner regression. Since the piezoelectric elements will have no charge under zero strain, the linear regression is performed with the y-intercept of the regression line fixed to the origin. The typical regression lines for the normal and shear impacts are shown in Figure C2.

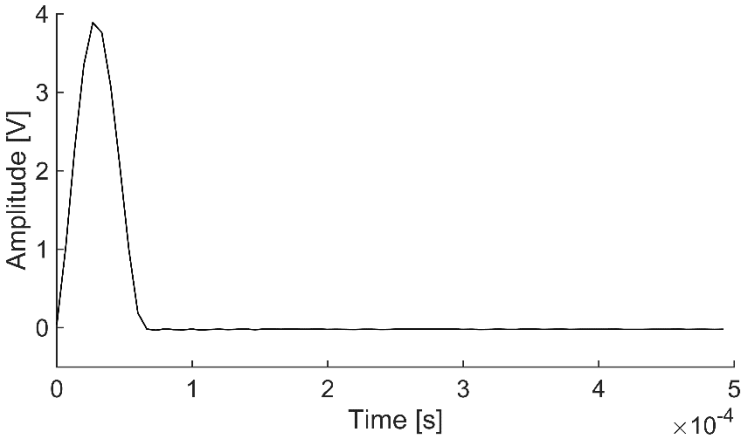

(a)

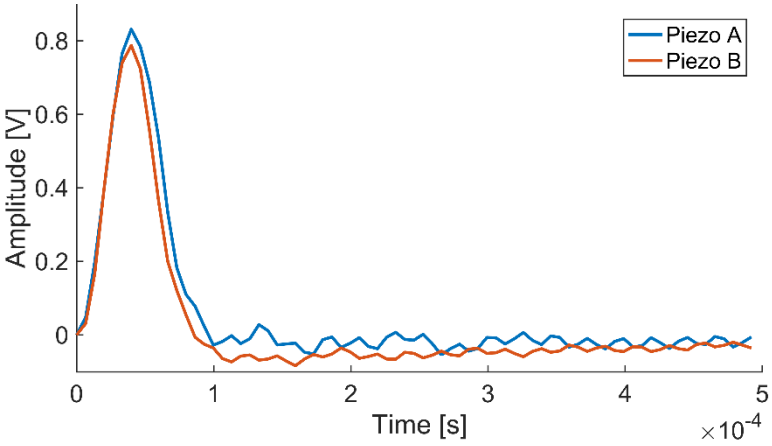

(b)

Figure C1. (a) Time domain plots of force hammer response and (b) piezo voltage responses for normal impact.

The slopes of the regression lines indicate the calibration constants [V/N]. The calibration method and the normal and shear sensitivity equations for a typical sensor are calculated in Appendix G. The calibration method was developed in [62], and has been validated in [63].

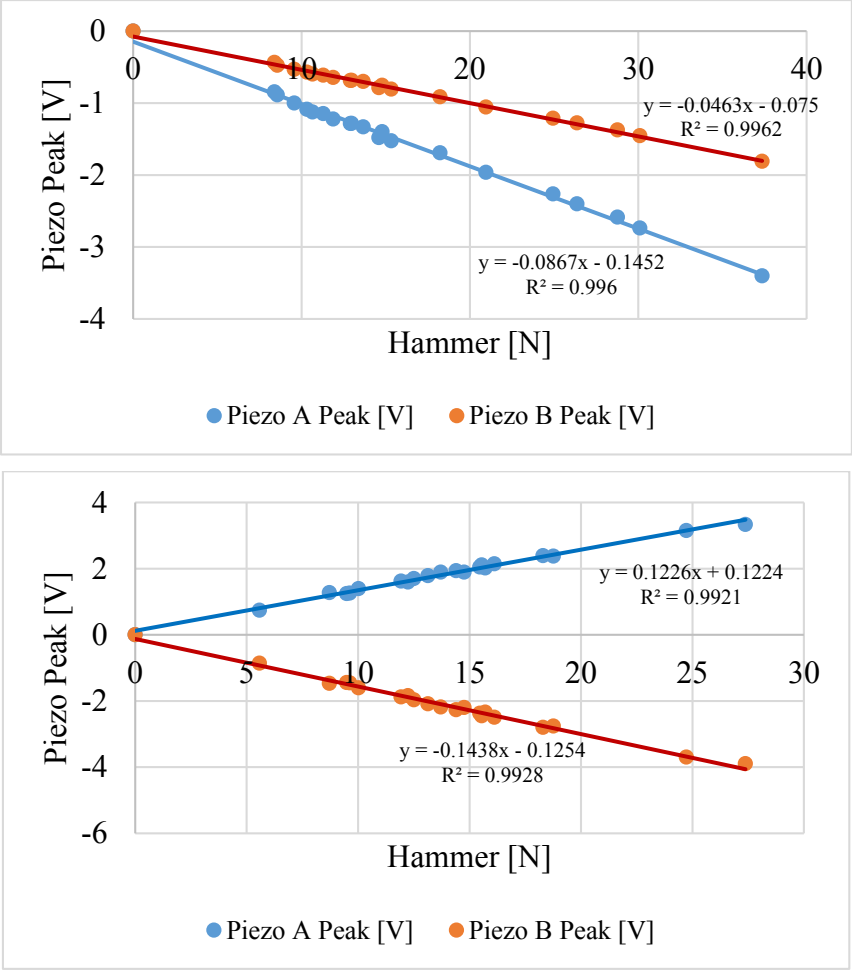

Figure C2. Typical peak voltage of piezo versus peak forces and the regression lines for the normal (top) and shear (below) impact calibration.

Environmental tests were also performed to ensure that the sensors are not compromised by refiner conditions and confirm the integrity of the O-ring seals and wires egress sealants application. In these tests, the sensors were placed inside a distilled water-filled custom pressure vessel located in an oven set to the temperature of the planned refiner trials (i.e. 100º C). After four hours, the sensors were cooled and then calibrated.

Appendix D

Operating Conditions of the Pilot-Scale Trials

Table 1: Operating conditions for pilot-scale low consistency refining trials at PPC-UBC, Canada, February 2015

Parameter	Condition
Refiner speed	800 rpm, 1000 rpm, 1200 rpm
Consistency	3.5 %
Flow rate	250 liter/min
Plate gap	1200 rpm, 2.0 mm - 0.25 mm (12 gaps) 800 rpm, 2.0 mm - 0.25 mm (12 gaps) 1000 rpm, 2.0 mm - 0.40 mm (9 gaps)
Refining temperature	60°C
Quantity of pulp	3500 liter
Operating mode	Mono-flo
Pulp type	Mechanical SPF softwood pulp, 378 ml CSF

Table 2: Plate gap, net power, and length-weighted fiber length data for pilot-scale low consistency refining trials at PPC-UBC, Canada, February 2015

Rotational speed (rpm)	Plate gap (mm)	Net power (kW)	Length-weighted fiber length (mm)
1200	3.51	0.00	--
	2.04	-0.51	1.876
	1.07	1.22	1.872
	0.80	2.75	1.869
	0.69	4.81	1.853
	0.59	9.95	1.859
	0.55	11.77	1.869
	0.50	16.78	1.813
	0.46	22.51	1.764
	0.39	29.94	1.706
	0.35	35.64	1.574
	0.30	41.10	1.465
	0.25	44.73	1.345

1000	3.49	0.00	--
	2.03	0.10	1.846
	1.02	1.14	1.833
	0.80	2.09	1.885
	0.69	2.93	1.850
	0.60	5.09	1.842
	0.55	6.01	1.851
	0.50	9.67	1.844
	0.43	14.46	1.830
	0.40	16.84	1.779
800	3.53	0.00	--
	2.03	0.29	1.872
	1.03	0.81	1.860
	0.80	1.60	1.875
	0.70	2.12	1.896
	0.61	2.75	1.907
	0.53	3.38	1.883
	0.51	4.00	1.843
	0.45	5.22	1.889
	0.39	6.52	1.897
	0.35	8.83	1.842
	0.30	13.43	1.839
	0.25	16.17	1.784

Table 3: Operating condition for pilot-scale low consistency refining trials at PPC-UBC, Canada, November 2015

Parameter	**Condition**	
Refiner speed	800 rpm, 1000 rpm, 1200 rpm	1200 rpm
Consistency	3.5 %	2.5 %
Flow rate	250 liter/min	
Plate gap	1200 rpm, 3.5 mm - 0.25 mm (15 gaps) 800 rpm, 3.5 mm - 0.25 mm (15 gaps) 1000 rpm, 3.5 mm - 0.25 mm (15 gaps)	1200 rpm, 3.5 mm – 0.25 mm (12 gaps)
Operating mode	Mono-flo	
Pulp type	Mechanical SPF softwood pulp, 378 ml CSF	

Table 4: Plate gap, net power, fine percentage, curl index, kink index, and length-weighted fiber length data for pilot-scale low consistency refining trials at PPC-UBC, Canada, November 2015

Rotational speed (rpm)	Plate gap (mm)	Net power (kW)	Fine percentage	Curl index	Kink index	Length-weighted fiber length (mm)
1200 rpm	3.54	0.00	10.43	0.038	0.46	1.835
At	2.03	-0.69	10.89	0.041	0.49	1.835
3.5%	1.07	1.54	11.05	0.036	0.48	1.846
consistency	0.78	2.68	10.34	0.037	0.46	1.858
	0.70	3.56	9.48	0.037	0.43	1.880
	0.61	5.68	9.63	0.036	0.43	1.878
	0.57	7.15	9.64	0.038	0.45	1.875
	0.55	7.49	9.52	0.035	0.43	1.837
	0.51	10.55	9.59	0.032	0.40	1.846
	0.51	10.61	9.70	0.034	0.42	1.837
	0.44	19.61	10.00	0.033	0.41	1.816
	0.39	26.52	10.30	0.032	0.41	1.742
	0.36	31.54	11.79	0.032	0.43	1.608
	0.29	44.03	12.22	0.034	0.38	1.472
	0.25	48.32	13.44	0.033	0.38	1.363
1200 rpm	3.50	0.00	11.61	0.039	0.50	1.816
at	2.01	-0.73	12.14	0.036	0.50	1.831
2.5%	0.75	3.73	11.98	0.036	0.49	1.837
consistency	0.60	7.38	10.57	0.036	0.45	1.858
	0.57	8.31	11.04	0.034	0.46	1.855
	0.55	10.01	11.46	0.035	0.48	1.827
	0.53	10.67	10.47	0.036	0.44	1.839
	0.50	13.59	10.46	0.036	0.45	1.825
	0.46	17.48	11.66	0.034	0.45	1.811
	0.41	22.27	11.30	0.035	0.42	1.775
	0.36	30.55	10.81	0.033	0.40	1.647
	0.26	43.51	13.59	0.034	0.40	1.367
1000 rpm	3.53	0.00	9.29	0.035	0.43	1.880
	2.03	-0.13	9.64	0.035	0.43	1.868
	1.00	0.94	9.77	0.036	0.43	1.848
	0.79	1.64	9.38	0.036	0.43	1.855
	0.68	2.48	10.13	0.036	0.44	1.846
	0.62	3.33	10.61	0.037	0.47	1.852
	0.56	4.13	10.18	0.036	0.45	1.842
	0.50	6.13	9.66	0.034	0.42	1.851
	0.46	8.06	9.55	0.036	0.43	1.854
	0.44	9.28	9.16	0.036	0.43	1.850

	0.41	11.71	9.61	0.036	0.43	1.832
	0.39	13.63	9.46	0.033	0.42	1.840
	0.33	20.54	11.51	0.036	0.47	1.714
	0.30	27.54	10.80	0.034	0.40	1.644
	0.25	31.68	12.79	0.034	0.42	1.596
800 rpm	3.51	0.00	10.44	0.037	0.49	1.846
	1.99	0.28	10.28	0.036	0.46	1.838
	1.03	0.61	10.33	0.037	0.48	1.846
	0.80	1.07	9.30	0.037	0.447	1.885
	0.68	1.63	9.08	0.035	0.44	1.865
	0.60	2.14	9.55	0.037	0.47	1.861
	0.54	2.47	10.25	0.037	0.47	1.840
	0.50	2.72	10.15	0.036	0.44	1.838
	0.45	3.52	9.60	0.036	0.45	1.857
	0.43	3.98	9.45	0.036	0.45	1.849
	0.40	4.61	9.53	0.037	0.45	1.841
	0.37	6.01	9.51	0.036	0.45	1.850
	0.35	6.86	9.90	0.035	0.42	1.853
	0.30	10.29	9.95	0.036	0.45	1.828
	0.25	12.93	10.61	0.035	0.44	1.757

Table 5: Operating condition for pilot-scale low consistency refining trials at PPC-UBC, Canada, August 2016

Parameter	Condition
Pulp furnish	Hemlock/balsam SW TMP, 240 ml Canadian standard freeness (CSF)
	SPF SW TMP, 630 ml CSF
	NBSK, 700 ml CSF
	Aspen HW TMP, 500 ml CSF
Refiner speed, rpm	1200, 1400
Consistency	3-3.5%
Flow rate, l/min	250
Plate gap, mm	3.5-0.2
Operating mode	Mono-flo
Sample duration	10 s

Table 6: Plate gap, net power, length-weighted fiber length, freeness, tear index, and tensile index data for pilot-scale low consistency refining trials at PPC-UBC, Canada, August 2016

Pulp type (rpm)	Plate gap (mm)	Net power (kW)	Freeness (ml)	Tear index (mNm^2/g)	Tensile index (kNm/kg)	Length-weighted fiber length (mm)
Hemlock/balsam						
SW TMP	3.529	0.00	192	7.5	24.5	1.622
at 1200 rpm	2.012	-0.27				1.725
	1.028	1.18	184			1.720
	0.770	2.18				1.668
	0.648	2.41	182			1.711
	0.595	4.01				1.694
	0.580	3.36				1.719
	0.549	4.67	182	8.1	25.7	1.711
	0.521	4.28				1.681
	0.485	6.03				1.706
	0.473	5.18				1.686
	0.453	7.43	178			1.686
	0.397	11.35				1.666
	0.349	17.09	166	8.1	26.9	1.668
	0.294	27.88				1.555
	0.254	36.81	135	6.6	28.7	1.454
	0.201	42.72				1.370
SPF SW TMP	3.522	0.00	638	10.2	32.4	2.177
at 1200 rpm	2.025	-0.60				2.202
	1.014	4.33	631			2.176
	0.794	6.96				2.202
	0.648	11.12	628	11.3	34.1	2.166
	0.598	13.75				2.166
	0.587	13.61				2.148
	0.551	15.72	612	11.2	34.0	2.183
	0.523	17.49				2.167
	0.494	19.64				2.141
	0.472	19.65				2.18
	0.457	22.82	586	11.4	36.2	2.15
	0.395	27.90		11.0	38.7	2.080
	0.340	33.55	571			1.999
	0.302	39.83				1.951
	0.236	49.86	458	9.2	46.5	1.764
SPF SW TMP	3.453	0.00	627	11.5	33.1	2.208
at 1400 rpm	1.996	-0.85				2.229
	1.008	7.51	626			2.231

	0.788	12.41				2.188
	0.656	18.34	600			2.227
	0.589	22.29				2.184
	0.577	23.47				2.186
	0.548	25.07	590	10.6	38.3	2.179
	0.532	27.24				2.127
	0.508	29.89				2.13
	0.472	34.51				2.08
	0.461	34.69	548	10.6	38.4	2.10
	0.395	44.81				1.976
	0.353	56.30	417			1.751
	0.300	60.36				1.496
	0.245	56.53	263	6.0	48.2	1.229
	0.196	55.76				1.107
NBSK	3.513	0.00	638	25.2	45.2	2.632
at 1200 rpm	1.990	-0.11				2.653
	1.003	1.87	612			2.646
	0.792	5.64				2.647
	0.659	7.28	609			2.645
	0.617	9.72				2.655
	0.585	11.03				2.621
	0.553	13.69	578	18.4	60.6	2.626
	0.525	18.75				2.645
	0.496	21.88				2.649
	0.479	25.07				2.644
	0.447	30.01	548	16.4	74.2	2.641
	0.411	33.12				2.610
	0.353	42.21	511			2.595
	0.298	52.52				2.61
	0.241	57.95	359	11.9	87.4	2.552
	0.207	63.47				2.507
Aspen HW TMP	3.509	0.00	491	1.7	12.1	0.891
at 1200 rpm	1.950	-1.47				0.886
	1.010	-1.19	479			0.890
	0.785	-0.61				0.906
	0.645	-0.21	474			0.902
	0.597	-0.08				0.921
	0.584	0.03				0.906
	0.556	0.15	463	1.6	11.5	0.894
	0.522	0.60				0.898
	0.493	0.96				0.904
	0.463	1.89				0.892
	0.452	2.37				0.896
	0.389	6.52	435	1.7	14.0	0.888
	0.349	15.48	392			0.855

	0.301	22.28				0.836
	0.257	29.09	328	1.9	17.0	0.787
	0.201	31.80				0.752
Aspen HW TMP	3.508	0.00	484	1.7	11.7	0.898
at 1400 rpm	2.001	-2.48				0.896
	1.041	-2.58	480			0.898
	0.793	-2.09				0.906
	0.665	-1.47	479	1.6	12.3	0.905
	0.602	-1.17				0.896
	0.574	-0.97				0.907
	0.544	-0.89	471	1.6	12.1	0.895
	0.529	-0.54				0.896
	0.498	0.02				0.901
	0.479	0.56		1.7	12.6	0.903
	0.439	1.79	477	1.5	12.3	0.899
	0.407	4.63				0.887
	0.353	13.78	434	1.9	15.1	0.863
	0.303	24.07				0.834
	0.256	32.86	332	2.0	16.7	0.731
	0.199	40.44				0.676
	0.142	42.70				0.665

Table 7: Operating condition for pilot-scale low consistency refining trials at PPC-UBC, Canada, March 2017

Parameter	Condition
Pulp furnish	SPF SW TMP, 666 ml Canadian standard freeness (CSF)
	SPF SW TMP, 456 ml CSF
	NBSK, 686 ml CSF
	Aspen HW TMP, 566 ml CSF
Refiner speed, rpm	1200, 1400
Consistency	3.3-3.6%
Flow rate, l/min	250
Plate gap, mm	3.5-0.2
Operating mode	Mono-flo
Sample duration	10 s

Table 8: Plate gap, net power, length-weighted fiber length, freeness, tear index, and tensile index data for pilot-scale low consistency refining trials at PPC-UBC, Canada, March 2017

Pulp type (rpm)	Plate gap (mm)	Net power (kW)	Freeness (ml)	Tear index (mNm^2/g)	Tensile index (kNm/kg)	Length-weighted fiber length (mm)
SPF SW TMP						
666 ml CSF	3.547	0.00	629	10.1	32.2	2.145
at 1200 rpm	2.059	0.93	634			2.185
	0.796	9.19				2.131
	0.650	12.62	621			2.163
	0.584	15.30				2.167
	0.549	16.23	607	10.5	33.2	2.165
	0.533	18.51				2.187
	0.499	20.60				2.176
	0.468	23.28	609			2.190
	0.434	29.91				2.146
	0.405	32.86	583	10.9	36.8	2.132
	0.382	36.77				2.083
	0.348	41.11	546			2.020
	0.314	43.69				1.951
	0.307	44.52				1.954
	0.247	52.74	475			1.829
	0.201	56.72		8.6	45.8	1.732
	0.162	61.89				1.617
	0.151	63.46				1.594
SPF SW TMP						
666 ml CSF at						
1400 rpm	3.542	0.00	635	11.0	33.4	2.190
	2.008	1.30	640			2.199
	0.793	15.39				2.180
	0.646	22.97	617			2.174
	0.611	25.91				2.152
	0.568	30.61				2.152
	0.545	35.85	595	10.7	40.1	2.154
	0.526	39.13	567	10.7	38.9	2.145
	0.496	44.35				2.139
	0.466	49.93				2.117
	0.450	52.77	534	10.1	42.3	2.029
	0.405	54.04				1.921
	0.352	63.67	458			1.790
	0.293	74.04				1.673
	0.251	77.80	365			1.608

	0.219	78.35		6.9	53.9	1.524
Aspen HW TMP						
at 1200 rpm	3.460	0.00	506	1.6	12.0	0.879
	2.015	-0.08	512			0.902
	0.811	0.90				0.887
	0.655	1.75	507			0.880
	0.614	2.07				0.886
	0.575	2.41				0.879
	0.546	2.63	510	1.7	12.1	0.882
	0.518	3.01				0.883
	0.502	3.49				0.896
	0.470	4.04				0.891
	0.446	4.88	503			0.886
	0.424	5.54				0.879
	0.410	6.51				0.873
	0.373	7.93				0.888
	0.356	10.62	478	1.8	13.2	0.872
	0.327	16.38				0.852
	0.299	19.22				0.844
	0.265	27.45	432			0.825
	0.190	35.59		2.2	18.9	0.779
	0.149	39.67				0.763
Aspen HW TMP						
at 1400 rpm	3.487	0.00	511	1.8	12.7	0.904
	1.985	0.08	501			0.898
	0.797	1.22				0.898
	0.646	2.33	500			0.884
	0.599	2.79				0.900
	0.571	3.00				0.900
	0.539	3.35	497	2.0	13.5	0.908
	0.529	3.78				0.890
	0.479	5.18				0.895
	0.448	7.13	482			0.897
	0.422	9.34				0.904
	0.402	12.36				0.887
	0.379	14.68	458	1.9	14.9	0.884
	0.347	26.20	423			0.845
	0.314	30.18				0.839
	0.299	34.27				0.816
	0.277	38.45				0.785
	0.254	41.87	353			0.778
	0.197	46.78		2.1	20.4	0.738
	0.181	49.25				0.729

SPF SW TMP 456 ml CSF at 1200 rpm	3.514	0.00	428	10.9	37.9	1.887
	2.038	0.56	431			1.921
	0.802	5.48				1.943
	0.649	7.24	404			1.928
	0.582	9.09				1.953
	0.538	10.64	411	9.7	36.7	1.934
	0.527	12.75				1.920
	0.495	14.48				1.908
	0.472	16.99				1.881
	0.451	18.60	398			1.856
	0.432	22.78				1.908
	0.390	25.70	372	10.2	41.5	1.901
	0.377	28.65				1.827
	0.360	38.97	322			1.770
	0.317	44.70				1.730
	0.298	47.71				1.698
	0.254	55.70	268			1.574
	0.233	61.41				1.502
	0.208	63.24		7.8	46.5	1.459
NBSK at 1200 rpm	3.476	0.00	647	23.3	38.9	2.605
	1.986	1.32	646			2.565
	0.799	6.41				2.632
	0.648	8.70	630			2.607
	0.578	10.10				2.634
	0.542	10.75	625	24.0	46.5	2.646
	0.521	11.90				2.599
	0.475	15.06				2.621
	0.465	16.71	613			2.662
	0.423	23.46				2.633
	0.374	33.51				2.650
	0.350	39.91	556			2.626
	0.304	45.99	538	15.6	73.1	2.639
	0.260	56.04	482			2.607
	0.201	63.06	432	14.4	79.6	2.590
	0.149	65.07				2.564
	0.128	67.39				2.531

Appendix E

Orientation of Piezoelements and Modal Analysis of the Refiner Force Sensor

The orientations of piezo elements used in the refiner force sensor for measuring the shear forces perpendicular and parallel to the major axis of the refiner bar are shown Figure E1.

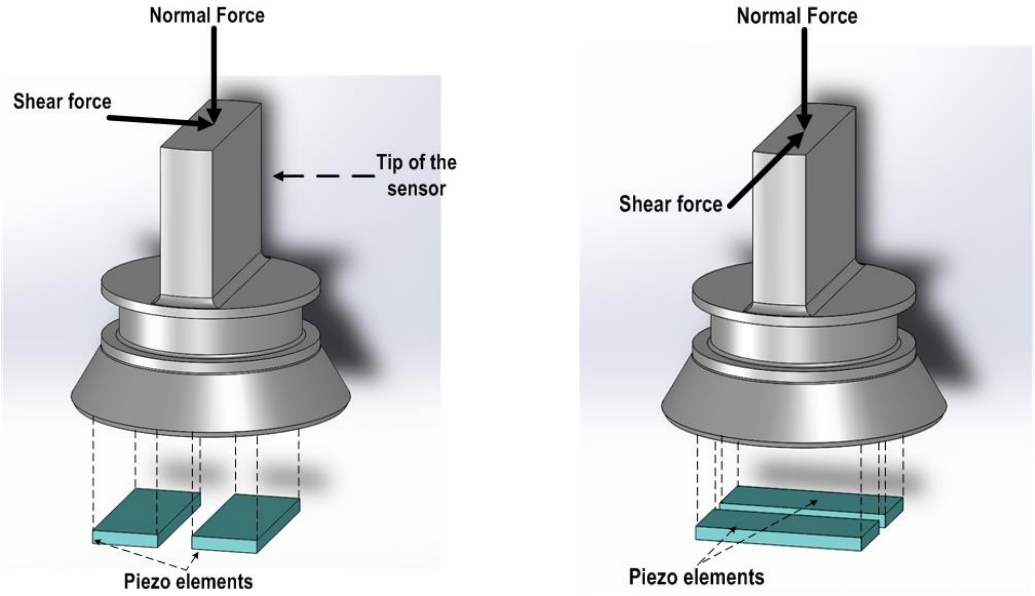

Figure E1. Orientation of piezo elements for measuring the normal force and the shear force perpendicular to (left) and parallel to (right) the direction of the major axis of the refiner bar.

The maximum bar-passing frequency, f_{BP}, is calculated by Equation 16:

$$f_{BP} = \frac{\pi \, \mathrm{D} \, \omega}{(\mathrm{W+G})} cos\emptyset \qquad 16$$

where D is the rotor diameter at the sensor location, ω is the refiner rotating frequency in radians per second, W is the bar width in mm, G is the groove width in mm, and ∅ is the bar angle. The maximum bar-passing frequency of the plate with BEL=2.74 km/rev, based on bar spacing and rotor speed, was calculated to be 5.1 kHz.

The mode shape for the first natural frequency of the sensor, installed in the plate with BEL=2.74 km/rev, is shown in Figure E2.

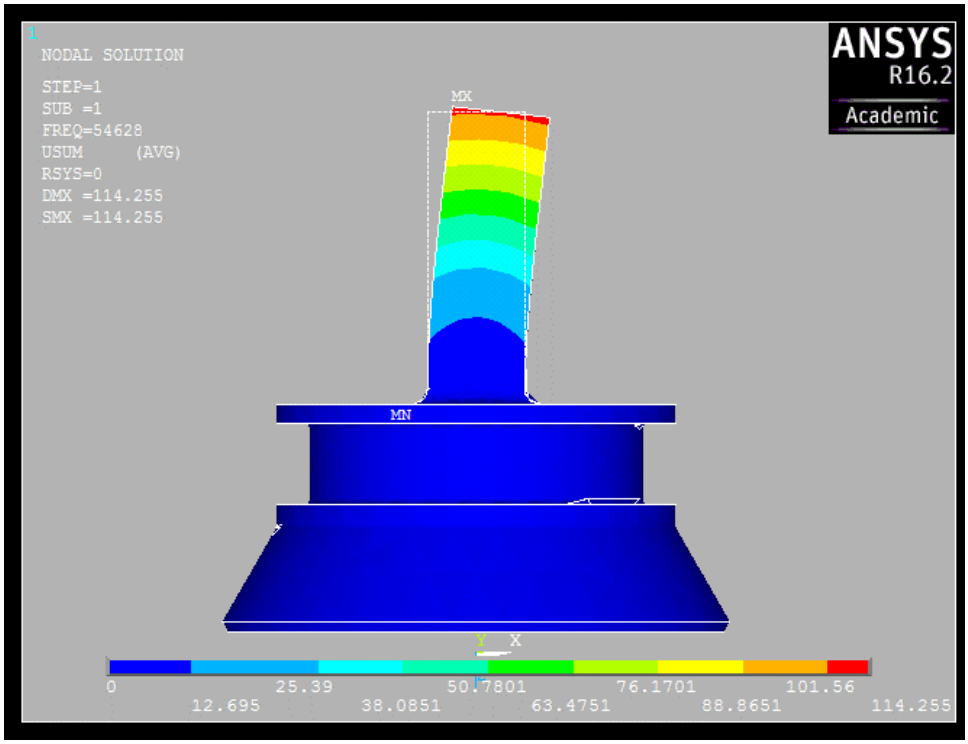

Figure E2. Sensor probe peak deflections at lowest resonant frequency based on modal analysis using ANSYS. FREQ is the resonance frequency of the sensor in Hz while DMX is the maximum deflection. The undeformed probe is shown in dashed white lines.

Appendix F

Details of Fabrication of Refiner Force Sensor

Figure F1a shows the hole made in the stator plate for accommodating the sensor. The RFS-type sensors were then custom designed and built at the University of Victoria based on the design previously used in refiner trials with some minor modifications. The components of the sensor including housing, probe, O-ring used between probe and housing, conical spacer, plug, set-screw, castellated spacer which provides the backing-screw to an uninterrupted mating surface, and backing-screw for affixing the sensor to the refiner plate are depicted in Figure F1b, prior to assembly. Sensor wiring is routed to the outside through two small conduits in the housing. The wiring passages, not shown in the figure, were sealed with silicone. The sealing method operates in an 180^0 C and 1MPa saturated steam test environment [73]. Finally, the LC refiner door was drilled to enable sensor wires pass from the back side of the sensors through a custom gland located in the door of the refiner, to which the stator plate is secured, as shown in Figure F1c and F1d. The approach offers effective sealing against the steam test environment.

(a)

(b)

(c)

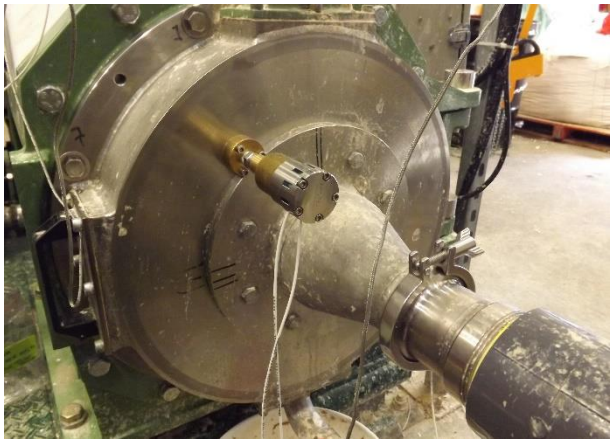

(d)

Figure F1. (a) The hole in the stator plate for accommodating the sensor, (b) components of the sensor before assembly, (c) drill of LC refiner door to enable sensor wires pass from the back side of the sensors, (d) custom gland

Appendix G

The Method of Calibration of Refiner Force Sensor

The relation between piezo and force hammer voltage responses are expressed are follows:

$$(v_A)_{normal} = k_1 F_n \quad \text{Equation 1}$$

$$(v_B)_{normal} = k_2 F_n \quad \text{Equation 2}$$

$$(v_A)_{shear} = k_3 F_s \quad \text{Equation 3}$$

$$(v_B)_{shear} = k_4 F_s \quad \text{Equation 4}$$

where v_A and v_B are the voltages measured from piezo A and piezo B, respectively and F_N and F_S are normal and shear forces, respectively. By applying superposition:

$$v_A = k_1 F_n + k_3 F_s \quad \text{Equation 5}$$

$$v_B = k_2 F_n + k_4 F_s \quad \text{Equation 6}$$

Equations 5 and 6 can be written in matrix format as follows:

$$\begin{Bmatrix} v_A \\ v_B \end{Bmatrix} = \begin{bmatrix} k_1 & k_3 \\ k_2 & k_4 \end{bmatrix} \begin{Bmatrix} F_n \\ F_s \end{Bmatrix} \quad \text{Equation 7}$$

The normal and shear forces are then related to piezoelectric voltage responses by inverting Equation 7. The formulas are referred as the normal and shear sensitivity equations.

$$\begin{Bmatrix} F_n \\ F_s \end{Bmatrix} = \frac{1}{det[K]} \begin{bmatrix} k_4 & -k_3 \\ -k_2 & k_1 \end{bmatrix} \begin{Bmatrix} v_A \\ v_B \end{Bmatrix} \quad \text{Equation 8}$$

$$F_n = \frac{1}{k_1 k_4 - k_3 k_2} (k_4 v_A - k_3 v_B) \quad \text{Equation 9}$$

$$F_s = \frac{1}{k_1 k_4 - k_3 k_2} (-k_2 v_A + k_1 v_B) \quad \text{Equation 10}$$

The calibration constants and the normal and shear sensitivity equations are calculated for a typical sensor:

$$\left.\begin{matrix} k_1 = -0.0646 \\ k_2 = -0.0714 \\ k_3 = 0.2831 \\ k_4 = 0.1258 \end{matrix}\right\} [V/N] \quad \text{Equation 11}$$

$$\left.\begin{matrix} F_n = (-4.4384 v_A - 9.988 v_B) \\ F_s = (2.5188 v_A - 2.2802 v_B) \end{matrix}\right\} \quad \text{Equation 12}$$

Appendix H

Harirforoush, R., Olson, J., Wild, P. (2017): In-process detection of fiber cutting in low consistency refining based on measurement of forces on refiner bars. TAPPI Journal, 16(4), 189-199.

In-process detection of fiber cutting in low consistency refining based on measurement of forces on refiner bars

R. HARIRFOROUSH, J. OLSON, AND P. WILD

ABSTRACT: A major drawback of low consistency refining is the degradation of mechanical properties due to fiber cutting at high refining energies. Conventional strategies to avoid fiber cutting are based on post-refining measurement of pulp properties and, typically, this does not enable rapid adjustment of refiner operation in response to the onset of fiber cutting. The objective of this study is to detect the onset of fiber cutting by using custom-designed piezoelectric force sensors that measure shear and normal forces applied to pulp fibers by the refiner bars. Trials are performed in an AIKAWA/Advanced Fiber Technologies Inc. 16-in. single-disc low consistency refiner. The trials are run using mechanical softwood SPF (spruce, pine, and fir) pulp with 378 ml CSF at 2.5% and 3.5% consistency at rotational speeds of 800 rpm, 1000 rpm, and 1200 rpm. Distributions of the peak normal and shear forces and peak coefficient of friction are determined for each operating condition, and a two-parameter Weibull function is fit to each of these distributions. The scale parameter, which is one of the key parameters of the Weibull function, is calculated, and length-weighted fiber length is plotted as a function of this parameter. The results show that the onset of fiber cutting consistently corresponds to a distinct transition in the plot of length-weighted fiber length versus scale parameter. This transition is believed to be caused by a fundamental transition in the fiber-bar interaction. Moreover, frequency analysis of the sensor data shows that the magnitude of the dominant frequency remains relatively constant while the plate gap is reduced, up to a threshold value, which corresponds to the onset of fiber cutting. These results suggest that these sensors have potential to be used for in-process detection of the onset of fiber cutting.

Application: The application of this study is in-process detection of fiber cutting in low-consistency mechanical refining.

Mechanical pulping is an energy intensive process. For example, in British Columbia (BC), 78 refiners consume 5400 GWh/yr or 11% of BC's total electrical energy production [1], and the bulk of this energy is consumed in the mechanical pulping process. With the increasing cost of energy, the long-term survival of mechanical pulping may depend on reducing energy consumption of this process.

One method of diminishing energy consumption in mechanical pulping is to decrease the number of refining treatments at high consistency (HC) and increase the number of treatments at low consistency (LC). LC refining of mechanical pulp has been shown to be more energy efficient than conventional HC refining [2-5]. Moreover, LC refining is effective for removal of shives, external fibrillation of fibers, removal of latency, and improving fiber networking and bonding capabilities [6,7]. However, the degradation of mechanical properties due to fiber cutting at high refining energies has limited the widespread adoption of LC refining [1]. Understanding the relation between refiner operating conditions and resulting pulp properties is essential to reduce fiber cutting.

In mechanical refining, as the plate gap is closed, fibers are subjected to increasing compressive and shear forces that lead to an increase in net refiner power. Based on pilot and mill-scale LC refining studies, Luukkonen et al. found that the plate gap is a key link between the refiner process variables and resulting changes in pulp properties [1]. In a separate study, Luukkonen et al. [8] proposed a methodology to correlate operating conditions to pulp quality by relating the refiner operating conditions (i.e., power, flow rate, rotational speed, and plate gap) to fiber quality (i.e., fiber length and freeness) and then relating fiber quality to pulp handsheet quality (i.e., tensile, tear, and bulk). They also showed that pulp quality remains constant as the gap is closed, until a critical gap, which is characterized by the onset of significant fiber cutting, is reached. Beyond the critical gap, fiber cutting commences and paper strength is reduced. Moreover, beyond this point, the relationship between refining power and plate gap deviates from linearity [9].

Similar results were observed by Nugroho [10] for various mixes of softwood and hardwood chemical pulps in LC refining. Refining power increased as the plate gap decreased and, at a critical gap between 0.3 to 0.5 mm, the power sharply increased. Moreover, the fiber length and freeness decreased

when the plate gap reached the critical gap. This transition occurred for all of the trial conditions.

Elahimehr et al. [11] studied the relationship between fiber length and plate gap in a AIKAWA 16-in. pilot-scale LC refiner. Trials were run at three rotational speeds, with four refiner plate patterns, and at 3% consistency. They found that mean fiber length was unchanged until the plate gap reached a critical gap, near 0.25 mm. The mean fiber length significantly decreased for the plate gaps smaller than the critical gap. Results also showed that increasing the rotational speed increases the critical gap.

Berg et al. [12] found that power increases linearly as the plate gap is reduced over the range of 0.1–0.2 mm in a two-zone TwinFlo72 LC refiner. They calculated average forces applied to fibers using the expression developed by Kerekes [13]. Fiber cutting was defined as the point where the ratio of outlet to inlet fiber length was equal to 0.95. Plate gap, forces on fibers, and specific edge load (SEL), defined as the energy expended per unit refiner bar length over one bar-crossing event, were found to predict fiber cutting.

In all of the studies previously discussed here, fiber cutting is detected by post-refining measurement of pulp properties. Typically, this approach does not enable rapid in-process adjustment of refiner operation in response to the onset of fiber cutting. These studies also do not address the mechanical interactions between fibers and refiner bars. Kerekes [14] suggests that bar force (i.e., the force applied to pulp fibers by the refiner bars) is the key parameter between bars and fibers in refining that cause important changes in fiber properties.

A piezoelectric sensor has been developed to measure bar forces. The sensor uses the piezoelectric effect, which is the ability of certain materials to generate an electric charge in response to applied mechanical stress. This sensor, referred to here as the refiner force sensor (RFS), has a sensing probe that replaces a short length of a refiner bar, enabling measurement of forces normal to and tangential to the refiner bars. The RFS has been used in a number of studies in both low consistency [15,16] and high consistency refining [17,18]. In a recent study, Harirforoush et al. [19] investigated the relation between net power, gap, and forces on bars in LC refining using the RFS. They found that, as the plate gap is reduced, the length-weighted fiber length remains relatively constant while net refiner power and the mean peak normal and shear forces increase up to threshold values. Here, peak refers to the maximum value that occurs as a bar on the rotor passes over the sensor. Above these thresholds, the mean peak normal and shear forces continue to increase, but the length-weighted fiber length exhibits negative linear relationship with these forces.

The objective of this study is to investigate the onset of fiber cutting based on analysis of bar forces measured with the RFS at a wide range of rotational speeds at 2.5% and 3.5% consistency. Distributions of the peak normal and shear forces, and peak coefficient of friction (i.e., peak shear force divide by peak normal force) are determined for each operating condition. Distinct transitions occur in these distributions that correspond to the onset of fiber cutting. In addition, frequency analysis of the sensor data shows that the magnitude of the dominant frequency can be used as an indication of the onset of fiber cutting.

MATERIALS AND METHODS

Trials were conducted using the AIKAWA 16-in. single-disc refiner at the Pulp and Paper Center at the University of British Columbia (Vancouver, BC, Canada). The refiner is equipped with a power meter, plate actuation, and a variable speed drive. The plate used in these trials is manufactured by AIKAWA FINEBAR, which has bar edge length of 2.74 km/rev and bar angle of 15° from radial. The bar width, groove width, and groove depth of the plate are 1.6 mm, 3.2 mm, and 4.8 mm, respectively.

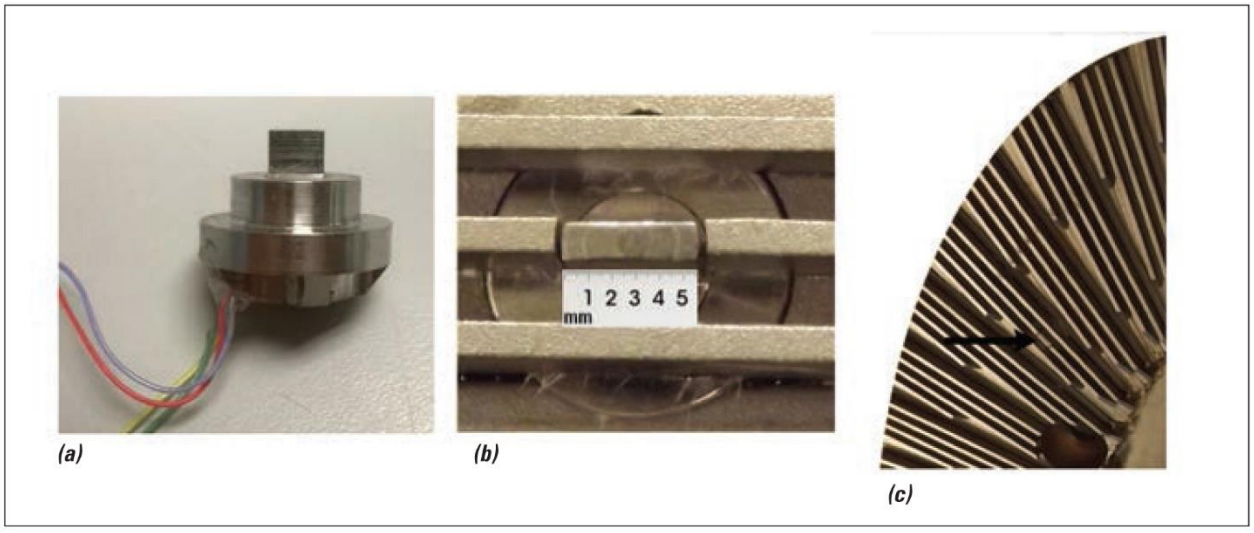

1. (a) Refiner force sensor (RFS) used at the Pulp and Paper Center, University of British Columbia (Vancouver, BC, Canada) trials, (b) a close-up of RFS installed in the stator plate, and (c) the location of the sensor in the stator plate [19].

An RFS-type sensor was custom designed and fabricated based on the design previously used in refiner trials [20]. A photograph of the RFS used in this work is shown in **Fig. 1a**. The sensor is installed in a custom recess that is machined into the back of the stator plate. The sensor wires pass from the back side of the sensor and through a custom gland located in the door of the refiner. The sensor recess is located so that the tip of the sensor replaces a short length of the refiner bar (i.e., 5 mm), as shown in Fig. 1b. The sensor measures force normal to the plate surface (i.e., parallel to the axis of the refiner bar) and the shear force perpendicular to the major axis of the refiner bar and normal to the bar edge. The sensor is positioned in the second bar of a three-bar cluster at a radius of 151 mm, as shown in Fig 1c. At this radius, the heads of the bolts do not pass over the sensor. The 144 bars on the rotor, grouped into 48 three-bar clusters, cross over the sensor in one revolution of the refiner.

Calibration and environmental tests were performed as described in [19,21]. Modal analyses were performed to ensure that the first natural frequency of the sensor is well above the bar-passing frequency of the refiner so that phase and magnitude distortion due to sensor resonance is avoided. The ratio of the first natural frequency of the sensor to the maximum bar-passing frequency is 8.2, which provides a sufficient margin above the bar passing frequency.

A custom charge amplifier converts the high impedance charge output of the sensors to a low impedance voltage signal that is read by a National Instruments (Austin, TX, USA) PXI 1042 Q high-speed board. National Instrument BNC-2110, Shielded Connector Blocks are used to connect the high-speed DAQ board to the charge amplifier. A custom LabVIEW (National Instruments; Austin, TX, USA) interface is used to control data acquisition. A sampling rate of 150 kHz is used, which is more than twenty times the maximum bar-passing frequency that occurs during the trials.

Mechanical SPF (40% spruce; 45% pine; 10% balsam fir and 5% Douglas fir) softwood pulp, produced at Quesnel River Pulp Mill, with 378 ml CSF at 2.5% and 3.5% consistency was used in all trials. The operating conditions for the trials are shown in **Table I**. The refining operating mode was mono-flo with one inlet perpendicular to the outlet. The refiner speed was set with a variable frequency drive (VFD). The plate gaps were adjusted using a controller from no-load position (3.5 mm) to the smaller plate gaps (0.25 mm). The flow rate was held constant at 250 L/min. Sensor signals were recorded using the LabVIEW interface for approximately 10 s once reaching stable condition at each target point. At each operating condition, the refiner was held steady for about 10 s to give the pulp time to move from the refining zone to the sample collection point. A 2-L pulp sample was collected over a 5 s interval. The process was repeated until all of the target points were achieved for one rotational speed. Then, the plate gap was increased to the no-load position and the refiner was adjusted to the next rotational speed using the VFD.

The length-weighted fiber length (L_W) was measured for all pulp samples using a Fiber Quality Analyzer (HiRes FQA, Optest Equipment Inc.; Hawkesbury, ON, Canada). Length-weighted fiber length is calculated based on Eq. (1) [22]:

$$L_w = \frac{\sum n_i L_i^2}{\sum n_i L_i} \quad (1)$$

where, n_i and L_i are the number of the fibers in the ith class and mean length of the ith class, respectively.

An algorithm was created in MATLAB (Mathworks; Natick, MA, USA) to identify bar-passing events in the force data. A bar-passing event is defined to occur when the passage of a rotor bar over the sensor results in a maximum or peak value in the force data that exceeds a predefined threshold value. The algorithm and its verification are described in [19].

For each bar-passing event, peak force is defined as the difference between the force at the base of the local valley that precedes the peak and the force at the peak [16]. The peak coefficient of friction is calculated by dividing the peak shear force by the peak normal force. The peak force and peak coefficient of friction data are assessed in the form of distributions to which the two-parameter Weibull distribution function is fit.

The Weibull distribution function is widely used because of its ability to characterize a wide variety of distributions, and

Parameter	Condition	
Refiner speed, rpm	800, 1000, 1200	1200
Consistency	3.5 %	2.5 %
Flow rate, L/min	250	
Plate gap, mm	3.5–0.25 (15 gaps)	3.5–0.25 (12 gaps)
Operating mode	Mono-flo	
Pulp type	Mechanical SPF softwood pulp, starting freeness at 378 ml CSF	

I. Operating conditions for the pilot-scale low consistency refining trials at the Pulp and Paper Center, University of British Columbia.

it has been used in previous HC and LC refining studies [15,17]. The Weibull distribution function is shown in Eq. (2) [23]:

$$f(x) = \frac{\beta}{\eta}\left(\frac{x-\gamma}{\eta}\right)^{\beta-1} exp^{-\left(\frac{x-\gamma}{\eta}\right)^{\beta}} \quad (2)$$

where, β, η, and γ are shape, scale and location parameters, respectively. The effects of these parameters on the Weibull distribution are discussed by Lee [24]. The two-parameter Weibull distribution function is obtained by setting in Eq. (2). In this study, the Weibull scale and shape parameters of the peak normal, shear force, and peak coefficient of friction distributions are calculated for each operating condition. Each of these parameters are then correlated to both plate gap and L_W.

RESULTS

The relation between net power and the inverse of plate gap for three rotational speeds (i.e., 1200 rpm, 1000 rpm, and 800 rpm) at 3.5% consistency and 1200 rpm at 2.5% consistency is shown in **Fig. 2**. In all cases, the net power increases as the plate gap is reduced. However, a considerable increase in energy transferred to the fibers is seen for gaps of less than 0.5 mm (or more than 2 mm^{-1}). At a constant gap and consistency, increasing the rotational speed increases the net power. The relationships are similar to the results of Nugroho [10], Elahimehr et al. [11], and Harirforoush et al. [19]. Across the full range of gaps at 1200 rpm, the net power for 3.5% and 2.5% consistency are approximately equal.

The relation between L_W and the inverse of plate gap for three rotational speeds (i.e., 1200 rpm, 1000 rpm, and 800 rpm) at 3.5% consistency and 1200 rpm at 2.5% consistency is shown in **Fig. 3**. In each case, L_W remains relatively constant as the plate gap is closed until the gap reaches the critical value, indicated by the dashed lines. The critical values are determined based on transitions in the plot of L_W versus the inverse of plate gap. For plate gaps smaller than the critical gap, L_W decreases in an approximately linear manner.

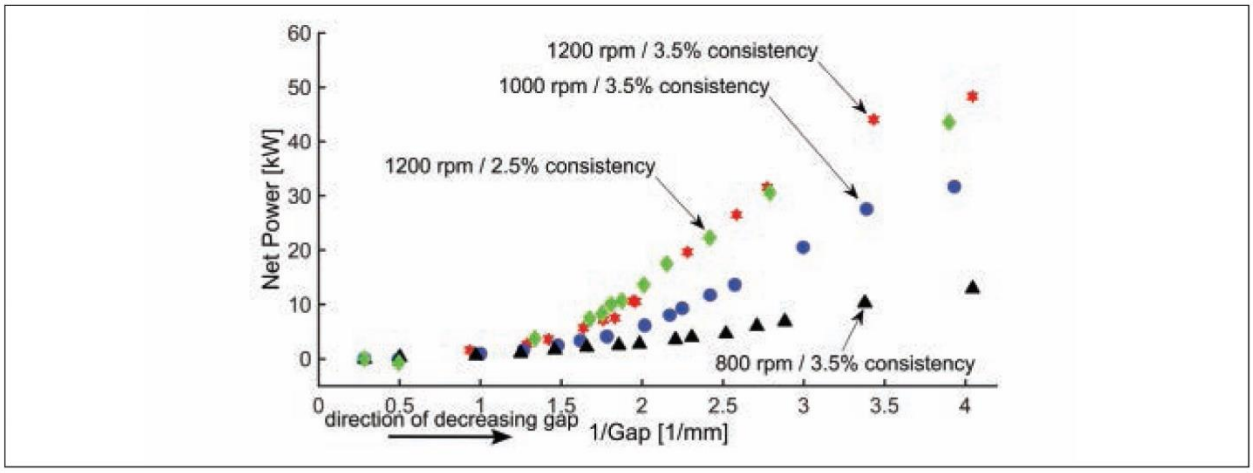

2. Net power versus the inverse of plate gap for three rotational speeds (i.e., 1200 rpm, 1000 rpm, and 800 rpm) at 3.5% consistency. Data is also shown for 1200 rpm at 2.5% consistency.

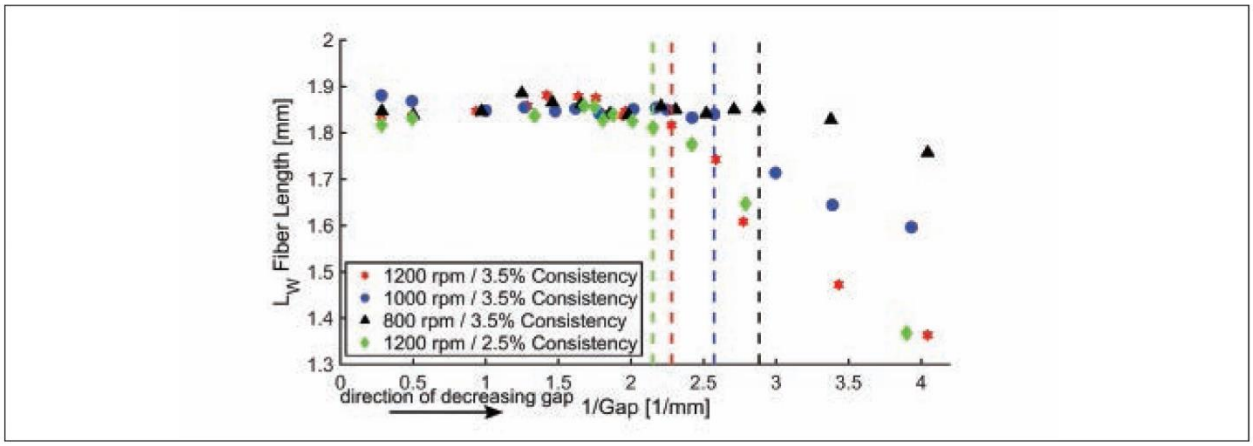

3. L_w versus the inverse of plate gap for three rotational speeds (i.e., 1200 rpm, 1000 rpm, and 800 rpm) at 3.5% consistency. Data is also shown for 1200 rpm at 2.5% consistency.

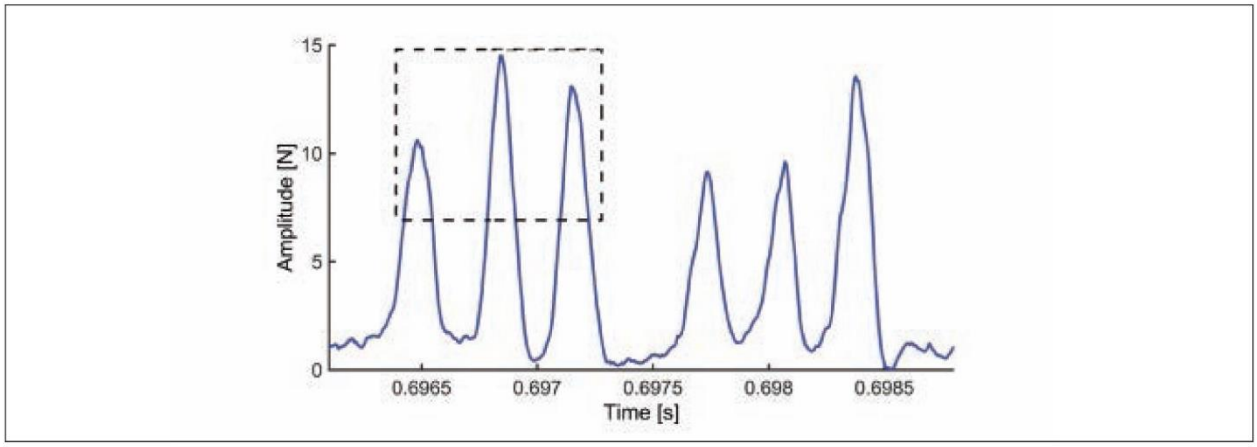

4. Typical unfiltered normal force data at 1000 rpm and 0.45 mm plate gap.

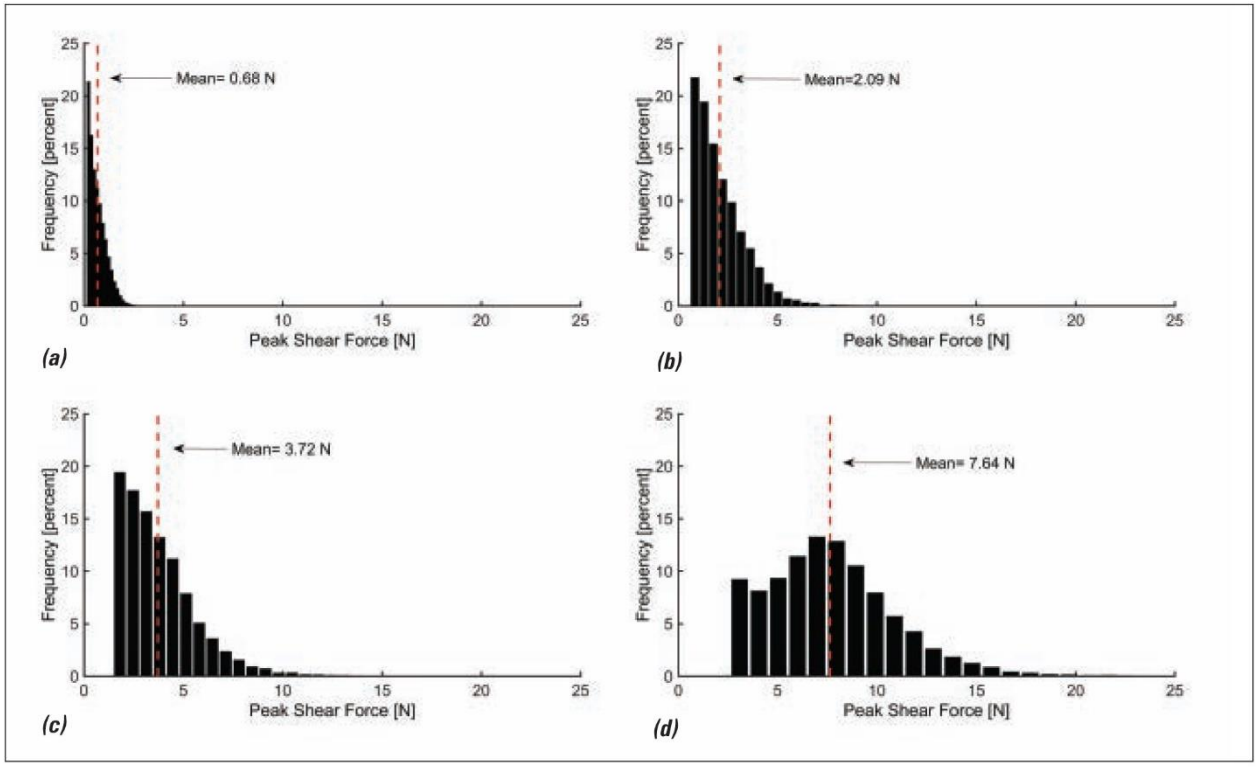

5. Normalized distributions of peak shear force for plate gaps of (a) 3.5 mm, (b) 0.55 mm, (c) 0.4 mm, and (d) 0.3 mm for rotational speed of 1200 rpm at 3.5% consistency.

Figure 3 also shows that, at the same consistency (i.e., 3.5%), the critical gap decreases as rotational speed decreases. This finding is consistent with the results of Nugroho [10], Elahimehr et al. [11], and Harirforoush et al. [19]. Moreover, the red dashed line representing the critical gap for 1200 rpm at 3.5% consistency occurs where 1/Gap = 2.282 (or gap = 0.438 mm), while the green dashed line indicating the critical gap for 1200 rpm at 2.5% consistency occurs where 1/Gap = 2.155 (or gap = 0.464 mm). Thus, at the same rotational speed, decreasing the consistency from 3.5% to 2.5% slightly increases the critical gap. This trend is not in agreement with Lundin [25], who reported that decreasing the consistency from 6% to 3% decreases the critical gap from 0.27 mm to 0.2 mm.

Typical unfiltered normal force data, taken at 1000 rpm and a plate gap of 0.45 mm, is shown in **Fig. 4**. Each peak represents a bar-passing event. As highlighted by the dashed rectangle, bar-passing events appear as clusters of three peaks, since the bars of the rotor that cross over the force sensor are grouped in three-bar clusters.

Normalized distributions of peak shear force data for plate gaps of 3.5 mm (no-load), 0.55 mm, 0.4 mm, and 0.3 mm for 1200 rpm at 3.5% consistency are shown in **Fig. 5**. The mean

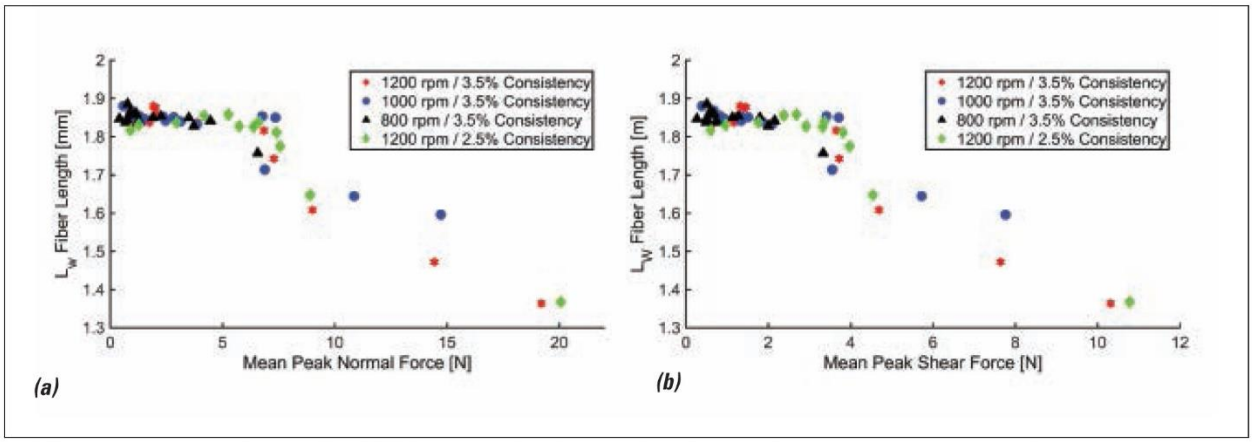

6. (a) L_w versus mean peak normal and (b) shear force for three rotational speeds (i.e., 1200 rpm, 1000 rpm, and 800 rpm) at 3.5% consistency. Data is also shown for 1200 rpm at 2.5% consistency.

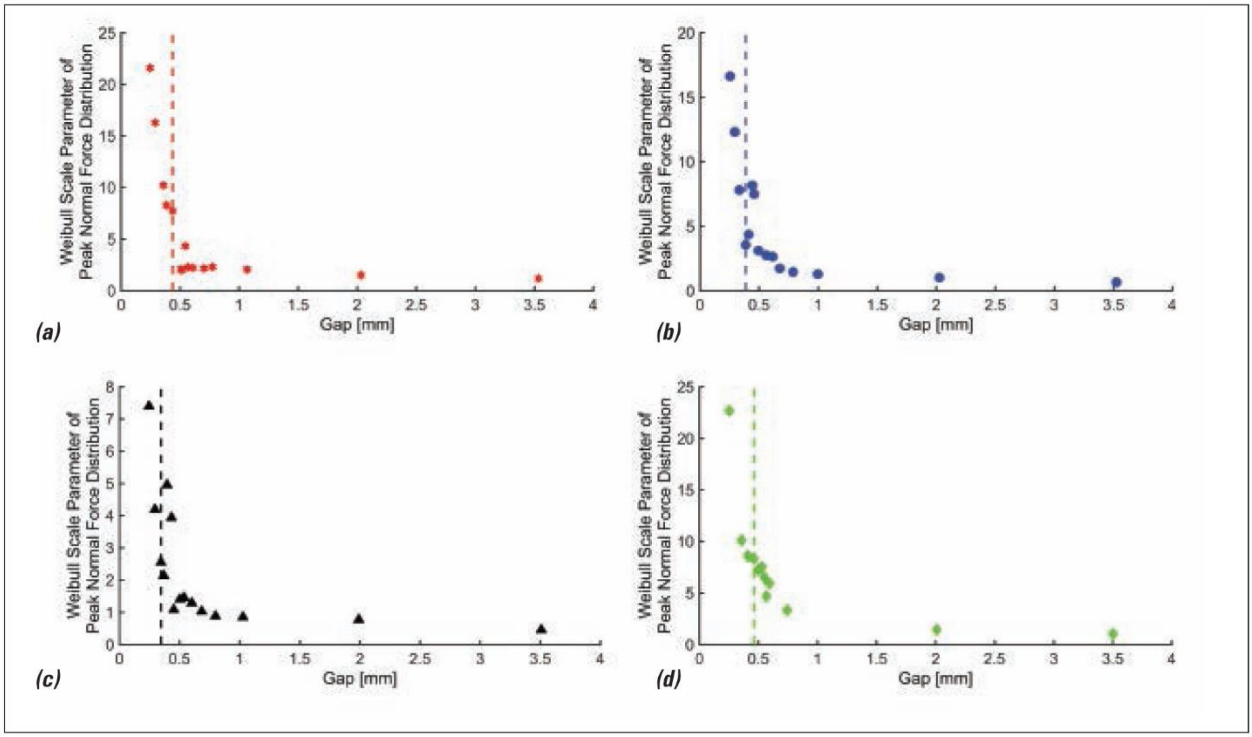

7. The Weibull scale parameter of peak normal force distribution versus plate gap for rotational speeds of (a) 1200 rpm, (b) 1000 rpm, (c) 800 rpm at 3.5% consistency, and (d) 1200 rpm at 2.5% consistency.

value of the peak shear force distribution, highlighted by the dashed line, increases as the plate gap decreases, which is consistent with the increase in net refiner power. This result is in agreement with the results of Prairie et al. [15], who showed that the median forces increase with increasing specific edge load (SEL). Moreover, as the plate gap is closed, the distribution of peak shear forces is extended to the right, its height decreases, and the shape of the distribution changes from positively skewed to an approximately normal distribution. The truncation of the left-hand end of the distributions shown in Figs. 5b, 5c, and 5d is an artefact of the algorithm used to identify bar-passing events. This algorithm, which is described in [19], discards events that fall below a prescribed threshold.

Figure 6 shows the relationship between L_W and mean peak force for three rotational speeds (i.e., 1200 rpm, 1000 rpm, and 800 rpm) at 3.5% consistency and 1200 rpm at 2.5% consistency. As shown in Fig. 6a, L_W remains relatively unchanged as mean peak normal force increases up to a threshold value that corresponds to the critical gap. The L_W value decreases in an approximately linear manner beyond the critical gap threshold. The trend is consistent with the results of Harirforoush et al. [19]. The mean peak normal force at this

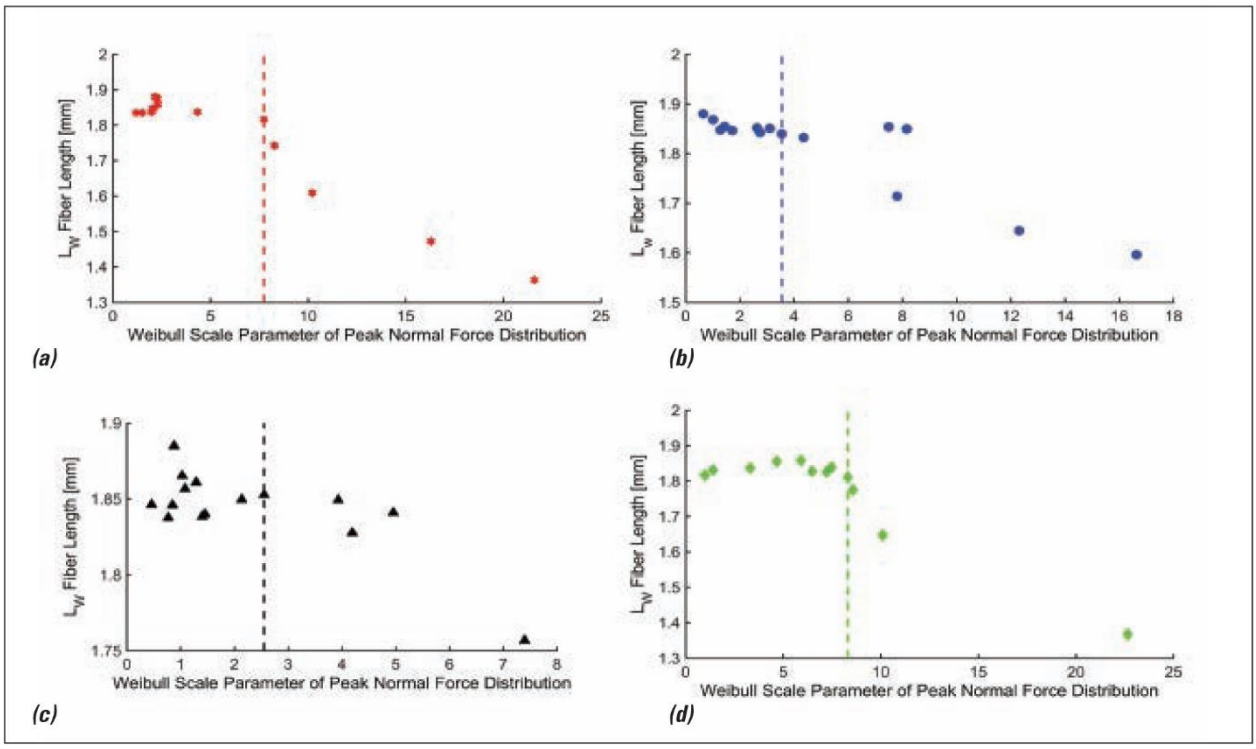

8. L_w versus the Weibull scale parameter of peak normal force distribution for rotational speeds of (a) 1200 rpm, (b) 1000 rpm, (c) 800 rpm at 3.5% consistency, and (d) 1200 rpm at 2.5% consistency.

threshold is relatively constant, approximately 7 N, for all rotational speeds at 3.5% consistency. Decreasing the consistency from 3.5% to 2.5% slightly increases this threshold value.

A similar trend is seen in the relationship between L_W and mean peak shear force (Fig. 6b). However, the threshold value at which the transition occurs is lower, approximately 3.8 N. For 800 rpm, possibly due to insufficient data for the plate gaps less than the critical gap, the trend cannot be seen.

To explore the relationship between the distribution of peak force and plate gap, the Weibull scale parameter of peak normal force distribution is plotted versus plate gap for three rotational speeds (i.e., 1200 rpm, 1000 rpm, and 800 rpm) at 3.5% consistency and 1200 rpm at 2.5% consistency. As shown in **Fig. 7a**, as the plate gap is decreased, the scale parameter remains relatively constant up to a threshold value. The threshold, highlighted by dashed line, corresponds to the transition seen in the plot of L_W versus the inverse of plate gap for 1200 rpm at 3.5% consistency, Fig. 3. This transition is in agreement with the onset of the fiber cutting. The trend also appears in Figs. 7b, 7c and 7d but is less definitive for 800 rpm at 3.5% consistency, Fig. 7c, and 1200 rpm at 2.5% consistency, Fig. 7d.

The relation between the distribution of peak forces and fiber length is investigated by plotting L_W versus the Weibull scale parameter of peak normal force distribution for three rotational speeds (i.e., 1200 rpm, 1000 rpm, and 800 rpm) at 3.5% consistency and 1200 rpm at 2.5% consistency. As shown in **Fig. 8a**, the length-weighted fiber length remains relatively constant as the scale parameter increases up to a threshold value, highlighted by dashed line. The dashed line corresponds to the transition seen in the plot of L_W versus the inverse of plate gap, Fig. 3, and it is at the same position as the dashed line shown in Fig. 7a. The L_W value decreases beyond this point. This point corresponds to the onset of fiber cutting. Similar trends occur in Figs. 8b, 8c, and 8d but are less definitive for 1000 rpm, Fig. 8b, and 800 rpm, Fig. 8c. At 800 rpm, pulp flow rate was observed to be unstable which may reflect unstable conditions in the refiner and may also be the cause of anomalous data at this speed.

The mean coefficient of friction is plotted in **Fig. 9a** as a function of SEL for three rotational speeds (i.e., 1200 rpm, 1000 rpm, and 800 rpm) at 3.5% consistency and for 1200 rpm at 2.5% consistency. Mean coefficient of friction decreases with increasing SEL. This result is consistent with Prairie et al. [15]. As shown in Fig. 9b, the mean coefficient of friction decreases as the plate gap is reduced. This finding is in accordance with Senger et al. [26]. The mean coefficient of friction varies from 0.65 to 1.37.

The relationships between L_W and the Weibull scale parameter of the distribution of peak coefficient of friction for three rotational speeds (i.e., 1200 rpm, 1000 rpm, and 800 rpm) at 3.5% consistency and 1200 rpm at 2.5% consistency are shown in **Figs. 10a-10d**. As shown in Fig. 10a, L_W remains relatively constant as the scale parameter decreases to a threshold, highlighted by a dashed line. The dashed line is at the same point as the dashed lines shown in Fig. 7a and Fig 8a, and it is

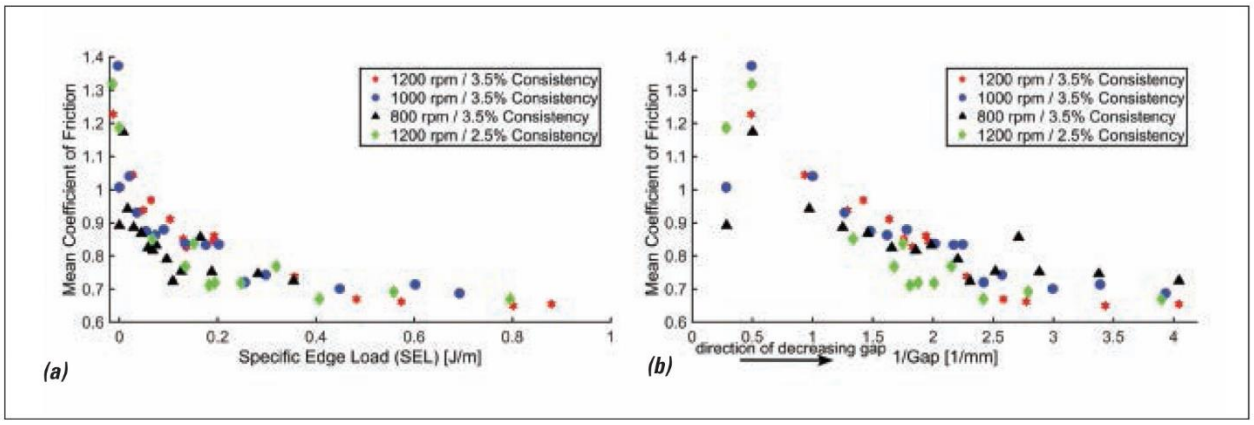

9. (a) Mean coefficient of friction versus specific edge load (SEL), and (b) mean coefficient of friction versus plate gap for three rotational speeds (i.e., 1200 rpm, 1000 rpm, and 800 rpm) at 3.5% consistency. Data is also shown for 1200 rpm at 2.5% consistency.

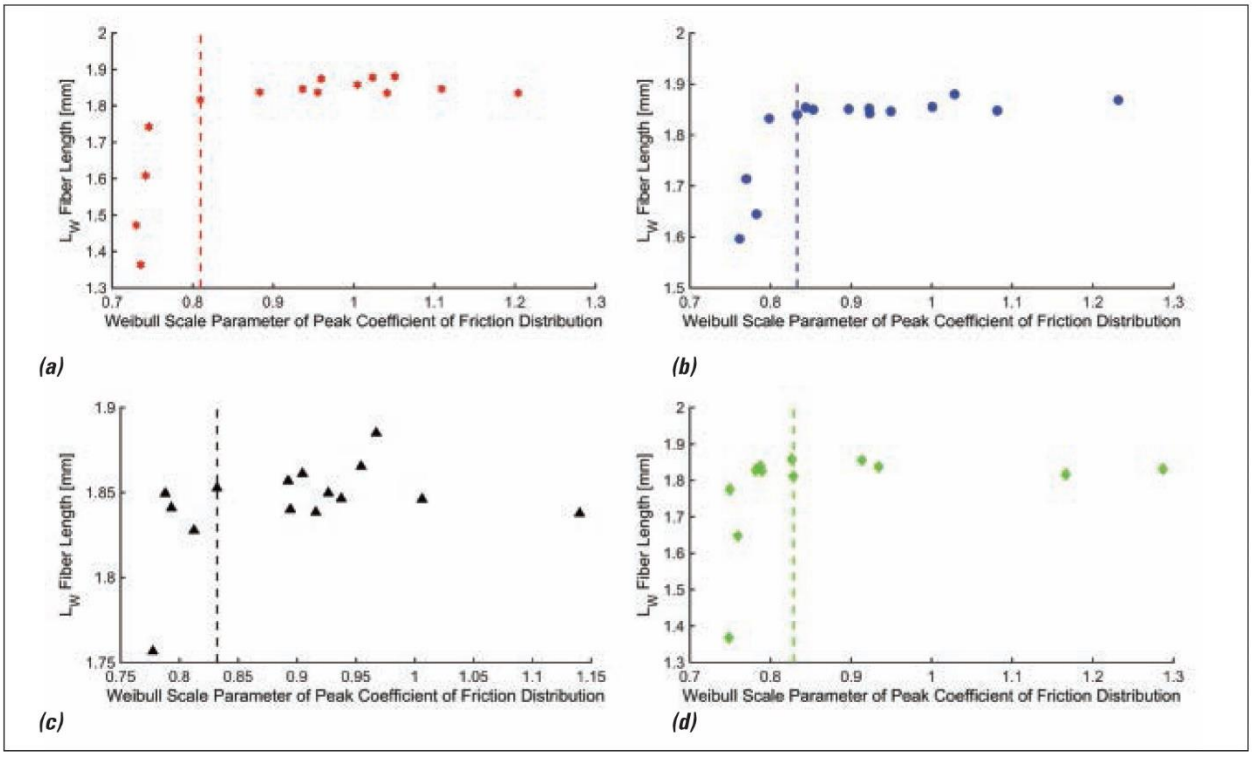

10. L_w versus Weibull scale parameter of peak coefficient of friction distribution for rotational speeds of (a) 1200 rpm, (b) 1000 rpm , (c) 800 rpm at 3.5% consistency, and (d) 1200 rpm at 2.5% consistency.

determined based on the transition seen in the plot of L_W versus the inverse of plate gap, Fig. 3. This point corresponds to the onset of fiber cutting. The L_W value decreases beyond this point. Similar transitions occur in Figs. 10b, 10c, and 10d.

The spectra of the normal force data at 1200 rpm, plate gaps of 0.45 mm and 0.55 mm, and 3.5% consistency show four maxima at frequencies of 3.82, 2.87, 1.90, and 0.95 kHz, highlighted by dashed circles, **Fig. 11**. The frequencies correspond to crossings of different bars within the three-bar clusters of the rotor, as described in [19]. The highest amplitude, marked by the arrow, corresponds to the passage of equivalent edges in adjacent three-bar clusters. This frequency, referred to here as the dominant frequency ($Freq_d$), appears in the frequency analysis for all of the operating conditions. Comparing Fig. 11a and Fig. 11b, it is apparent that the amplitude (magnitude) at this frequency is affected by the plate gap.

Figure 12 shows the magnitude of the dominant frequency, ($Freq_d$), versus plate gap for three rotational speeds (i.e., 1200 rpm, 1000 rpm, and 800 rpm) at 3.5% consistency and 1200 rpm at 2.5% consistency for normal force data. As shown in Fig. 12a, the magnitude remains relatively constant while the plate gap is reduced up to a threshold value, which

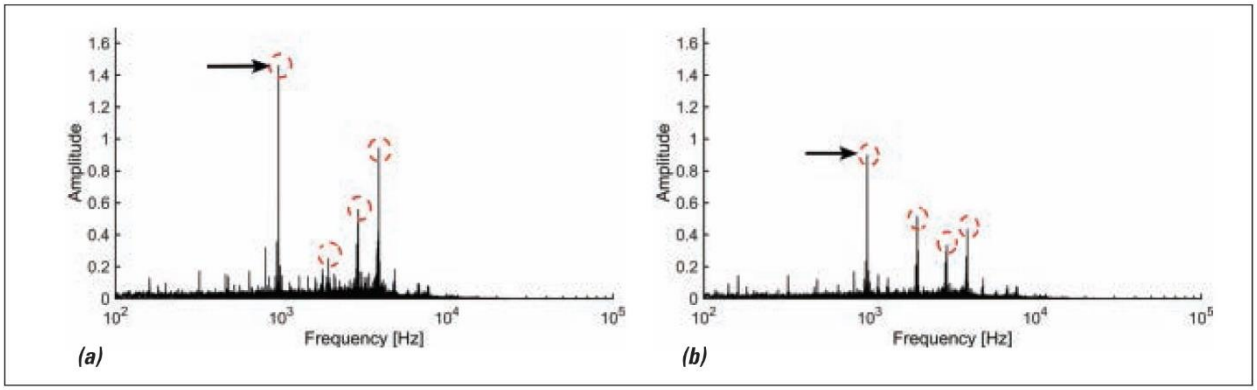

11. Spectrum of normal forces at plate gaps of (a) 0.45 mm and (b) 0.55 mm for rotational speed of 1200 rpm and 3.5% consistency.

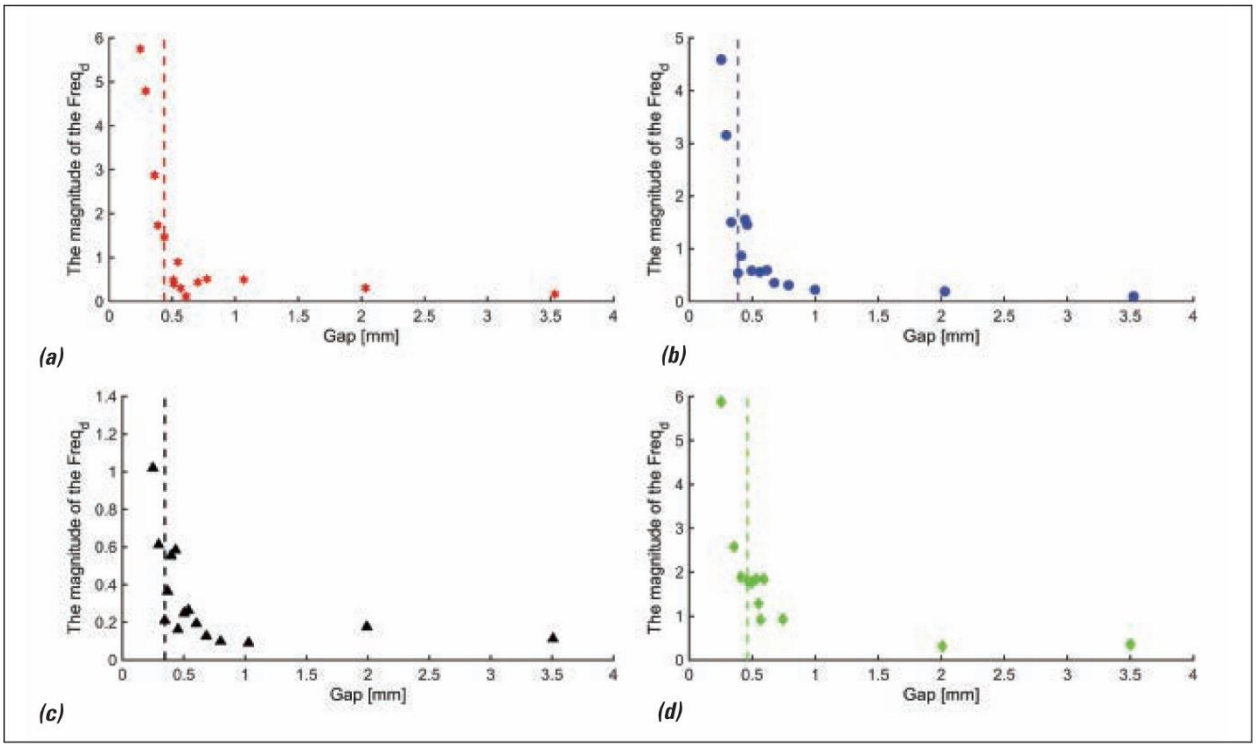

12. The magnitude of the frequency corresponds to the passage of equivalent edges in adjacent three-bar clusters versus the plate gap for rotational speeds of (a) 1200 rpm, (b) 1000 rpm, (c) 800 rpm at 3.5% consistency, and (d) 1200 rpm at 2.5% consistency.

corresponds to the onset of fiber cutting, indicated by dashed lines. This trend is present but less definitive for 800 rpm, Fig. 12c, and 1200 rpm at 2.5% consistency, Fig. 12d.

The trends shown in Figs. 7, 8, and 12 also appear in the peak shear force distributions. This data is not included here in the interest of brevity.

DISCUSSION

The RFS measures normal force and shear force, perpendicular to the major axis of the refiner bar, in a single-disc LC refiner. The bar-passing events are characterized as distributions of event parameters such as peak normal and shear forces and peak coefficient of friction. These distributions are used to compare refining conditions on the basis of data taken at each operating condition. Distinct transitions are observed in parameters that characterize these distributions; in particular, mean peak force and the Weibull scale parameter. These transitions consistently correspond to the onset of fiber cutting.

As the plate gap is reduced, mean peak normal and shear forces increase but L_W remains relatively constant, up to a threshold value of mean peak normal and shear force. The L_W value decreases in an approximately linear manner beyond these threshold values, as shown in Fig. 6. These transitions correspond to the onset of fiber cutting. Above these thresholds, mean peak forces continue to increase but L_W exhibits a

negative linear relationship with force that mirrors the established relationship between L_W and the inverse of plate gap (Fig. 3). The trend is consistent with the results in [19].

The Weibull scale parameter of the peak force distributions and of peak coefficient of friction distributions are also candidates for in-process detection of fiber cutting. As shown in Fig. 8 and Fig. 10, transitions occur in length-weighted fiber length at the values of the scale parameters that correspond to the onset of fiber cutting. Note that the position of these transitions, indicated by the dashed lines, correspond to the transitions seen in the plot of L_W versus the inverse of plate gap shown in Fig. 3.

In addition to these indicators of fiber cutting found in the time domain data, the power spectrum of the sensor data can also be used to detect the onset of fiber cutting. As shown in Fig. 12, as the plate gap is reduced, the magnitude of the dominant frequency, which is equal to the bar-passing frequency, remains relatively constant up to a threshold value that corresponds to the onset of fiber cutting. Beyond this threshold, the amplitude increases. According to Parseval's theorem, the magnitude of the spectrum at a given frequency is equal to the energy transferred at that frequency. Therefore, this transition in the spectrum may be due to a fundamental change in the mode of energy transfer to the pulp at the onset of fiber cutting.

These results suggest that the RFS has potential to be used for in-process detection of fiber cutting in mill operations. In previous mill trials, the sensors have been shown to be sufficiently rugged [17] for industrial use. Key challenges to such an application are modification of refiner plates to accommodate the sensors and passage of signal wires from the sensor to the refiner exterior.

CONCLUSION

This study investigates in-process detection of the onset of fiber cutting using a custom designed piezoelectric sensor measuring normal and shear forces, perpendicular to the major axis of the refiner bars, in an AIKAWA/Advanced Fiber Technologies Inc. 16-in. single-disc LC refiner. Trials were run using mechanical SPF softwood pulp with 378 ml CSF at 2.5% and 3.5% consistency for three rotational speeds (1200, 1000, and 800 rpm) and a wide range of plate gaps. The pulp was sampled at regular intervals, and the length-weighted fiber length was determined for each sample. The data recorded from the sensors were processed and the distributions of the peak normal and shear forces and peak coefficient of friction are determined for each operating condition. A two-parameter Weibull function is fit to each of these distributions. The Weibull scale parameter is calculated and length-weighted fiber length is plotted as a function of this parameter. The results show that the onset of fiber cutting consistently corresponds to a distinct transition in the plot of length-weighted fiber length versus scale parameter. In addition, the power spectrum of the sensor data indicates that the magnitude of the dominant frequency can be used as an indication of the onset of fiber cutting. This result suggests that the sensor has potential to be used for in-process detection of the onset of fiber cutting. **TJ**

ACKNOWLEDGEMENTS

This work is funded by a Collaborative Research and Development grant provided by National Sciences and Engineering Research Council of Canada (NSERC) and the following partners, who we thank for their ongoing support: AB Enzymes, Alberta Newsprint Company, Andritz, BC Hydro, Canfor, Catalyst Paper, FPInnovations, Holmen Paper, Meadow Lake Pulp (Paper Excellence), Millar Western, NORPAC, West Fraser, Westcan Engineering, and Winstone Pulp International.

A special thanks to M. Miller, E. Jahangir, E. Trudel, G. Burton, and G. Soong for their assistance during the preparation and execution of the refining trials at the Pulp and Paper Center at the University of British Columbia.

LITERATURE CITED

1. Luukkonen, A., Olson, J.A., and Martinez, D.M., *J. Pulp Pap. Sci.* 36(1-2): 28(2010).
2. Muenster H., Ferritsius O., Lecourt M., et al., *Proc. Int. Mech. Pulping Conf.*, TAPPI Press, Atlanta, GA, USA, 2005, p. 213.
3. Zha, Q., Lanouette, R., Law, K.-N., et al., *Prepr. - PAPTAC Annu. Meet., 94th*, Pulp and Paper Technical Association of Canada, Montreal, 2008, p. B481.
4. Musselman, R., Letarte, D., and Simard, R., *Int. Refin. Conf., 4th*, Pira International, Leatherhead, UK, 1997, pp.139–148.
5. Sandberg., C., Sundström, L., and Nilsson, L., *Proc. Int. Mech. Pulping Conf.*, TAPPI Press, Atlanta, 2009, p. 186.
6. Kappel, J., *Mechanical Pulps: From Wood to Bleached Pulp*, TAPPI Press, Atlanta, 1999.
7. Smook, G.A., *Handbook for Pulp and Paper Technologists*, 2nd Edn., Angus Wilde Publications, Vanouver, BC, Canada, 1992.
8. Luukkonen, A., Olson, J.A., and Martinez, D.M., *J. Pulp Pap. Sci.*, 36(3-4): 107(2010).
9. Luukkonen, A., Ph.D. thesis, "Development of a methodology to optimize low consistency refining of mechanical pulp," University of British Columbia, Vancouver, 2011.
10. Nugroho, D.D.P., "Low consistency refining of mixtures of softwood and hardwood bleached kraft pulp: Effects of refining power," M.Sc. thesis, Asian Institute of Technology, Khlong Nung, Thailand, 2012.
11. Elahimehr, A., Olson, J.A., and Martinez, D.M., *Nord. Pulp Pap. Res. J.* 28(3): 386(2013).
12. Berg, J.E., Sandberg, C., Engberg, B., et al., *Nord. Pulp. Pap. Res. J.* 30(2): 225(2015).
13. Kerekes, R.J. and Senger, J.J., *J. Pulp Pap. Sci.* 32(1): 1(2006).
14. Kerekes, R.J., *Nord. Pulp Pap. Res. J.* 26(1): 14(2011).
15. Prairie, B., Wild, P., Byrnes, P., et al., *J. Pulp Pap. Sci.* 34(1): 1(2008).
16. Prairie, B., Wild, P., Byrnes, P., et al., *J. Pulp Pap. Sci.* 108(9): 34(2007).
17. Olender, D., Wild, P., Byrnes, P., et al., *J. Pulp Pap. Sci.* 33(3): 163(2007).

18. Olender, D., Wild, P., Byrnes, P., et al., *Nord. Pulp Pap. Res. J.* 23(2): 218(2008).

19. Harirforoush, R., Wild, P., and Olson, J., *Nord. Pulp Pap. Res. J.* 31(1): 71(2016).

20. Olender, D., Wild, P., and Byrnes P., *J. Process Mech. Eng.* 222(Part E): 115(2008).

21. Prairie, B.C., "Measurement of forces in a low consistency refiner," M.Sc. thesis, University of Victoria, Victoria, BC, Canada, 2005.

22. Graca Carvalho, M., Ferriera, P.J., Martins, A.A., et al., *TAPPI J.* 80(2): 137(1997).

23. Prabhakar Murthy, D.N., Xie, M., and Jiang, R., *Weibull Models*, John Wiley & Sons, Hoboken, NJ, USA, 2003.

24. Lee, S., *Int. J. Basic Appl. Sci.* 14(2): 18(2014).

25. Lundin, T., Ph.D. thesis, "Tailoring pulp fibre properties in low consistency refining," Laboratory of Fiber and Cellulose Technology, Abo Akademyi University, Turku, Finland, 2008.

26. Senger, J., Siadat, A., Ouellet, D., et al., *J. Pulp Pap. Sci.* 30(9): 247(2004).

ABOUT THE AUTHORS

Low consistency (LC) refining of mechanical pulp has been shown to be more energy efficient than conventional high consistency refining. However, degradation of mechanical properties due to fiber cutting at high refining energies has limited the widespread adoption of LC refining. In-process detection of the onset of fiber cutting is essential to reduce fiber cutting.

In 2016, we investigated relationships between local bar forces, plate gap, and fiber length in a single-disc low consistency refiner (Harirforoush et al. [19]). The results showed that the sensors have potential for the onset detection of fiber cutting.

Developing the sensor to withstand the harsh conditions inside the refiner was the most difficult aspect of the research here. Our results suggest that these sensors have potential to be used for in-process detection of the onset of fiber cutting.

The most interesting findings we observed were the distinct transitions in parameters that characterize the distributions of bar forces (forces applied to pulp fibers by the refiner bars). These transitions consistently correspond to the onset of fiber cutting. In addition, the power spectrum of the sensor data indicates that the magnitude of the dominant frequency can be used as an indication of the onset of fiber cutting.

For mills, detection of the onset of fiber cutting conditions is potentially beneficial in low consistency refining as it may reduce fiber cutting, optimize fiber quality improvements, and increase energy efficiency. Our next step is to understand the effect of pulp furnish on the distribution of bar forces and investigate the onset of fiber cutting by using the sensor data.

Harirforoush

Wild

Olson

Harirforoush is a Ph.D. candidate in the Department of Mechanical Engineering and the Institute for Integrated Energy Systems (IESVic), and Wild is professor of Mechanical Engineering and director of IESVic, at the University of Victoria, Victoria, BC, Canada. Olson is associate dean of Research and Industrial Partnership, Faculty of Applied Science; professor of Mechanical Engineering; and FPInnovations professor at the University of British Columbia – Point Grey Campus, Vancouver, BC, Canada. Email Harirforoush at rharirfo@uvic.ca.

Appendix I

Harirforoush, R., Olson, J., Wild, P. (2018): Indications of the onset of fiber cutting in low consistency refining using a refiner force sensor: the effect of pulp furnish. Nordic Pulp and Paper Research Journal, 33(1). "Reprinted with permission from Nordic Pulp & Paper Research Journal, accepted for publication in issue 33(1), 2018, http://www.npprj.se/html/main.asp?i=167&h=1&b=1&m=739"

MECHANICAL PULPING
Nordic Pulp & Paper Research Journal Vol 33 no 1, 2018 – DOI

Indications of the onset of fiber cutting in low consistency refining using a refiner force sensor: the effect of pulp furnish

R. Harirforoush, J. Olson and P. Wild

KEYWORDS: Force measurement, Low consistency refining, Sensor, Fiber cutting, Mechanical pulping

ABSTRACT: Detection of the onset of fiber cutting is beneficial in low consistency refining as it may prevent reduction of average fiber length, optimize fiber quality improvements by operating at gaps just wider than the critical gap, avoid decreasing the strength properties of paper, and increase energy efficiency. The objective of this study is to understand the effect of pulp furnish on measured bar forces and, more specifically, on the detection of fiber cutting. Bar forces, i.e. forces applied to pulp fibers by the refiner bars, are measured with a custom-designed piezoelectric force sensor. Trials were conducted with an AIKAWA 16-in. single-disc refiner using hemlock/balsam softwood thermomechanical pulp, SPF softwood thermomechanical pulp, northern bleached softwood kraft pulp, and aspen hardwood thermomechanical pulp at 3.0 to 3.5% consistency at rotational speeds of 1200 and 1400 rpm. The power of the time domain signal of the measured forces is introduced as an indicator of the onset of fiber cutting. Our results show that this new fiber cutting metric is a sensitive and reliable metric for determination of fibre cutting for a range of pulp furnishes. The study suggests that the refiner force sensor has potential to be exploited for in-process detection of fiber cutting.

ADDRESSES OF THE AUTHORS: R. Harirforoush (rharirfo@uvic.ca), University of Victoria, Department of Mechanical Engineering, P.O. Box 3055 STN CSC, V8W 3P6, Victoria, BC, Canada. **J. Olson** (james.olson@ubc.ca), University of British Columbia, Department of Mechanical Engineering, Point Grey Campus, 5000-2332 Main Mall, V6T 1Z4, Vancouver, BC, Canada. **P. Wild** (pwild@uvic.ca), University of Victoria, Department of Mechanical Engineering, P.O. Box 3055 STN CSC, V8W 3P6, Victoria, BC, Canada
Corresponding author: R. Harirforoush

Introduction

A crucial parameter in the production of mechanical pulp through refining is energy consumption. The specific energy consumption of refiner mechanical pulp, defined as the total energy expended per unit mass of fiber, is typically between 1600 and 3000 kWh/t (Bajpai 2016), and the majority of this energy is consumed in refining. In British Columbia (BC), 78 refiners consume 5400 GWh/yr or 11% of BC's total electrical energy production (Luukkonen et al. 2010a). With the increasing cost of energy, the long term survival of mechanical pulping may depend on reducing energy consumption of this process.

One method of reducing energy consumption in mechanical pulping is to decrease the number of refining treatments at high consistency (HC) and increase the number of treatments at low consistency (LC). LC refining of mechanical pulp has been shown to be more energy efficient than conventional HC refining (Muenster et al. 2005; Zha et al. 2008). A reduction of 5-8% in specific energy has been reported without loss in pulp quality (Musselman et al. 1997). It is hypothesized that the uniformity of treatment of LC refining causes the increased efficiency of this approach (Luukkonen et al. 2010a). Moreover, LC refining is effective for removal of shives, external fibrillation of fibers, removal of latency and improving fiber networking and bonding capabilities (Kappel 1999; Smook 1992). However, the degradation of mechanical properties due to fiber cutting at high refining energies has limited the widespread adoption of LC refining. Understanding the relation between refiner operating conditions and resulting pulp properties is essential to reduce fiber cutting.

In mechanical refining, as the plate gap is closed, fibers are subjected to increasing compressive and shear forces. This leads to increasing net refiner power and Specific Edge Load (SEL), which is defined as the energy expended per unit refiner bar length over one bar-crossing event. SEL, introduced by Brecht (1967), is widely used in industry to characterize refining performance. However, Roux and Joris (2005) showed that SEL cannot be used to predict fiber cutting since the effect of plate geometry parameters (i.e. bar width, groove width, and bar angle) are not considered in this theory.

Modified edge load (MEL) theory, developed by Meltzer (1994), is an improvement over SEL theory that includes plate geometry parameters which are absent from SEL theory. However, MEL theory does not account for some important parameters such as consistency, rotational speed, groove depth, and fiber properties (Senger 1998). The relationship between MEL and the length-weighted fiber length indicates that the theory does not predict changes in fiber length (Elahimehr et al. 2015).

Roux and Mayade (1999) developed a comminution model for the kinetics of fiber shortening in LC refining. The model predicts the potential of fiber cutting in the given conditions as a function of the energy per unit mass consumed by the solid phase and the average impact intensity. Olson et al. (2003) also investigated the use of comminution model of LC refining to calculate fiber cutting rate as a function of fiber length for a wide range of operating conditions. They concluded that the probability of fiber cutting during refining is proportional to the applied energy and to the fiber length.

Theoretical net tangential and net normal force per number of bar-crossing have also been proposed to assess refining intensity and to predict changes in fiber length (Roux et al. 2009). The correlation between the average

weighted fiber length and these two parameters indicates that the net normal force per number of bar-crossing is adequate to quantify and predict the cutting effect on fibers.

Based on pilot and mill-scale LC refining studies, Luukkonen et al. (2010a) found that the plate gap is a key link between the refiner process variables and resulting changes in pulp properties. Luukkonen et al. (2010b) also proposed a methodology to correlate operating conditions to pulp quality by relating the refiner operating conditions (*i.e.* power, flow rate, rotational speed and plate gap) to fiber quality (*i.e.* fiber length and freeness) and then relating fiber quality to pulp handsheet quality (*i.e.* tensile index, tear index, and bulk). They also showed that pulp quality remains constant as the gap is closed, up to a *critical gap* which was first introduced by Roux (2001). Beyond the critical gap, fiber cutting commences and paper strength is reduced. Moreover, beyond this point, the relationship between refining power and plate gap deviates from linearity (Luukkonen 2011) which is consistent with the results in Chaussy et al. (2011).

Similar results were observed by Nugroho (Nugroho 2012) for various mixes of softwood (SW) and hardwood (HW) chemical pulps in LC refining. Refining power increases as the plate gap decreased and, at a critical gap between 0.3 to 0.5 mm, the power increases sharply. Moreover, the fiber length and freeness decrease as the plate gap is reduced below the critical gap. This transition occurs for all of the trial conditions.

Elahimehr et al. (2013) studied the effect of plate gap, rotational speed of refiner, and plate pattern on LC refining performance in an AIKAWA 16-inch pilot-scale LC refiner. They found that the non-dimensional power-plate gap relationship is a function of refiner plate geometry and pulp furnish. They also found that mean fiber length was constant for gaps larger than a critical gap, near 0.25 mm. The mean fiber length significantly decreased for the plate gaps smaller than the critical gap. Results also show that increasing the rotational speed increases the critical gap. In addition, Elahimehr et al. (2015) defined intensity as the net energy per leading edges of bar-crossing to predict fiber length reduction in LC refining of mechanical pulp. They found that fiber cutting occurs at 0.03 J/m for all plates and rotational speeds.

Berg et al. (2015) found that power increases linearly with decreasing the plate gap over the range of 0.1-0.2 mm in a two-zone TwinFlo72 LC refiner. They calculated average forces applied to fibers using an expression developed by Kerekes and Senger (2006). Fiber cutting was defined as the point where the ratio of outlet to inlet fiber length was equal to 0.95. Plate gap, calculated forces on fibers, and SEL were found to predict fiber cutting.

In all of the studies discussed above, the onset of fiber cutting is detected by post-refining measurement of pulp properties. Typically, this approach does not enable rapid in-process adjustment of refiner operation in response to the onset of fiber cutting. Nor do these studies address the mechanical interactions between fibers and refiner bars. Kerekes (2011) suggests that *bar force* (*i.e.* the force applied to pulp fibers by the refiner bars) is the key parameter between bars and fibers in refining that cause important changes in fiber properties.

A piezoelectric sensor, referred to here as the refiner force sensor (RFS), has been developed to measure the forces applied by refiner bars to the pulp. The RFS has a probe which replaces a short length (i.e. 5 mm) of a refiner bar. Forces normal to and tangential to this probe are measured by the RFS, as explained in (Prairie 2005) and in (Olender et al. 2008a). The RFS has been used in a number of studies in both low consistency (Prairie et al. 2007, 2008) and high consistency refining (Olender et al. 2008b, 2007).

Harirforoush et al. (2016) investigated the relation between net power, gap and forces on bars in a LC refining using the RFS in experiments conducted on AIKAWA 16-inch single-disc refiner. As the plate gap is reduced, *mean peak normal force* and *mean peak shear force* increase up to threshold values. Here, peak refers to the maximum value that occurs as a bar on the rotor passes over the sensor (Harirforoush et al. 2016; Olender et al. 2007). Beyond these thresholds, the mean peak normal and shear forces continue to increase but the length-weighted fiber length exhibits a negative linear relationship with these forces. In a subsequent study, Harirforoush et al. (2017) found distinct transitions in the parameters characterizing the distributions of bar forces which consistently corresponded to the onset of fiber cutting.

The objective of this study is to understand the effect of pulp furnish on measured bar forces and, more specifically, on the detection of the onset of fiber cutting using the RFS. Tests are conducted using an AIKAWA 16-inch single-disc refiner using hemlock/balsam SW thermomechanical pulp (TMP), SPF (spruce, pine, fir) SW TMP, NBSK (northern bleached SW kraft) pulp, and aspen HW TMP at 3.0 to 3.5% consistency at 1200 and 1400 rpm. A parameter used in signal processing, the *power* of the time domain signal of the measured forces, is shown to be a sensitive and consistent indicator of the onset of fiber cutting. It is also shown that the fiber cutting indicators previously used in (Harirforoush et al. 2017) can be extended to different pulp furnishes and operating conditions.

Materials and Methods

Trials were performed using the AIKAWA 16-inch single-disc refiner at the Pulp and Paper Centre at the University of British Columbia, BC, Canada. The refiner is equipped with a power meter, plate actuation and a variable speed drive. The plate used in these trials is manufactured by AIKAWA FINEBAR®, and has bar edge length of 2.74 km/rev and bar angle of 15º from radial. The bar width, groove width, and groove depth of the plate are 1.6 mm, 3.2 mm, and 4.8 mm, respectively.

Two RFS-type sensors were custom designed and fabricated, based on the design previously used in refiner trials (Olender et al. 2008a). The RFS used in this work is shown in *Fig 1a*. The sensors are installed in a custom recess that are machined into the back of the stator plate. The sensor wires pass from the back side of the sensor and through a custom gland located in the door of the refiner. The sensor recesses are located so that the tip of the sensor replaces a short length of the refiner bar (i.e. 5 mm), as shown in *Fig 1b*. The sensor measures force normal to the plate surface (*i.e.* parallel to the axis of the refiner) and the

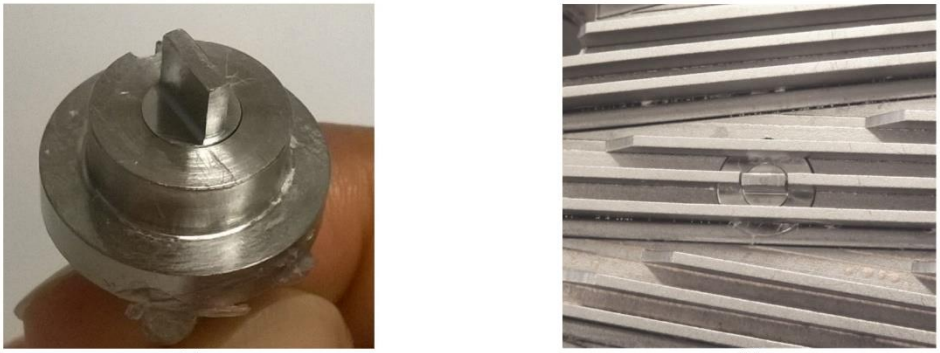

(a) (b)

Fig 1 – (a) RFS sensor (b) close-up of the stator plate with the RFS installed

shear force normal to the bar edge and in the plane of the refiner plate. Two sensors are located on opposite sides of the stator plate. The sensors are positioned in the second bar of a three-bar cluster at a radius of 151 mm. At this radius, the heads of the bolts do not pass over the sensor. 144 bars on the rotor, grouped into 48 three-bar clusters, cross over the sensor in one revolution of the rotor.

Calibration and environmental tests were performed as described in (Harirforoush et al. 2016; Prairie 2005). Modal analyses were performed to ensure that the first natural frequency of the sensor is well above the bar-passing frequency of the refiner so that phase and magnitude distortion due to sensor resonance is minimised. The ratio of the first natural frequency of the sensor to the maximum bar-passing frequency is 8.2 which provides a sufficient margin above the bar passing frequency.

A custom charge amplifier converts the high impedance charge output of the sensors to a low impedance voltage signal which is read by a National Instruments (Austin, TX, USA) PXI 1042 Q high-speed board. National Instrument BNC-2110, Shielded Connector Blocks are used to connect the high-speed DAQ board to the charge amplifier. A custom LabVIEW™ (National Instruments; Austin, TX, USA) interface is used to control data acquisition. A sampling rate of 150 kHz is used which is more than twenty times the maximum bar-passing frequency that occurs during the trials.

Four pulp types, hemlock/balsam SW TMP, SPF SW TMP, NBSK, and aspen HW TMP, at 3 to 3.5% consistency were used in all trials. Pulp freeness and operating conditions for the trials are shown in *Table 1*. The refining operating mode was mono-flo with one inlet perpendicular to the outlet. The refiner speed was set with a Variable Frequency Drive. The plate gaps were adjusted from no-load position (3.5 mm) to the smaller plate gaps (0.2 mm). The flow rate was held constant at 250 liter/min. Sensor signals were recorded using the LabVIEW™ interface for approximately 10 s once reaching stable condition at each target point. At each operating condition, the refiner was held steady for about 10 s to give the pulp time to move from the refining zone to the sample collection point. A ten-liter pulp sample was collected over a 5 s interval. The process was repeated until all of the target points were achieved for one rotational speed. Note that the refining machine operated in continuous mode and the pulp was not recirculated.

All pulp samples were collected and measured for *length-weighted fiber length* (L_w) using a Fiber Quality Analyzer (HiRes FQA, Optest Equipment Inc.; Hawkesbury, ON, Canada), and freeness, defined as the drainage resistance of pulp slurry, (using TAPPI standard T227). Handsheets were made and paper properties of bulk, tear index and tensile index (using TAPPI standard T220) were measured. The calculation of length-weighted fiber length is presented in (Carvalho et al. 1997).

The critical gap is identified based on fiber length data and *Eq 1-2*:

$$\frac{(L_w)_{i+1}-(L_w)_i}{(L_w)_i} < -2\% \qquad i = 1, \dots, n-1 \qquad [1]$$

$$\left.\begin{matrix}(L_w)_{i+2} - (L_w)_{i+1} < 0\\ (L_w)_{i+3} - (L_w)_{i+2} < 0\\ (L_w)_{i+4} - (L_w)_{i+3} < 0\end{matrix}\right\} \qquad [2]$$

In these equations, L_w, is length-weighted fiber length, *i*, is the index of data point, and n is the total number of data points at each trial. The data point index, *i*, ascends as the gap is closed. When the conditions presented in *Eq 1 and 2* are both satisfied, then fibre cutting is determined to have begun.

The bar force data is processed to identity the passage of rotor bars over the sensor. A bar passing event is defined to have occurred when a maximum or peak value in the force data exceeds a predefined threshold value. The algorithm and its verification are described in (Harirforoush et al. 2016).

For each bar-passing event, peak force is defined as the difference between the force at the base of the local valley that precedes the peak and the force at the peak (Prairie et al. 2007). The mean peak normal force and mean peak shear force are calculated for each operating condition. The peak coefficient of friction is calculated by dividing the peak shear force by the peak normal force. The peak normal and shear force data are assessed in the form of distributions to which the two-parameter Weibull distribution function is fit. The Weibull distribution function has been used in previous HC and LC refining studies (Olender et al. 2007; Prairie et al. 2008).

The *average power* (*P*) of a time domain signal $f(t)$ can be defined as the sum of absolute squares of time-domain

Table 1 – Operating conditions for the pilot-scale refining trials

Parameter	Condition
Pulp furnish	Hemlock/balsam SW TMP, 240 ml Canadian standard freeness (CSF) SPF SW TMP, 630 ml CSF NBSK, 700 ml CSF Aspen HW TMP, 500 ml CSF
Refiner speed, rpm	1200, 1400[1]
Consistency	3-3.5%
Flow rate, l/min	250
Plate gap, mm	3.5-0.2
Operating mode	Mono-flo
Sample duration	10 s

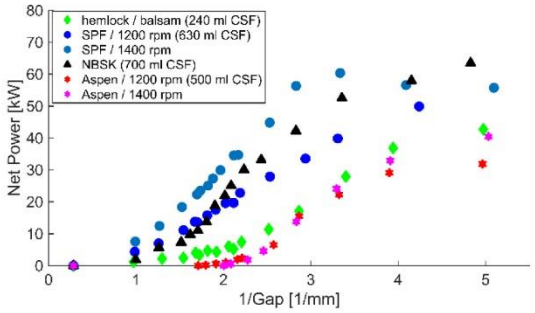

Fig 2 – Net power versus the inverse of plate gap for hemlock/balsam SW TMP (diamond), SPF SW TMP (circle), NBSK (triangle), and aspen HW TMP (hexagram)

samples divided by the signal length, and defined by *Eq 3.* (Papoulis 1962):

$$P = \lim_{T\to\infty} \frac{1}{2T} \int_{-T}^{T} |f(t)|^2 \, dt \qquad [3]$$

where T is the signal length. Note that this term is not equal to the mechanical power that is dissipated on the sensor probe. Rather this is a signal processing term which is equivalent to the square of RMS (root-mean-square) magnitude of a signal.

In this study, the power of the normal force signals and the shear force signals are calculated at each operating condition. As the gap is closed, a transition in the relation between the power of the normal force signal and the plate gap is identified when the conditions shown in *Eq 4-5* are satisfied:

$$\Delta_j = (P_{norm})_{j+1} - (P_{norm})_j > 0.01; \;\; j = 1, \dots, n-1 \quad [4]$$

$$\left\{\begin{matrix}\Delta_{j+1} > 0.01 \\ \Delta_{j+2} > 0.01\end{matrix}\right\} \qquad [5]$$

where $(P_{norm})_j$ is the normalized power of normal force and is defined by *Eq 6.*:

$$(P_{norm})_j = \frac{P_j - \min(P_1 \dots P_i)}{\max(P_1 \dots P_i) - \min(P_1 \dots P_i)} \quad i = 1, \dots, n-1 \quad [6]$$

In these equations, P_j is the power of normal force signal, i and j are the indexes of data point, and n is the total number of data points at each trial.

Results

The relation between net power and the inverse of plate gap for each pulp furnish is shown in *Fig 2*. The net power increases as the plate gap is reduced. A considerable increase in net power is seen for the plate gaps of less than 0.5 mm ($2mm^{-1}$). At a constant gap, increasing the rotational speed increases the net power. This trend is similar to the results presented in (Elahimehr et al. 2013). Moreover, for all plate gaps, more energy is transferred to SW pulp than to HW pulp.

The relation between L_w and the inverse of plate gap for all pulp furnishes is shown in *Fig 3*. In each case, L_w remains relatively unchanged as the plate gap is reduced until the plate gap reaches the critical values, indicated by red dashed lines. The critical gaps, for all but the NBSK pulp, are determined based on an algorithm expressed in *Eq 1-2*.

For the NBSK pulp (*Fig 3d*), the critical gap defined by this algorithm is indicated by the circled data point. However, inspection of the data suggests that the data point indicated by the red dashed line is more likely to be the point of transition. During the NBSK pulp trials, the flow rate was unstable and this is thought to be the cause of this anomalous data.

L_w decreases in an approximately linear manner as a function of the inverse of plate gap for plate gaps smaller than the critical gap. This trend is in agreement with the results of (Harirforoush et al. 2016, 2017). In addition, our results show that the critical gap depends on both pulp furnish and rotational speed and it occurs at different SEL values. For example, the SEL at the onset of fiber cutting is 0.31 J/m for hemlock/balsam SW TMP while it is 0.42 J/m for SPF SW TMP.

Fig 4 shows the relation between the power of normal force and plate gap for all pulp furnishes. Note that the x-axis of these plots is the plate gap not the inverse of plate gap. This format is consistent with the format used in Harirforoush et al. (2017) to show the transitions that indicate fiber cutting.

For all pulp furnishes, as the plate gap is reduced, the power of normal force is relatively constant down to a gap at which there is a transition below which the power increases sharply. This transition gap, based on the algorithm expressed in *Eq 4-5*, is indicated by the blue dotted line. The critical gap, based on the fiber length data (see *Eq 1-2* and *Fig 3*) is indicated by the red dashed line. For each pulp type, except the NBSK pulp (*Fig 4d*), there is an agreement between the transition gap and the critical gap. The difference between the critical gap and the transition gap for the NBSK pulp, shown in *Fig 4d*, is believed to be due to instability of the flow rate during these tests.

[1] Only SPF SW TMP and aspen HW TMP are tested at the rotational speed of 1400 rpm.

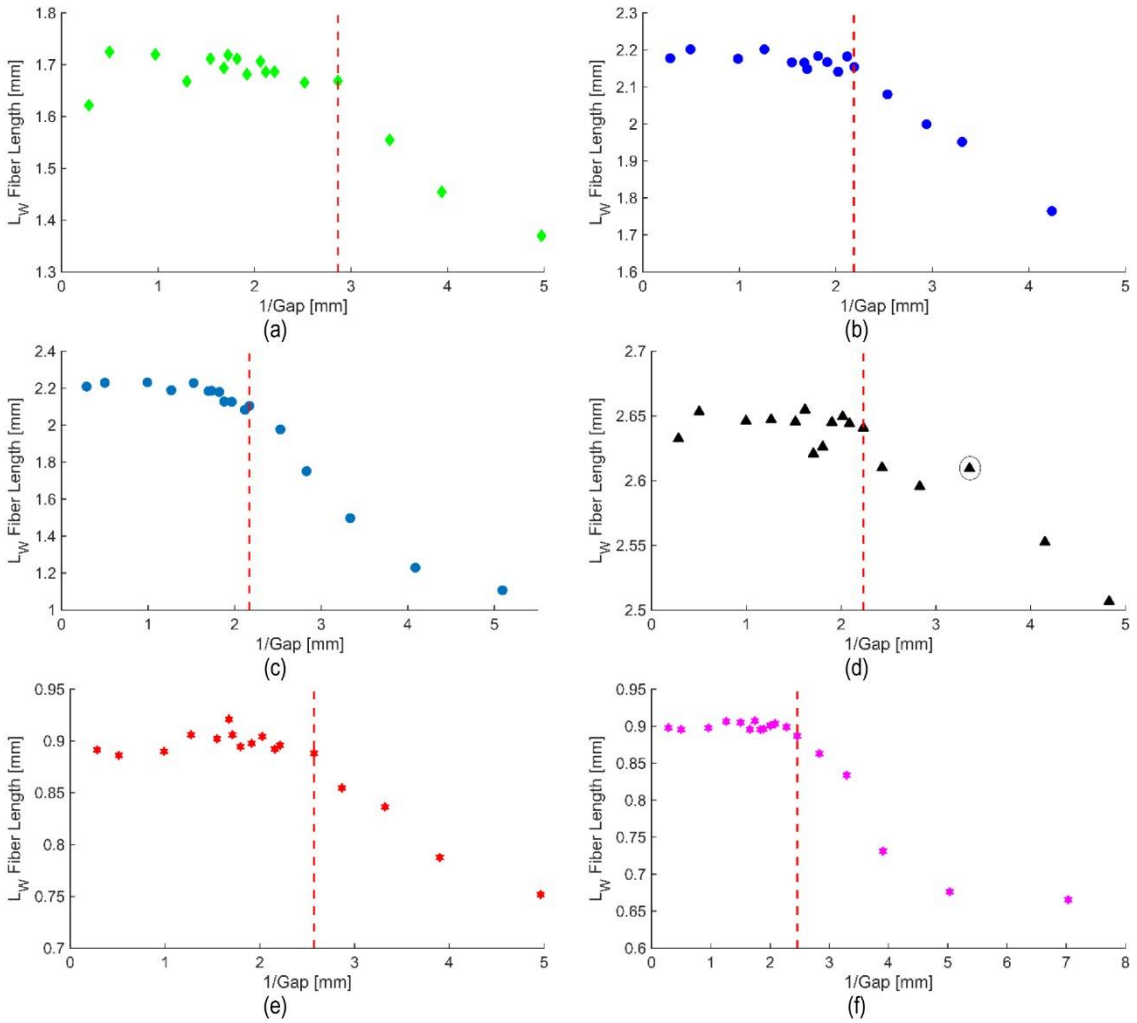

Fig 3 – L_w versus the inverse of plate gap for (a) hemlock/balsam SW TMP (b) SPF SW TMP at 1200 rpm (c) SPF SW TMP at 1400 rpm (d) NBSK (e) aspen HW TMP at 1200 rpm, and (f) aspen HW TMP at 1400 rpm

The relation between freeness, tear index, and tensile index at 1200 rpm is depicted in *Fig 5*. As it is shown in *Fig 5a* and *5b*, freeness changes with decreasing plate gap. This is consistent with the results of (Elahimehr et al. 2015; Luukkonen et al. 2010b) who showed the changes of freeness with specific energy. A substantial reduction of freeness occurs for the plate gaps smaller than the critical gap highlighted by dashed lines.

In *Fig 5a*, the tear index is relatively constant as the plate gap is decreased until the critical gap. After the critical gap, fibers start to cut and tear index drops considerably. This is in agreement with (Elahimehr et al. 2015). However, the trend is not apparent for aspen HW TMP, *Fig 5b*. In addition, the trend of decreasing tear index with increasing tensile index, *Fig 5a*, is in agreement with the results of (Luukkonen et al. 2010a). Similar trends to those shown in *Fig 5a* were observed for SPF SW TMP and NBSK pulp but the results are not presented here in the interest of brevity.

The relation between L_w and mean peak normal force for hemlock/balsam SW and aspen HW at 1200 rpm is shown in *Fig 6*. As shown in *Fig 6a*, L_w remains constant as mean peak normal force increases (*i.e.* as the gap is closed) up to a threshold value, indicated by the dashed circle, which corresponds to the critical gap, as determined by *Eq 1-2*. L_w decreases in an approximately linear manner beyond the critical gap. This trend is consistent with the results of (Harirforoush et al. 2016, 2017). The mean peak normal force at the critical gap is approximately 9 N. This threshold normal force is significantly higher than the equivalent force (*i.e.* 3 N) for the aspen HW pulp, *Fig 6b*.

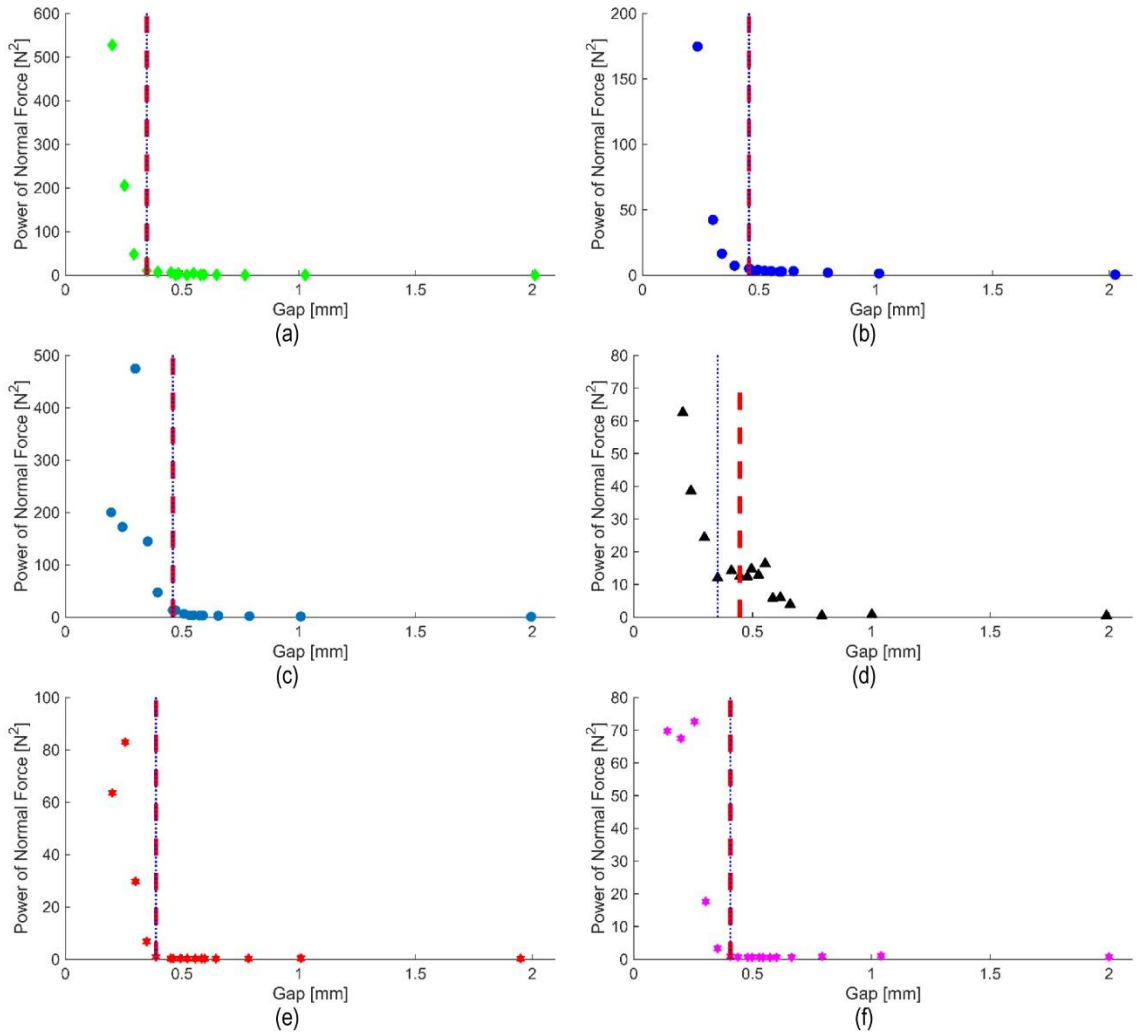

Fig 4 – Power of normal force versus plate gap for (a) hemlock/balsam SW TMP (b) SPF SW TMP at 1200 rpm (c) SPF SW TMP at 1400 rpm (d) NBSK (e) aspen HW TMP at 1200 rpm, and (e) aspen HW TMP at 1400 rpm

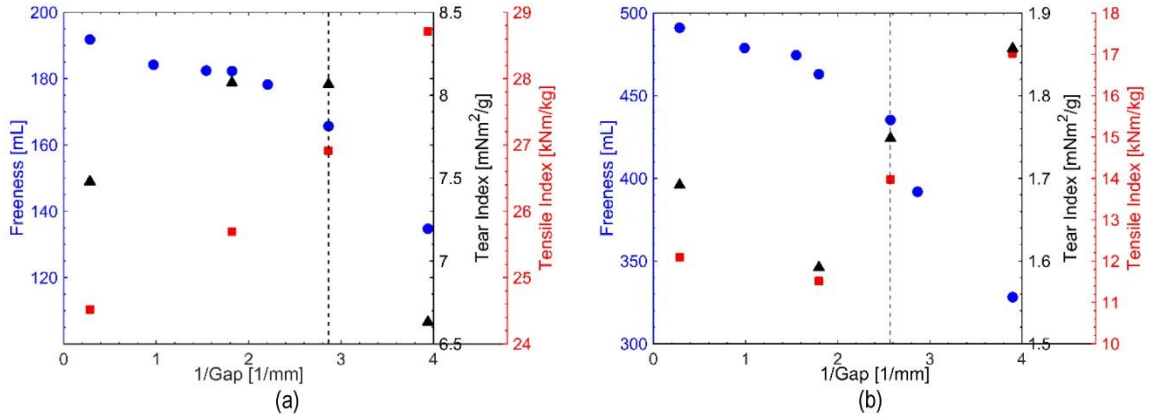

Fig 5 – Freeness (circle), tear index (rectangle), and tensile index (square) versus the inverse of plate gap for (a) hemlock/balsam SW TMP and (b) aspen HW TMP at 1200 rpm.

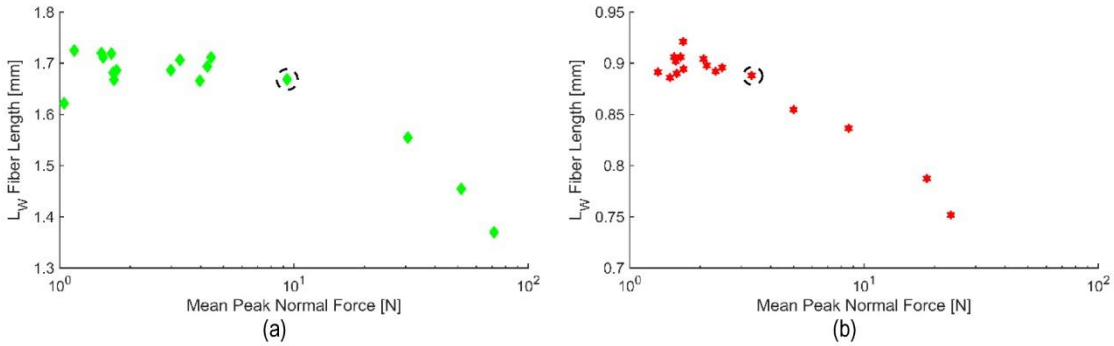

Fig 6 – L_w versus mean peak normal force for (a) hemlock/balsam SW TMP, and (b) aspen HW TMP at 1200 rpm.

A similar trend is seen in the relationship between L_w and mean peak shear force (*Fig 7*). However, the shear force at the critical gap is significantly lower than the threshold of mean peak normal force. Comparing the threshold values of *Fig 7a*, and *7b*, the mean peak shear force at the critical gap is of similar magnitude for both HW and SW pulps, approximately 1.4 N. If the average shear force is assumed to be one-half of the peak shear force, the average shear force per length of sensor tip is in relatively good agreement with Kerekes and Meltzer (2017) who showed that for zero length reduction, the threshold of bar shear force is 200 N/m.

The trends shown in *Fig 6* and *7* also appear in the relation between L_w and mean peak normal and shear forces for SPF SW TMP, and NBSK pulp. These results are not presented here due to the interest of brevity. However, as tabulated in *Table 2*, the mean peak force at the onset of fiber cutting depends on pulp furnishes.

The mean coefficient of friction is plotted in *Fig 8* as a function of the inverse of plate gap. As shown in *Fig 8a*, the mean coefficient of friction decreases as the plate gap is reduced. This finding is in accordance with Roux (2001), Senger et al. (2004), and Harirforoush et al. (2017). The trend indicates that by decreasing the plate gap, the changes in mean peak normal force are more significant than the changes in mean peak shear force. It can be hypothesized that the changes in pulp and paper properties that are associated with closure of the gap, in particular those properties affected by fiber cutting, are more strongly related to an increase in compressive force than to an increase in shear force. As an aside, the results show that the mean coefficient of friction at the critical gap depends on the pulp furnish. This value, as tabulated in *Table 2*, is 0.22, 0.54, and 0.41 for hemlock/balsam SW TMP, SPF SW TMP, and NBSK, respectively.

Similar trends are observed for aspen HW TMP, *Fig 8b*. However, the mean coefficient of friction increases up to the plate gap of 0.65 mm, and decreases beyond this point. For this pulp furnish, the onset of fiber cutting occurs when the mean coefficient of frictions equals to 0.49. At the same plate gap, the mean coefficient of friction is relatively constant at two different rotational speeds, *Fig 8b*.

Table 2- Mean peak normal force, mean peak shear force and mean coefficient of friction at the onset of fiber cutting for all pulp furnishes at 1200 rpm

	Mean peak normal force (N)	Mean peak shear force (N)	Mean coefficient of friction
Hemlock/balsam SW TMP	9.35	1.40	0.22
SPF SW TMP	5.69	1.69	0.54
NBSK	6.50	1.60	0.41
Aspen HW TMP	3.32	1.38	0.49

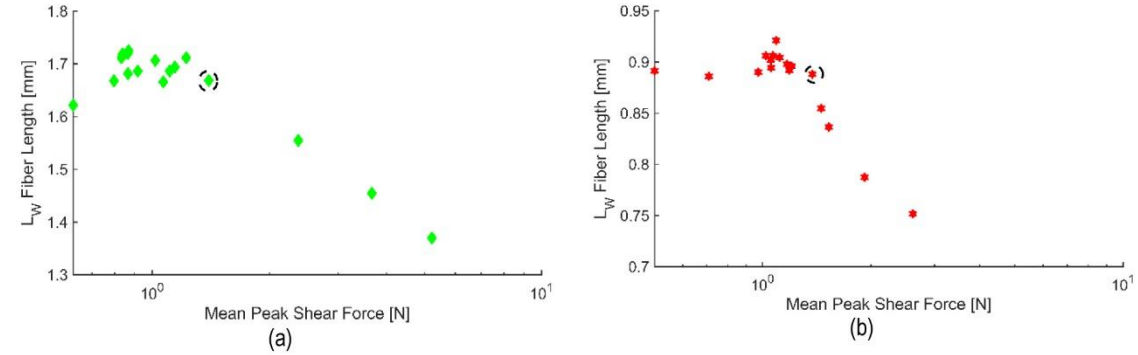

Fig 7 – L_w versus mean peak shear force for (a) hemlock/balsam SW TMP, and (b) aspen HW TMP at 1200 rpm.

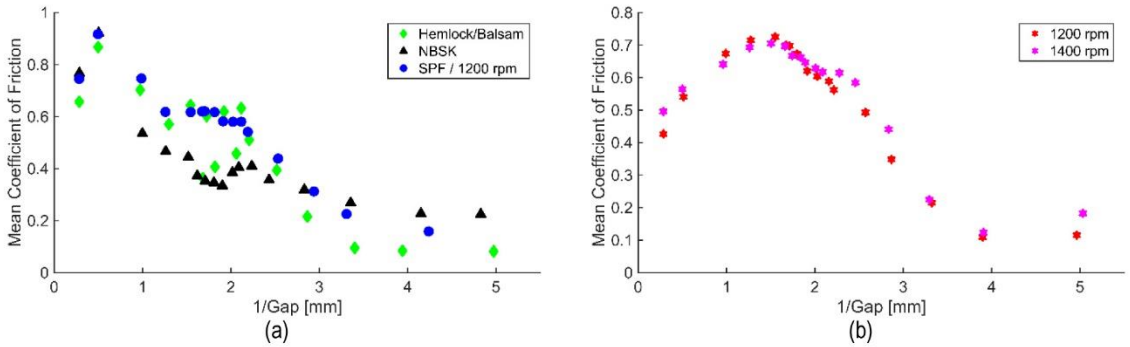

Fig 8 – Mean coefficient of friction versus the inverse of plate gap for (a) hemlock/balsam SW TMP, SPF SWTMP, NBSK, and (b) aspen HW TMP.

Our results also show that the scale parameter of Weibull distribution of peak forces, and the magnitude of dominant frequency, previously used as the indications of the onset of fiber cutting (Harirforoush et al. 2017), can be employed for different pulp furnishes. This data is not shown in the interest of brevity.

Discussion

In a previous work (Harirforoush et al. 2017), we observed distinct transitions in parameters that characterize the distributions of peak normal and shear forces, namely mean peak force and the Weibull scale parameter, as measured by the RFS during LC refining. These transitions consistently correspond to the onset of fiber cutting. In addition, the analysis of the power spectrum of the sensor data shows that the magnitude of the dominant frequency can be used as an indicator of fiber cutting.

In the current study, we investigate the generality of these findings by performing further trials measuring forces during LC refining of a range of pulp furnishes (i.e. SW, HW, TMP and chemical pulp). The results show that the RFS-based indications of the onset of fiber cutting apply to all of the tested pulp furnishes.

The power of the time domain signal of the normal force is shown to be a reliable and consistent indication of the onset of fiber cutting. This parameter consistently identifies the critical gap, as determined by fibre length data, for all pulp furnishes except the NBSK pulp. Flow instability during the NBSK trials is believed to account for this anomalous result.

This study also shows that the mean peak normal and shear force at the onset of fiber cutting depend on pulp furnish. At the onset of fiber cutting, the mean peak normal force of the SW pulp is much higher than for the HW pulp. The level of compressive strain in fibers imposed by fiber forces depends on the properties of the fibers (i.e. modulus of elasticity and fiber geometries such as length, diameter and wall thickness) as well as applied forces (Kerekes and Senger 2006). HW and SW have quite different geometries (i.e. SW fibers are longer than HW fibers) which result in different normal forces at the onset of fiber cutting. Kerekes and Senger (2006) estimate that, for low consistency refining, the normal force on a fiber is proportional to fiber length taken to the power of 3/2 and uncompressed fiber diameter.

However, the mean peak shear force for HW and SW pulps at the onset of fiber cutting are approximately equivalent. The shear force that is generated as opposed bars cross is comprised of two components (Batchelor et al. 1997): a corner or ploughing force at the bar edge and a friction force on axial-facing bar surface. Due to the dissimilar geometries of HW and SW fibres, we expect that the magnitude of the corner force for HW pulp will be different from the corner force of SW pulp. Similarly, we expect that the magnitude of the friction force for HW pulp will be different from the friction force for SW pulp. Our results suggest, however, that these two forces vary such that their sum is approximately equivalent for HW and SW pulps, at the onset of fiber cutting.

The mean coefficient of friction at the critical gap also depends on the pulp furnish. At 1200 rpm, the mean coefficient of friction is 0.22, 0.54, 0.41, and 0.49 for hemlock/balsam SW TMP, SPF SW TMP, NBSK, and aspen HW TMP, respectively. For all pulps, the coefficient of friction decreases as the plate gap is closed. Since the coefficient of friction is the ratio of peak shear force to peak normal force, it is hypothesized that the changes in pulp and paper properties that are associated with closure of the gap and, in particular, those properties affected by fiber cutting, may be caused by an increase in compressive forces rather than by an increase in shear forces on fibers.

Conclusion

This study investigates the effect of pulp furnish on measured bar forces and, more specifically, on the detection of fiber cutting using a custom designed piezoelectric force sensor measuring bar forces in an AIKAWA 16-in. single-disc refiner. Trials were performed using hemlock/balsam softwood thermomechanical pulp, SPF softwood thermomechanical pulp, northern bleached softwood kraft pulp, and aspen hardwood thermomechanical pulp at 3.0 to 3.5% consistency at rotational speeds of 1200 and 1400 rpm. The pulp was sampled at regular intervals, and the length-weighted fiber length, freeness, tear index, and tensile index were measured for each sample. Distinct transitions occur in the plot of the power of time domain signal of

measured normal force versus plate gap which consistently identifies the critical gap, as determined by fibre length data. This indication is a sensitive and reliable metric for in-process detection of fiber cutting. Moreover, our results show that at the onset of fiber cutting, the mean peak normal force, mean peak shear force, and mean coefficient of friction depend on pulp furnish. The results of this study suggest RFS as a potential sensor to detect the onset of fiber cutting.

Acknowledgment

This work is supported by a Collaborative Research and Development grant provided by Natural Sciences and Engineering Research Council of Canada (NSERC) and the following partners: AB Enzymes, Alberta Newsprint Company, Andritz, BC Hydro, Canfor, Catalyst Paper, FPInnovations, Holmen Paper, Meadow Lake Pulp (Paper Excellence), Millar Western, NORPAC, West Fraser, Westcan Engineering, and Winstone Pulp International. The authors also wish to thank M. Miller, E. Jahangir, R. Seifert, and G. Soong for their assistance during the preparation and execution of the refining trials, and for conducting the sample characterisations at the Pulp and Paper Centre at the University of British Columbia.

References

Bajpai, **P.** (2016). Pulp and Paper Industry: Energy Conservation, Elsevier.

Batchelor, **W.J.**, **Martinez**, **D.M.**, **Kerekes**, **R.J. and Ouellet**, **D.** (1997): Forces on fibres in low-consistency refining: Shear force. J. Pulp Pap. Sci., 23(1), J40–J45.

Berg, **J.-E.**, **Sandberg**, **C.**, **Engberg**, **B.A. and Engstrand**, **P.** (2015): Low-consistency refining of mechanical pulp in the light of forces on fibres. Nord. Pulp Pap. Res. J., 30(2), 225–229.

Brecht, **W.** (1967): A method for the comparative evaluation of bar-equppied beating devices. Tappi J., 50(8), 40A–44A.

Carvalho, **M.G.**, **Ferreira**, **P.J.**, **Martins**, **A.A. and Figueiredo**, **M.M.** (1997): A comparative study of two automated techniques for measuring fiber length. Tappi J., 80(2), 137–142.

Chaussy, **D.**, **Martin**, **C. and Roux**, **J.-C.** (2011). Rheological behavior of cellulose fiber suspensions: application to paper-making processing. Ind. Eng. Chem. Res. 50(6), 3524–3533.

Elahimehr, **A.**, **Olson**, **J.A. and Martinez**, **D.M.** (2013): Understanding LC refining: The effect of plate pattern and refiner operation. Nord. Pulp Pap. Res. J., 28(3), 386–391.

Elahimehr, **A.**, **Olson**, **J.A. and Martinez**, **D.M.** (2015): Low consistency refining of mechanical pulp: how plate pattern and refiner operating conditions change the final properties of pulp. Nord. Pulp Pap. Res. J., 30(4), 609–616.

Harirforoush, **R.**, **Wild**, **P.**, and **Olson**, **J.** (2016): The relation between net power, gap, and forces on bars in low consistency refining. Nord. Pulp Pap. Res. J., 31(1), 71–78.

Harirforoush, **R.**, **Olson**, **J. and Wild**, **P.** (2017): In-process detection of fiber cutting in low consistency refining based on measurement of forces on refiner bars. Tappi J., 16(4), 189-199.

Kappel, **J.** (1999): Mechanical pulps: From wood to bleached pulp, Tappi press, Atlanta.

Kerekes, **R.J.** (2011): Force-based characterization of refining intensity. Nord. Pulp Pap. Res. J., 26(1), 14–20.

Kerekes, **R.J. and Senger**, **J.J.** (2006): Characterizing refining action in loconsistency refiner by forces in fibres. J. Pulp Pap. Sci., 32(1), 1–8.

Kerekes, **R.J.**, **and Meltzer**, **F.P.** (2017): The influence of bar width on bar forces and fibre shortening in pulp refining. PTS Faserstoff Symposium, Dresden, Germany.

Luukkonen, **A.** (2011): Development of a methodology to optimize low consistency refining of mechanical pulp. Ph.D. thesis, University of British Columbia.

Luukkonen, **A.**, **Olson**, **J.A.**, **and Martinez**, **D.M.** (2010a): Low consistency refining of mechanical pulp, effect of gap, speed and power. J Pulp Pap. Sci., 36, 28–34.

Luukkonen, **A.**, **Olson**, **J.A.**, **and Martinez**, **D.M.** (2010b): Low consistency refining of mechanical pulp: A methodology to relate operating conditions to paper properties. J. Pulp Pap. Sci. 36, 107–111.

Meltzer, **F.P.** (1994): Neue Möglichkeiten zur Vorherbestimmung des technologischen Mahlergebnisses. Das Papier, 48, 578–583.

Muenster, **H.**, **Ferritsius**, **O.**, **Lecourt**, **M.**, **and Petit-Conil**, **M.** (2005): Energy savings in TMP by high temperature LC/MC refining. International Mechanical Pulping Conference, Oslo, Norway, 213–223.

Musselman, **R.**, **Letarte**, **D.**, **and Simard**, **R.** (1997): Third stage low consistency refining of TMP for energy savings and quality enhancement. 4th int. refining conf., Italy, 141–147.

Nugroho, **D.D.P.** (2012): Low consistency refining of mixtures of softwood & hardwood bleached kraft pulp: effects of refining power. M.Sc. thesis, Asian Institute of Technology School of Environment, resources and development, Thailand.

Olender, **D.**, **Wild**, **R.**, **Byrnes**, **R.**, **Ouellet**, **D.**, **and Sabourin**, **M.** (2007): Forces on bars in high-consistency mill-scale refiners: Trends in primary and rejects stage refiners. J. Pulp Pap. Sci., 33(3), 163–171.

Olender, **D.**, **Wild**, **P.**, **and Byrnes**, **P.** (2008a): A piezoelectric force sensor for mill-scale chip refiners. Proc. Inst. Mech. Eng. Part E-J. Process Mech. Eng. 222 (E2), 115–122.

Olender, **D.**, **Wild**, **P.**, **Byrnes**, **R.**, **Ouellet**, **D.**, **and Sabourin**, **M.** (2008b): Forces on bars in high-consistency mill-scale refiners: Effect of consistency. J. Pulp Pap. Sci., 23(2), 218–223.

Olson, **J.A**, **Drozdiak**, **J.**, **Martinez**, **M.**, **Garner**, **R.**, **Robertson**, **A.G. and Kerekes**, **R.** (2003): Characterizing fibre shortening in low-consistency refining using a comminution model. Powder Technol. 129(1), 122–129.

Papoulis, **A.** (1962): The Fourier Integral and Its Applications, New York, McGraw-Hill.

Prairie, **B.** (2005): Measurement of forces in a low consistenct refiner. M.Sc. thesis, University of Victoria, British Columbia, Canada.

Prairie, **B.**, **Wild**, **P.**, **Byrnes**, **P.**, **Olender**, **D.**, **Francis**, **D.W.**, **and Ouellet**, **D.** (2007): Forces during bar-passing events in low consistency refining: Effects of refiner tram. Pulp Pap. Can., 108(9), 34–37.

Prairie, **B.**, **Wild**, **P.**, **Byrnes**, **P.**, **Olender**, **D.**, **Francis**, **W.**, **and Ouellet**, **D.** (2008): Forces during bar-passing events in low-consistency refining: Distributions and rRelationships to specific edge load. J. Pulp Pap. Sci., 34(1), 1–8.

Roux, **J.C.** (2001): Review paper on pulp treatment processes. In Trans, 12th Fundamental Research Symposium, Oxford (Baker, C.F., ed.) The Pulp and Paper Fundamentals Research Society, Bury, U.K. , 19-80.

Roux, **J.C.**, **and Joris**, **J.** (2005): Angular parameters beyond specific edge load. TAPPSA J. Tech. Asso. Pulp Pap. Ind. South Afr., 1-10.

Roux, **J.C.**, **and Mayade**, **T.L.** (1999): Modeling of the particle breakage kinetics in the wet mills for the paper industry. Powder Technology, 105, 237–242.

Roux, **J.-C.**, **Bloch**, **J.-F.**, **Bordin**, **R.**, **and Nortier**, **P.** (2009): The net normal force per crossing point: a unified concept for the low consistency refining of pulp suspensions. 14th Fundamental research symposium, Oxford, 51-83.

Senger, **J.J.** (1998): The Forces on pulp fibres during refining. M.Sc. thesis, The University of British Columbia.

Senger, **J.**, **Siadat**, **A.**, **Ouellet**, **D.**, **and Wild**, **R.** (2004): Measurement of normal and shear forces during refining using a piezoelectric force sensor. J. Pulp Pap. Sci. 30(9), 247–251.

Smook, **G.A.** (1992): Handbook for pulp and paper technologists, 2nd Edition. Vancouver, BC, Angus Wilde Publications.

Zha, **Q.**, **Lanouette**, **R.**, **Law**, **K.N.**, **Bousquet, J.-P.**, **and Bussières**, **S.** (2008). Refining of long fibre fractions after fractionation. Prepr. 94th Ann. Mtg., PAPTAC, Montreal, Canada, 2008, p. B481–7.

Manuscript received September 15, 2017
Accepted December 12, 2017

Appendix J

Harirforoush, R., Olson, J., Wild, P. (2017): Bar force measueremnets in low consistency refining: the effect of plate pattern. Under Review, Nordic Pulp and Paper Research Journal. ”With permission from Nordic Pulp & Paper Research Journal, manuscript submitted for publication , 2018, Under Review"

Bar force measurement in low consistency refining: the effect of plate pattern

R. Harirforoush[1], J. Olson[2], P. Wild[1]

KEYWORDS: Force measurement, sensor, low consistency, plate pattern, mechanical pulping

ABSTRACT: The effect of plate pattern on forces applied to pulp fibers by refiner bars in low consistency refining is investigated in an AIKAWA 16-inch single-disc refiner. These forces are measured using a custom-built piezoelectric sensor. Trials are conducted using SPF softwood thermomechanical pulp, northern bleached softwood kraft pulp, and aspen hardwood thermomechanical pulp at 3.3 to 3.6% consistency at rotational speeds of 1200 and 1400 rpm. The pulp is sampled at regular intervals, and the length-weighted fiber length, freeness, tear Index, and tensile Index are measured for each sample. The results show that the plate with higher bar edge length results in lower mean peak normal and shear forces. The mean peak normal and shear forces at the onset of fiber cutting depend on rotational speed, pulp furnish and plate pattern, and these parameters are lower for a plate pattern with higher bar edge length. In addition, the mean coefficient of friction is a function of plate gap, pulp furnish, and plate pattern. The plate having higher bar edge length results in higher mean coefficient of friction.

ADDRESSES OF THE AUTHORS: R. Harirforoush (rharirfo@uvic.ca), University of Victoria, Department of Mechanical Engineering, P.O. Box 3055 STN CSC, V8W 3P6, Victoria, BC, Canada. **J. Olson** (james.olson@ubc.ca), University of British Columbia, Department of Mechanical Engineering, Point Grey Campus, 5000-2332 Main Mall, V6T 1Z4, Vancouver, BC, Canada. **P. Wild** (pwild@uvic.ca), University of Victoria, Department of Mechanical Engineering, P.O. Box 3055 STN CSC, V8W 3P6, Victoria, BC, Canada

Corresponding author: R. Harirforoush

Introduction

It has been shown that energy consumption in mechanical pulping can be reduced by decreasing the number of refining treatments at high consistency (HC) and increasing the number of treatments at low consistency (LC) (Muenster et al. 2005; Musselman et al. 1997; Zha et al. 2008). However, a drawback of LC refining is fiber cutting which may occur at high refining energies and has limited the widespread adoption of LC refining. To reduce fiber cutting, one approach is to use a plate pattern with narrower bars and grooves to provide lower intensity treatments (Luukkonen et al. 2010a). However, the effect of plate pattern on the relationship between refiner operating conditions, measured bar forces (i.e. forces applied to pulp fibers by the refiner bars), and resulting pulp properties has not been investigated.

Plate patterns are conventionally characterized by the length of intersecting edges between the opposing plates, bar edge length (BEL). BEL, defined as the total length of bar edges swept by bar-crossing during a single rotation of the disc, is related to the bar width and groove width and is calculated using TAPPI standard TIP 0508-05 (Stationwala et al. 1994). BEL is also inversely proportional to the intensity of refining.

Pilot and mill-scale LC refining studies have investigated the effect of BEL, rotational speed, power and plate gap on resulting pulp properties (Luukkonen et al. 2010a). Trails were carried out using an Andritz TwinFlow 22-in refiner for the plates of BEL of 10.29 km/rev and 14.65 km/rev while consistency was held constant. The results show that the relation between tensile strength and specific refining energy, defined as the ratio of the net power to the mass of the flow rate of fibers, is strongly affected by plate design and operating conditions. The plate having lower BEL exhibits slightly higher tensile strength development than higher BEL plate. However, at the same rotational speed, a slightly greater drop in tear index is shown for higher BEL plate.

The effect of plate gap, rotational speed and plate pattern on LC refining has been studied experimentally using an AIKAWA 16-inch pilot-scale LC refiner (Elahimehr et al. 2013). The results show that power varies with cube of rotational speed and with the inverse of plate gap for a wide range of plate patterns. It was also shown that the form of the non-dimensional power-plate gap relationship is related to refiner plate pattern, as characterized by BEL, and pulp furnish. In a later study, Elahimehr et al. (Elahimehr et al. 2015) showed that, at a certain specific refining energy, plates with larger *bar interaction length*, defined as the net energy per leading edge of bar-crossing, perform a lower intensity treatment and avoid fiber length reduction.

In mechanical refining, as the plate gap is closed, fibers are subjected to increasing compressive and shear forces which leads to increasing net refiner power. Kerekes suggests that the interaction forces between bars and fibers is the key parameter governing changes in fiber properties (Kerekes, 2011). Bar forces have been analyzed in several studies

both theoretically (Batchelor et al. 1997; Kerekes 2006; Martinez et al. 1997) and experimentally (Backlund 2004; Senger et al. 2005). A piezoelectric sensor, referred to here as the refiner force sensor, RFS, has been developed to measure bar forces. The RFS has a probe which replaces a short length (i.e. 5 mm) of a refiner bar. The sensor measures forces normal and tangential to the probe and, thus, to the refiner bar. The RFS has been used in a number of studies in both low consistency (Harirforoush et al. 2016; Prairie et al. 2007, 2008) and high consistency refining (Olender et al. 2008a, 2007).

In a recent study, Harirforoush et al. (2017) used the RFS in experiments conducted on an AIKAWA 16-inch single-disc LC refiner and found distinct transitions in the parameters characterizing the distributions of bar forces which consistently corresponded to the onset of fiber cutting. In a subsequent study, it was shown that the fiber cutting indicators can be extended to different pulp furnishes and operating conditions (Harirforoush et al. 2018). Both of these studies were conducted using a plate with BEL=2.74 km/rev.

The objective of this study is to examine the effect of plate pattern and, more specifically, BEL on the relationship between refiner operating conditions, measured bar forces, and resulting pulp properties. Trials are conducted using an AIKAWA 16-inch single-disc refiner with the plate of BEL=5.59 km/rev using SPF (spruce, pine, fir) softwood (SW) thermomechanical pulp (TMP) at two different freeness, NBSK (northern bleached SW kraft) pulp, and aspen hardwood (HW) TMP at 3.3 to 3.6% consistency at 1200 and 1400 rpm. The results of these trials are compared with the trial results which used the plate of BEL=2.74 km/rev. It is shown that higher BEL plate results in lower mean peak normal and shear forces. Here, peak refers to the maximum value that occurs as a bar on the rotor passes over the sensor. In addition, it is found that the mean coefficient of friction is a function of plate gap, pulp furnish, and plate pattern. The mean coefficient of friction increases with the plate having higher BEL. It is also observed that the fiber cutting indicators previously found in (Harirforoush et al. 2017, Harirforoush et al. 2018) can be extended to different plate patterns.

Materials and Methods

Trials were performed using the AIKAWA 16-inch single-disc refiner at the Pulp and Paper Centre at the University of British Columbia, BC, Canada. The refiner is equipped with a power meter, plate actuation and a variable speed drive. The plate used in these trials is manufactured by AIKAWA FINEBAR®, and has bar edge length of 5.59 km/rev and bar angle of 15° from radial. The bar width, groove width, and groove depth of the plate are 1 mm, 2.4 mm, and 4.8 mm, respectively.

Two RFS-type sensors were custom designed and fabricated, based on the design previously used in refiner trials (Olender et al. 2008b). The RFS used in this work is shown in *Fig 1a*. The sensors are installed in custom recesses that are machined into the back of the stator plate. The sensor wires pass from the back side of the sensor and through a custom gland located in the door of the refiner. The sensor recesses are located so that the tip of the sensor replaces a short length of the refiner bar (i.e. 5 mm), as shown in *Fig 1b*. The sensor measures force normal to the plate surface (*i.e.* parallel to the axis of the refiner) and the shear force normal to the bar edge and in the plane of the refiner plate. Two sensors are located on the opposite sides of the stator plate in the second bar of four-bar cluster at a radius of 151 mm. To compare the bar force results of the plate patterns with BEL=2.74 km/rev and BEL=5.59 km/rev, the RFS sensors are installed at the same radial position of the sensors previously accommodated in the plate with BEL=2.74 km/rev to avoid the effect of radial position on bar forces. At this position, the heads of the bolts do not pass over the sensor. 192 bars on the rotor, grouped into 48 four-bar clusters, cross over the sensor in one revolution of the rotor.

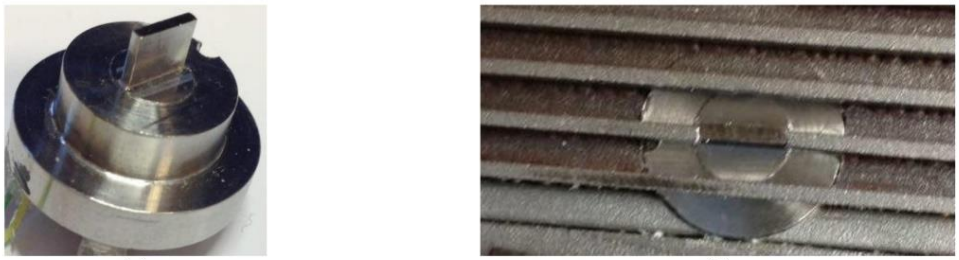

(a) (b)

Fig 1- (a) RFS sensor (b) close-up of the stator plate with the RFS installed in the plate with BEL=5.59 km/rev

Calibration and environmental tests were performed as described in (Harirforoush et al. 2016; Prairie 2005). Modal analyses were performed to ensure that the first natural frequency of the sensor is well above the bar-passing frequency of the refiner so that phase and magnitude distortion due to sensor resonance are minimised. The ratio of the first

natural frequency of the sensor to the maximum bar-passing frequency is approximately 4 which provides a sufficient margin above the bar-passing frequency.

A custom charge amplifier converts the high impedance charge output of the sensors to a low impedance voltage signal which is acquired by a National Instruments (Austin, TX, USA) PXI 1042 Q high-speed board. National Instrument BNC-2110, Shielded Connector Blocks are used to connect the high-speed DAQ board to the charge amplifier. A custom LabVIEW™ (National Instruments; Austin, TX, USA) interface is used to control data acquisition. A sampling rate of 150 kHz is used which is more than twenty times the maximum bar-passing frequency that occurs during the trials.

Three pulp furnishes, SPF SW TMP at two different freeness, NBSK, and aspen HW TMP at 3.3 to 3.6% consistency were used in the trials. Pulp freeness and operating conditions for the trials are shown in *Table 1*. The refiner operating mode was mono-flo with one inlet perpendicular to the outlet. The refiner speed was set with a Variable Frequency Drive. The plate gaps were adjusted from no-load position (3.5 mm) to the smaller plate gaps (0.15 mm). The flow rate was held constant at 250 liter/min. Once the refiner was stabilized at each target operating condition, sensor signals were recorded using the LabVIEW™ interface for approximately 10 s. Then, the refiner was held steady for another 10 s to give the pulp time to move from the refining zone to the sample collection point. A ten-liter pulp sample was collected over a 5 s interval. Note that the pulp was not recirculated during trials. The process was repeated until all of the target points were achieved for one rotational speed.

All pulp samples were collected and measured for *length-weighted fiber length* (L_w) using a Fiber Quality Analyzer (HiRes FQA, Optest Equipment Inc.; Hawkesbury, ON, Canada), and freeness (using TAPPI standard T227). Handsheets were made and paper properties of tear index and tensile index (using TAPPI standard T220) were measured. The calculation method for length-weighted fiber length is presented in (Carvalho et al. 1997).

The critical gap is identified based on fiber length data and the algorithm described in (Harirforoush et al. 2018). The bar force data is processed to identity the passage of rotor bars over the sensor. A bar-passing event is defined to have occurred when a maximum or peak value in the force data exceeds a predefined threshold value. The algorithm and its verification are described in (Harirforoush et al. 2016).

For each bar-passing event, peak force is defined as the difference between the force at the base of the local valley that precedes the peak and the force at the peak (Prairie et al. 2007). For each operating condition, the mean peak normal force, mean peak shear force, and the mean coefficient of friction, defined as the ratio of the peak shear force by the peak normal force, are calculated. The normal and shear stresses are obtained by divining the peak normal and shear forces by the area of the "top" of the sensor probe, i.e., the bar width multiplied by the length of the probe. The results of these trials are compared with the trial results in (Harirforoush et al. 2017; Harirforoush et al. 2018) which used the plate of BEL=2.74 km/rev (bar width, groove width, and groove depth are 1.6 mm, 3.2 mm, and 4.8 mm, respectively). The peak normal and shear force data are assessed in the form of distributions and the indications of the onset of fiber cutting discussed in (Harirforoush et al. 2017; Harirforoush et al. 2018) are also calculated.

Table 1- Operating conditions for the pilot-scale refining trials

Parameter	Condition
Pulp furnish	SPF SW TMP, 666 ml Canadian standard freeness (CSF)[1]
	SPF SW TMP, 456 ml CSF
	NBSK, 686 ml CSF
	Aspen HW TMP, 566 ml CSF
Refiner speed, rpm	1200, 1400[2]
Consistency	3.3-3.6%
Flow rate, l/min	250
Plate gap, mm	3.5-0.15
Operating mode	Mono-flo
Sample duration	10 s

[1] In this study, SPF SW TMP, 666 ml CSF, and SPF SW TMP, 456 ml CSF, are referred as SPF SW HF TMP and SPF SW LF TMP, respectively,

[2] Only SPF SW HF TMP and aspen HW TMP are tested at the rotational speed of 1400 rpm.

Results

Typical unfiltered normal and shear force data, taken at 1200 rpm and a plate gap of 0.15 mm, for aspen HW TMP is shown in *Fig 2*. Each peak represents a bar-passing event. As noted earlier, the bars of the rotor that cross over the force sensor are grouped in four-bar clusters. Therefore, bar-passing events appear in *Fig 2* as clusters of four peaks, an example of which is highlighted in the dashed rectangle.

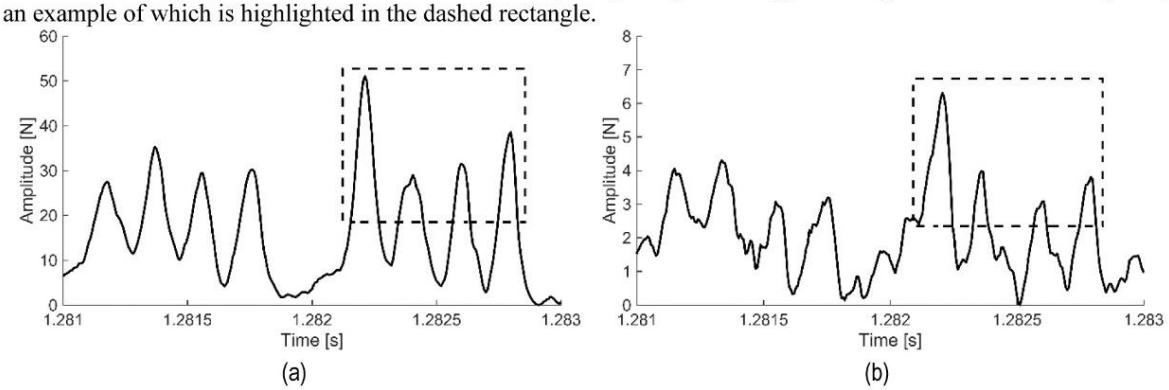

Fig 2- Typical unfiltered (a) normal force and (b) shear force at 1200 rpm and 0.15 mm plate gap for aspen HW TMP

The power spectrum of the sensor data at 1200 rpm and plate gap of 0.15 mm shows local maxima which correspond to the crossing of different bars within the four-bar clusters of the rotor (*Fig 3*). The highest amplitude, marked by the dashed circle, corresponds to the passage of equivalent edges of the four-bar clusters on the rotor. This frequency is referred as the dominant frequency (Harirforoush et al. 2017) and its value depends on the bar width, groove width, bar angle, and rotational speed. This frequency appears in the frequency analysis of the plate patterns designed as clusters of bars.

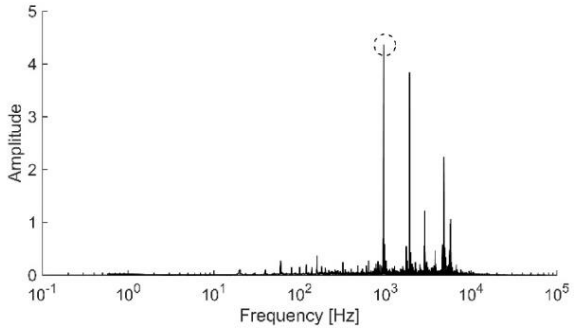

Fig 3- Spectrum of normal force at 1200 rpm and 0.15 mm plate gap for aspen HW TMP

The relation between specific refining energy (SRE) and the inverse of plate gap for SPF SW HF TMP, aspen HW TMP, and NBSK pulp at 1200 rpm for two plate patterns is shown in *Fig 4*. The SRE increases as the plate gap is reduced. At the same plate gap and pulp furnish, the energy transferred to pulp fibers is relatively equivalent for two plate patterns. Moreover, for all plate gaps, more energy is transferred to SW pulp than to HW pulp which is consistent with the results of (Harirforoush et al. 2018).

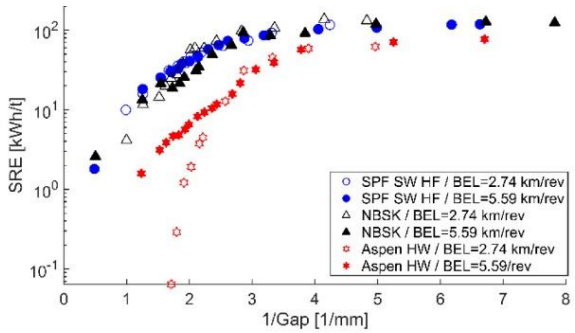

Fig 4- Specific refining energy versus the inverse of plate gap for SPF SW HF TMP (circle),NBSK (triangle), and aspen HW TMP (hexagram) at 1200 rpm for the plates of BEL =5.59 km/rev and BEL=2.74 km/rev[3]

The relation between L_w and the inverse of plate gap for SPF SW HF TMP and aspen HW TMP at 1200 rpm is shown in *Fig 5*. In each case, L_w remains relatively constant as the plate gap is reduced until the plate gap reaches a critical gap, indicated by red dashed lines. The critical gap is determined based on fibre length data using the algorithm described in (Harirforoush et al. 2018). Similar trends to those shown in *Fig 5* were observed for SPF SW LF TMP and NBSK pulp but the results are not presented here in the interest of brevity.

Comparing the critical gap values of the plates of BEL=5.59 km/rev and BEL=2.74 km/rev used in (Harirforoush et al. 2017; Harirforoush et al. 2018) shows that for the same pulp furnish, the critical gap slightly decreases with the plate pattern having higher BEL. However, this trend is more considerable for NBSK pulp. As an aside, the critical gaps happens at different specific edge load (SEL), defined as the energy expended per unit refiner bar length over one bar-crossing event, which is consistent with (Harirforoush et al. 2018). Furthermore, at the critical gaps, the SEL values of SW pulp is much higher than HW pulp.

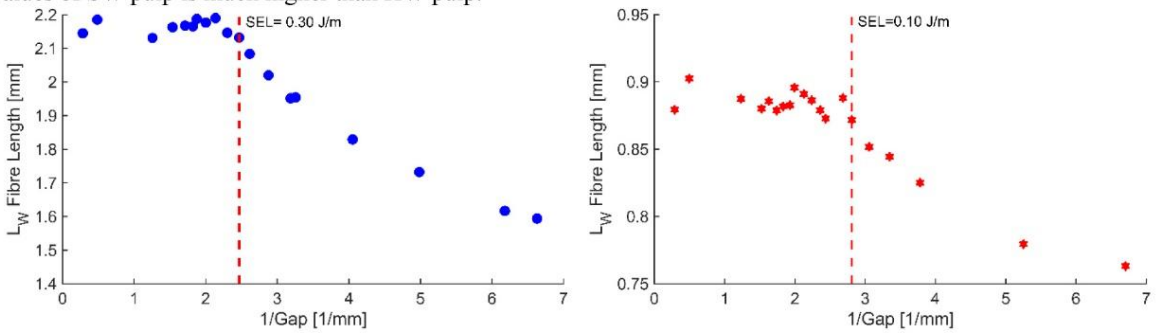

Fig 5- L_w versus the inverse of plate gap for (a) SPF SW HF TMP and (b) aspen HW TMP at 1200 rpm

The relation between freeness and the inverse of plate gap for SPF SW HF TMP and aspen HW TMP at 1200 rpm for two plate patterns is shown in *Fig 6.* For SW pulp, at the same gap, the freeness is relatively constant for two plate patterns. However, for HW pulp, at the same gap, the freeness slightly increases with the plate having higher BEL. The results of tear index and tensile index are not presented here in the interest of brevity. However, same trend seen in the plate of BEL=2.74 km /rev in (Harirforoush et al. 2018) appears in data for the plate with BEL=5.59 km/rev. The trend of change of freeness with decreasing plate gap is in accordance with the results of (Elahimehr et al. 2015; Luukkonen et al. 2010b) who showed the changes of freeness with SRE.

[3] Note that in this paper, the data for the plate of BEL=2.74 km/rev is taken from (Harirforoush et al. 2017; Harirforoush et al. 2018).

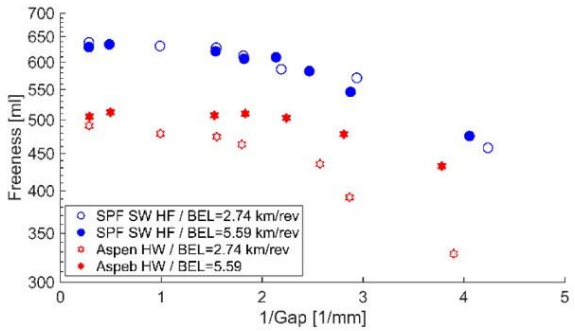

Fig 6- Freeness versus the inverse of plate gap for SPF SW HF TMP, and aspen HW TMP at 1200 rpm for the plates of BEL =5.59 km/rev and BEL=2.74 km/rev

The relation between mean peak normal force and the inverse of plate gap for SPF SW HF TMP, aspen HW TMP, and NBSK pulp at 1200 rpm for the plate patterns of BEL=2.74 km/rev and BEL=5.59 km/rev is shown in *Fig 7*. As the plate gap is reduced, the mean peak normal force increases. However, this trend is not observed in the data for NBSK pulp, *Fig 7a*. Flow instability during the NBSK trials is believed to account for this result.

For all pulp furnishes and at all plate gaps, the plate with higher BEL, which has smaller bar width and groove width, results in lower mean peak normal force. Moreover, the mean peak normal force at the onset of fiber cutting, tabulated in *Table 2*, depends on the plate pattern and pulp furnish and is reduced for the plate pattern having higher BEL. The difference between mean peak normal force at the onset of fiber cutting for two plate patterns is more significant for SW pulp than HW pulp.

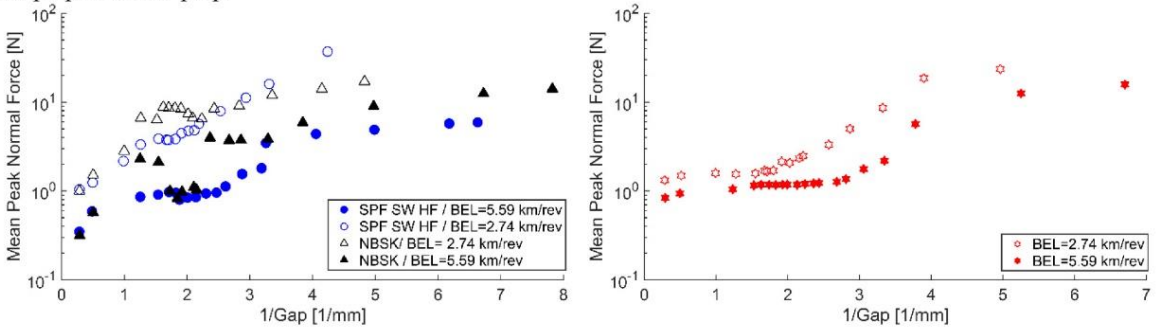

Fig 7- Mean peak normal force versus the inverse of plate gap for (a) SPF SW HF TMP, NBSK, and (b) aspen HW TMP at 1200 rpm for the plates of BEL =5.59 km/rev and BEL=2.74 km/rev

Table 2- Mean peak normal force, mean peak shear force and coefficient of friction at the onset of fiber cutting (i.e. critical gap) for all pulp furnishes at 1200 rpm for plates of BEL=5.59 km/rev and BEL=2.74 km/rev

	Mean peak normal force (N)	**Mean peak shear force (N)**	**Mean coefficient of friction**
SPF SW TMP HF / Plate BEL=2.74 km/rev	5.69	1.69	0.54
SPF SW TMP HF / Plate BEL=5.59 km/rev	0.95	0.58	0.92
SPF SW TMP LF / Plate BEL=2.74 km/rev	6.85	3.68	0.74
SPF SW TMP LF / Plate BEL=5.59 km/rev	0.94	0.56	0.99
NBSK / Plate BEL=2.74 km/rev	6.50	1.60	0.41
NBSK / Plate BEL=5.59km/rev	3.84	1.45	0.68
Aspen HW TMP / Plate BEL=2.74 km/rev	3.32	1.38	0.49
Aspen HW TMP /Plate BEL=5.59km/rev	1.36	0.95	0.91

A similar trend to *Fig 7* is seen in the relationship between mean peak shear force and the inverse of plate gap (*Fig 8*). Higher BEL plate results in lower mean peak shear force for all pulp furnishes. However, the trend is less definitive for NBSK pulp. As tabulated in *Table 2*, for all pulp furnishes and plate patterns, the mean peak shear force at the critical gap is lower than the mean peak normal force which is consistent with the results of (Harirforoush et al. 2018).

For the plate of BEL=5.59 km/rev, the mean peak shear force at the onset of fiber cutting is different for HW and SW which is in the contrary with the result of (Harirforoush et al. 2018) that showed for the plate of BEL=2.74 km/rev, the mean peak shear force at critical gap is of similar magnitude for both HW and SW pulps.

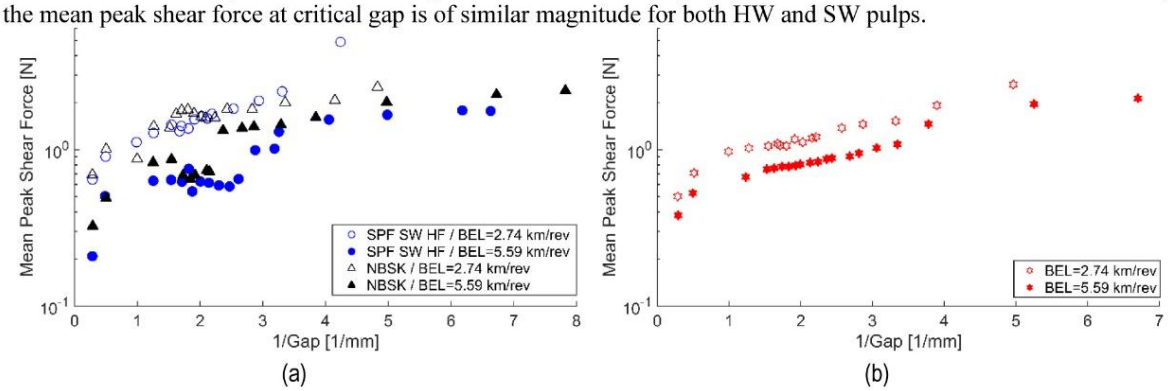

Fig 8- Mean peak shear force versus the inverse of plate gap for (a) SPF SW HF TMP, NBSK, and (b) aspen HW TMP at 1200 rpm for the plates of BEL =5.59 km/rev and BEL=2.74 km/rev

The relation between normal stress and shear stress and the inverse of plate gap for SPF SW HF TMP, aspen HW TMP, and NBSK pulp at 1200 rpm for two plate patterns is shown in *Fig 9*. For both SW and HW, normal stress decreases with the plate pattern having higher BEL, *Fig 9a-9b*. However, the data for the NBSK pulp does not show this trend. For SW pulp, the shear stress is relatively similar for two plates, *Fig 9c*, while for HW pulp the shear stress slightly increases with the plate having higher BEL, *Fig 9d*.

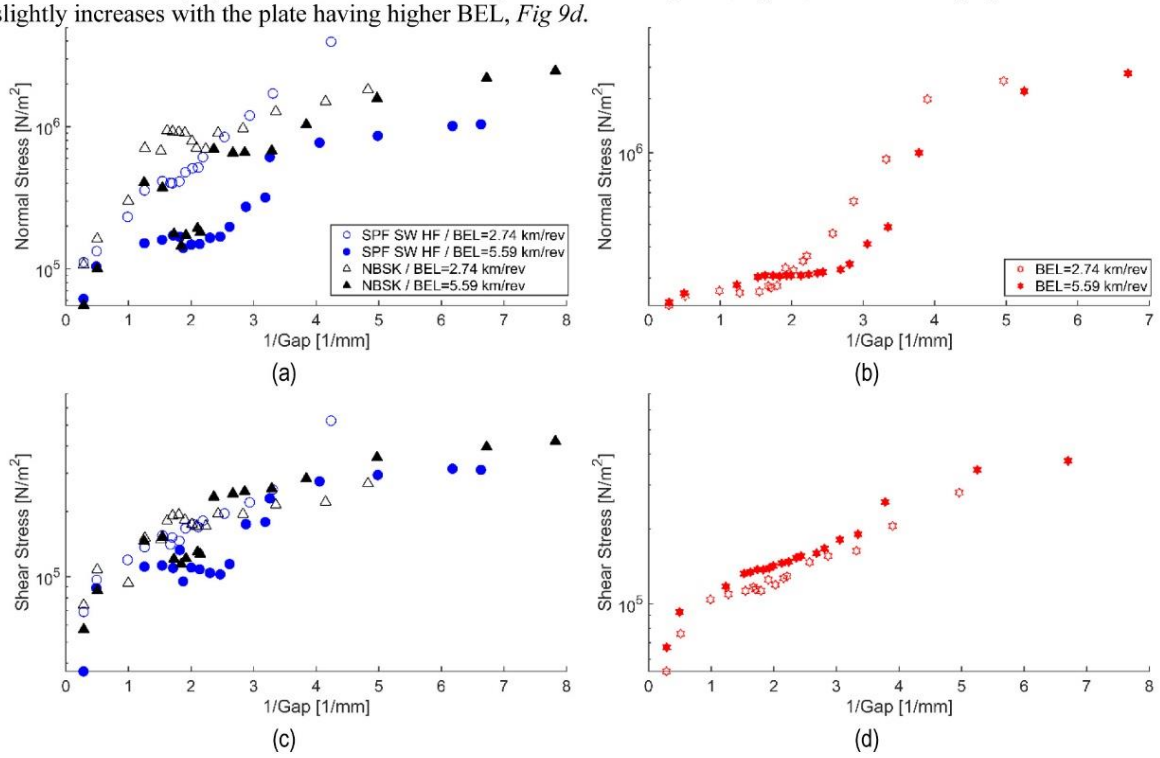

Fig 9- Normal stress versus the inverse of plate gap for (a) SPF SW HF TMP, NBSK and (b) aspen HW TMP at 1200 rpm for the plates of BEL =5.59 km/rev and BEL=2.74 km/rev. Shear stress is also shown in (c) and (d).

The mean coefficient of friction is plotted in *Fig 10* as a function of the inverse of plate gap for SPF SW HF TMP, aspen HW TMP, and NBSK pulp at 1200 rpm for two plate patterns. As shown in *Fig 10a*, the mean coefficient of friction decreases as the plate gap is reduced. This finding is in accordance with (Harirforoush et al. 2017; Roux, 2001; Senger et al. 2004). Similar trends are observed for aspen HW TMP, *Fig 10b*. However, the mean coefficient of

friction increases up to a peak value, and decreases beyond this point which is consistent with (Harirforoush et al, 2018).

Moreover, the results show that at all plate gaps and for all pulp furnishes, the mean coefficient of friction is higher for the plate pattern having higher BEL. In addition, the mean coefficient of friction at the onset of fiber cutting, tabulated in *Table 2*, depends on of plate gap, pulp furnish, and plate pattern. The plate with smaller bar width and groove width results in higher mean coefficient of friction at the onset of fiber cutting.

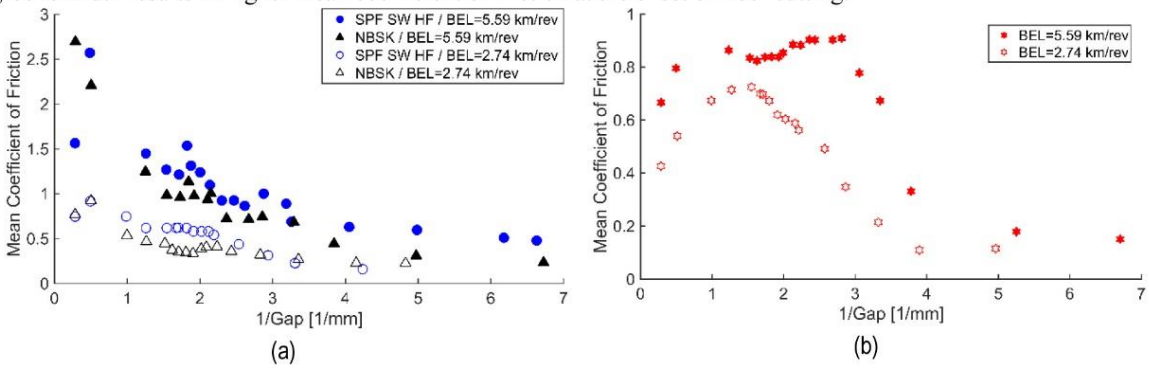

Fig 10- Mean coefficient of friction versus the inverse of plate gap for (a) SPF SW HF TMP (circle), NBSK (triangle), and (b) aspen HW TMP at 1200 rpm for the plates of BEL =5.59 km/rev and BEL=2.74 km/rev

The results shown in *Fig 4* to *Fig 10* also appear for SPF SW LF TMP at 1200 rpm, SPF SW HF TMP at 1400 rpm, and aspen HW TMP at 1400 rpm. In addition, our results also show that the indications of the onset of fiber cutting reported in (Harirforoush et al. 2017; Harirforoush et al. 2018) are reliable for a different plate pattern. This data is not shown here, in the interest of brevity.

Discussion

In this study, we investigate the effect of plate pattern on bar forces using the RFS in a single-disc LC refiner. For all tested pulp furnishes and at all plate gaps, mean peak normal force and mean peak shear force decreases with higher BEL plate, *Fig 7* and *Fig 8*.

SRE is the product of the number of impacts per unit mass of the pulp and the intensity of each impact (Kerekes, 2015). The number of impacts per unit mass of pulp is higher for the plate pattern with higher BEL. In one revolution, the rotor bars cross over the sensor for the plate with BEL=5.59 km/rev and the plate with BEL=2.74 km/rev are 192 and 144, respectively. As shown in *Fig 4*, at the same plate gap and pulp furnish, the SRE for the two plates are approximately equivalent. So, we expect that the intensity of the plate with BEL=2.74 km/rev is higher than the plate with BEL=5.59 km/rev. Decreasing intensity by increasing BEL is consistent with our results that show higher BEL plate results in lower mean peak forces.

This study also shows that the mean peak normal and shear force at the onset of fiber cutting depend on pulp furnish and plate pattern. Both of these forces are lower for the plate pattern having higher BEL, *Table 2*. Moreover, at the onset of fiber cutting, the mean peak normal force of the SW pulp is higher than for the HW pulp. This is consistent with (Harirforoush et al. 2018). However, the difference between mean peak normal force at the onset of fiber cutting for two plate patterns is more significant for SW pulp than HW pulp.

For the plate of BEL=5.59 km/rev, the mean peak shear force at the onset of fiber cutting is different for HW and SW. This is not consistent with the results of (Harirforoush et al. 2018) which showed, for the plate of BEL=2.74 km/rev, the mean peak shear force for HW and SW pulps at the onset of fiber cutting are approximately equivalent. We hypothesize that, the relative magnitudes of two components of shear force (i.e. corner or ploughing force, at the bar edge, and friction force on axial-facing bar surface) differ for these two plate patterns. For the plate of BEL=2.74 km/rev, these two forces vary such that their sum is approximately equivalent for HW and SW pulps, at the onset of fiber cutting. But, for the plate of BEL=5.59 km/rev, the magnitude of the friction force/corner force for HW pulp will be higher (or lower) from the friction force/corner force for SW pulp that cause different mean peak shear forces at the onset of fiber cutting.

At the same plate gap and pulp furnish, normal stress is lower for the plate pattern with higher BEL. However, for SW pulp, shear stress is relatively similar for two plates, *Fig 9c*, while, for HW pulp, shear stress is slightly higher for the plate having higher BEL, *Fig 9d*.

Our results, *Fig 10* and *Table 2*, also show that the mean coefficient of friction at the onset of fiber cutting is a function of plate gap, pulp furnish, and plate pattern. Decreasing the bar width and groove width of the plate results in a higher mean coefficient of friction at all plate gaps and for all pulp furnishes.

As the plate gap is closed, mean peak normal and shear forces increase but mean coefficient of friction decreases. However, increase in mean peak normal force is more significant than the increase in mean peak shear force. This implies a hypothesis that the normal forces are the dominant forces in LC refining that are responsible for development of fibre and paper properties, particularly those properties affected by fiber cutting. This hypothesis is in accordance with (Harirforoush et al. 2018) and (Fernando et al. 2013).

Conclusion

This study investigates the effect of plate pattern on measured bar forces using a custom-designed piezoelectric force sensor measuring bar forces in an AIKAWA 16-in. single-disc refiner with the plate of BEL=5.59 km/rev. Trials were performed using SPF softwood thermomechanical pulp, northern bleached softwood kraft pulp, and aspen hardwood thermomechanical pulp at 3.3 to 3.6% consistency at rotational speeds of 1200 and 1400 rpm. The pulp was sampled at regular intervals, and the length-weighted fiber length, freeness, tear Index, and tensile Index were measured for each sample. Comparing the results of the plate of BEL=5.59 km/rev and BEL=2.74 km/rev indicate that the mean peak normal and shear forces decrease with higher BEL plate. The mean peak of normal and shear forces at the onset of fiber cutting depends on pulp furnish and plate pattern, and they decrease with plate having higher BEL. In addition, the mean coefficient of friction is a function of plate gap, pulp furnishes, and BEL. The plate having higher bar edge length results in higher mean coefficient of friction. We also hypothesize that the normal force is the dominant force in LC refining. In addition, fiber cutting metrics previously introduced in our studies are reliable to be used for different plate patterns.

Acknowledgment

This work is supported by a Collaborative Research and Development grant provided by Natural Sciences and Engineering Research Council of Canada (NSERC) and the following partners: AB Enzymes, Alberta Newsprint Company, Andritz, BC Hydro, Canfor, Catalyst Paper, FPInnovations, Holmen Paper, Meadow Lake Pulp (Paper Excellence), Millar Western, NORPAC, West Fraser, Westcan Engineering, and Winstone Pulp International. The authors also wish to thank M. Miller, E. Jahangir, R. Seifert, D. Bernard, and G. Soong for their assistance during the preparation and execution of the refining trials, and for conducting the sample characterisations at the Pulp and Paper Centre at the University of British Columbia.

References

Backlund, **H.-O.** (2004). Measurement of shear force, temperature profiles and fibre development in mill-scale TMP refiners. PhD. Thesis, Mid Sweden University

Batchelor, **W.J.**, **Martinez**, **D.M.**, **Kerekes**, **R.J.**, and **Ouellet**, **D.** (1997). Forces on fibres in low-consistency refining: Shear force. J. Pulp Pap. Sci. 23 (1), J40–J45.

Carvalho, **M.G.**, **Ferreira**, **P.J.**, **Martins**, **A.A.**, and **Figueiredo**, **M.M.** (1997). A comparative study of two automated techniques for measuring fiber length. Tappi J. 80 (2), 137–142.

Elahimehr, **A.**, **Olson**, **J.A.**, and **Martinez**, **D.M.** (2013). Understanding LC refining: The effect of plate pattern and refiner operation. Nord. Pulp Pap. Res. J. 28(3), 386–391.

Elahimehr, **A.**, **Olson**, **J.A.**, and **Martinez**, **D.M.** (2015). Low consistency refining of mechanical pulp: how plate pattern and refiner operating conditions change the final properties of pulp. Nord. Pulp Pap. Res. J. 30(4), 609–616.

Fernando, **D.**, **Gorski**, **D.**, **Sabourin**, **M.**, and **Daniel**, **G.** (2013). Characterization of fiber development in high- and low-consistency refining of primary mechanical pulp. Holzforschung 67(7), 735–745.

Harirforoush, **R.**, **Wild**, **P.**, and **Olson**, **J.** (2016). The relation between net power, gap, and forces on bars in low consistency refining. Nord. Pulp Pap. Res. J. 31(1), 71–78.

Harirforoush, **R.**, **Olson, J.**, and **Wild**, **P.** (2017). In-process detection of fiber cutting in low consistency refining based on measurement of forces on refiner bars. Tappi J. 16 (4), 189-198.

Harirforoush, **R.**, **Olson, J.**, and **Wild**, **P.** (2018). Indications of the onset of fiber cutting in low consistency refining using a refiner force sensor: the effect of pulp furnish. Nord. Pulp Pap. Res. J., 33(1), 48-57.

Kerekes, **R.J.** (1990). Characterization of pulp refiners by a C - factor. Nord. Pulp Pap. Res. J. 5 (1), 3-8.

Kerekes, **R.J.** (2011). Force-based characterization of refining intensity. Nord. Pulp Pap. Res. J. 26 (1), 14–20.

Kerekes, **R.J.** (2015). Perspectives on High and Low Consistency Refining in Mechanical Pulping. BioResource, 10 (4), 8795-8811

Kerekes, **R.J.**, **Senger**, **J.J.** (2006). Characterizing refining action in low consistency refiner by forces in fibres. J. Pulp Pap. Sci. 32 (1), 1–8.

Luukkonen, **A.**, **Olson**, **J.A.**, and **Martinez**, **D.M.** (2010a). Low Consistency Refining of Mechanical Pulp, Effect of Gap, Speed and Power. J. Pulp Pap. Sci. 36, 28–34.
Luukkonen, **A.**, **Olson**, **J.A.**, and **Martinez**, **D.M.** (2010b). Low Consistency Refining of Mechanical Pulp: A Methodology to Relate Operating Conditions to Paper Properties. J. Pulp Pap. Sci. 36, 107–111.
Martinez, D.M., **Batchelor**, **W.J.**, **Kerekes**, **R.J.**, and **Ouellet**, **D.** (1997). Forces on fibres in low-consistency refining: Normal force. J. Pulp Pap. Sci. 11–18.
Muenster, **H.**, **Ferritsius**, **O.**, **Lecourt**, **M.**, and **Petit-Conil**, **M.** (2005). Energy savings in TMP by high temperature LC/MC refining. International Mechanical Pulping Conference, Oslo, Norway, 213–223.
Musselman, **R.**, **Letarte**, **D.**, and **Simard**, **R.** (1997). Third stage low consistency refining of TMP for energy savings and quality enhancement. 4th Int. Refining Conf., 141–147.
Olender, **D.**, **Wild**, **R.**, **Byrnes**, **R.**, **Ouellet**, **D.**, and **Sabourin**, **M.** (2007). Forces on bars in high-consistency mill-scale refiners: Trends in primary and rejects stage refiners. J. Pulp Pap. Sci. 33(3), 163–171.
Olender, **D.**, **Wild**, **P.**, **Byrnes**, **R.**, **Ouellet**, **D.**, and **Sabourin**, **M.** (2008a). Forces on bars in high-consistency mill-scale refiners: Effect of Consistency. Nord. Pulp Pap. Res. J. 23(2), 218–223.
Olender, **D.**, **Wild**, **P.**, and **Byrnes**, **P.** (2008b). A piezoelectric force sensor for mill-scale chip refiners. Proc. Inst. Mech. Eng. Part E-J. Process Mech. Eng. 222, 115–122.
Prairie, **B.C.** (2005). Measurement of forces in a low consistenct refiner. M.Sc. Thesis, University of Victoria, BC, Canada.
Prairie, **B.**, **Wild**, **P.**, **Byrnes**, **P.**, **Olender**, **D.**, **Francis**, **D.W.**, and **Ouellet**, **D.** (2007). Forces during bar-passing events in low consistency refining: Effects of refiner tram. Pulp Pap. Can. 108 (9), 34–37.
Prairie, **B.**, **Wild**, **P.**, **Byrnes**, **P.**, **Olender**, **D.**, **Francis**, **W.**, and **Ouellet**, **D.** (2008). Forces during Bar-Passing Events in Low-Consistency Refining: Distributions and Relationships to Specific Edge Load. J. Pulp Pap. Sci. 34(1), 1–8.
Roux, **J.C.** (2001): Review paper on pulp treatment processes. The pulp and paper fundamentals research Soc., FRC editor, Oxford, 19-80.
Senger, **J.**, **Siadat**, **A.**, **Ouellet**, **D.**, and **Wild**, **P.** (2004). Measurement of normal and shear forces during refining using a piezoelectric force sensor. J. Pulp Pap. Sci. 30 (9), 247–251.
Senger, **J.**, **Olmstead**, **M.**, **Ouellet**, **D.**, and **Wild**, **P.** (2005). Measurement of normal and shear forces in the refining zone of a TMP refiner. J. Pulp Pap. Sci. 31 (1), 28–32.
Stationwala, **M.I.**, **Miles**, **K.B.**, and **Karnis**, **A.** (1994). Effect of feed rate on refining. J. Pulp Pap. Sci. 20 (8), 236–240.
Zha, **Q.**, **Lanouette**, **R.**, **Law**, **K.N.**, **Bousquet**, **J.-P.**, and **Bussières**, **S.** (2008). Refining of Long Fibre Fractions after Fractionation. 94th Annual meeting PAPTAC, Montreal, QC, Canada, B481–B487.